AIRCRAFT SIMULATION VALIDATION USING AN INSTRUMENTAL VARIABLE APPROACH

by

Christopher D. Weekley

Thesis Submitted to the Faculty of the

Virginia Polytechnic Institute and State University

in partial fulfillment of the requirements for the degree of

Master of Science

in

Aerospace Engineering

APPROVED:

Mark R. Anderson

Dr. M.R. Anderson

E M Cliff

Dr. E.M. Cliff

W C Durham

Dr. W.C. Durham

December, 1992

Blacksburg, Virginia

AIRCRAFT SIMULATION VALIDATION USING AN INSTRUMENTAL VARIABLE APPROACH

by

Christopher D. Weekley

Committee Chairman: Dr. M.R. Anderson

Department of Aerospace and Ocean Engineering

(ABSTRACT)

A procedure is developed which offers the potential to validate aircraft simulation models using noisy flight test measurements. The proposed validation procedure is based on the instrumental variable parameter identification method. The instrumental variable method requires a choice of "instruments." For this research, the "instruments" are chosen using the response predicted by an available simulation model. With the "instruments" chosen from the predicted response, it is shown that the parameter estimates are correlated with only the measured input noise vector. In contrast, the generally used least-squares approach is shown to be correlated with both the state and input noise vectors.

Several studies are presented to demonstrate the utility of the validation procedure. These studies include input variations and noise variations. The method is demonstrated using longitudinal and lateral/directional axis cases derived from a nonlinear simulation of a high performance fighter aircraft. The results are presented using time response comparisons, eigenvalue comparisons, and identified stability derivative comparisons. The case study results confirm that the instrumental variable method performs better than the least-squares technique when the state noise level is high and the input noise level is relatively low.

Acknowledgements

I would like to thank Dr. Mark R. Anderson for his helpful insight and direction during the formulation and writing of this thesis. Without his guidance this thesis could not have been written. Thanks also to Dr. W.C. Durham and Dr. E.M. Cliff for agreeing to be committee members. I would also like to thank the AOE department for allowing me to attend this University and learn a different, yet valuable engineering perspective. Finally, I want to thank my parents and my wonderful fiancée for their patience and encouragement.

Table of Contents

List of Tables

List of Figures

List of Appendix Figures

List of Symbols

A	Linear state matrix
A_p	Predicted linear state matrix
B	Linear control input matrix
B_p	Predicted linear control input matrix
C	Linear output state matrix
D	Linear output control matrix
e	Error measurement
f	State deterministic sensor function, random variable
f_d	State derivative function
g	Input function, random variable
L_α	Aerodynamic lift due to angle-of-attack (1/sec)
L_β	Aerodynamic rolling moment due to sideslip ($1/sec^2$)
L_{δ_a}	Aerodynamic rolling moment due to aileron deflection ($1/sec^2$)
L_{δ_h}	Aerodynamic lift due to elevator deflection (1/sec)
$L_{\delta r}$	Aerodynamic rolling moment due to rudder deflection ($1/sec^2$)
L_p	Aerodynamic rolling moment due to roll rate (1/sec)
L_q	Aerodynamic lift due to pitch rate (1)
L_r	Aerodynamic rolling moment due to yaw rate (1/sec)
M_α	Aerodynamic pitching moment due to angle-of-attack ($1/sec^2$)
M_{δ_h}	Aerodynamic pitching moment due to rudder deflection ($1/sec^2$)
M_q	Aerodynamic pitching moment due to pitch rate (1/sec)
N_β	Aerodynamic yawing moment due to sideslip ($1/sec^2$)
N_{δ_a}	Aerodynamic yawing moment due to aileron deflection ($1/sec^2$)

$N_{\delta r}$	Aerodynamic yawing moment due to rudder deflection ($1/sec^2$)
N_p	Aerodynamic yawing moment due to roll rate (1/sec)
N_r	Aerodynamic yawing moment due to yaw rate (1/sec)
p	Roll rate (rad/sec), parameter vector
q	Pitch rate (rad/sec)
r	Yaw rate (rad/sec)
u	Vector of control inputs
u_m	Vector of measured control inputs
$\hat{u}$	Vector of control input estimates
v	State noise vector
v_d	State derivative noise vector
w	Control input noise vector
x	State vector
X	Matrix of independent variables
x_m	Measured state vector
x_p	Predicted state vector
$\hat{x}$	State vector estimates
y	Dependent variables in normal form
Y_β	Aerodynamic side force due to sideslip (1/sec)
Y_{δ_a}	Aerodynamic side force due to aileron deflection (1/sec)
$Y_{\delta r}$	Aerodynamic side force due to rudder deflection (1/sec)
Y_p	Aerodynamic side force due to roll rate (1)
Y_r	Aerodynamic side force due to yaw rate (1)
Z	Matrix of instrumental variables

Greek Symbols

α	Angle-of-attack, alpha (rad)
β	Sideslip, beta (rad)
δ_a	Aileron deflection, delta_a (rad)
δ_h	Elevator deflection, delta_h (rad)
δ_r	Rudder deflection, delta_r (rad)
σ	Noise RMS value
ζ	Damping ratio

1.0 Introduction

Modern aircraft simulations play an increasingly important role in the design and analysis of modern aircraft. With the aide of high performance computers, highly sophisticated, nonlinear models of high performance aircraft are being used extensively in pilot and crew member training. The simulation should model the actual flight system as closely as possible to insure training utility. Accurate methods of simulation validation are therefore needed so that the fidelity of current and future simulations can be proven. The validation task has become increasingly difficult to accomplish because of the complexity of today's aircraft systems.

One method of simulation validation is to use parameter identification techniques to determine model parameters from actual flight data. The simulation is considered valid if the identified parameters match the parameters in the simulation. Frequency-response identification methods have been useful tools in validating rotorcraft simulations.[1,2] Statistical methods of parameter identification have also been applied to aircraft systems. For example, Friedrich [3] used a regression analysis to determine stability derivatives from flight test results. V. Klein [4-6] has used statistical methods of parameter estimation extensively in his studies of highly maneuverable and often unstable aircraft such as the High-Angle-of-Attack Research Aircraft (HARV) and the X-31. He has employed subset regression, fractional rank regression, and mixed estimation techniques (which are based on extensions of the least-squares technique) to deal with the many problems which can arise in the identification of aircraft models.

If a simulation of the aircraft is already available, parameter identification techniques can be used to identify an error model instead of the dynamics of the actual aircraft. If the terms of the identified error model are small, the simulation is considered valid. Or, the

dynamics of the identified error model can be added to the existing simulation to produce a new simulation which will compare favorably to the actual aircraft. For example, Hess, Stanka, and Purdy [7] developed a method in which unknown error terms are estimated such that the sum of the squared differences between the predicted output states and the measured output states are minimized. Hess and Ly [8] installed a simple estimation scheme (based on least-squares estimation) in a simulation environment to isolate deficiencies in simulation models as well as to identify error models.

Noise inherent in the measured aircraft states and controls can cause errors in the estimation of aircraft or error model parameters. If the noise is high relative to the measured signal, many of the previously mentioned identification methods will not be able to predict accurate stability and control derivatives. Although advances have been made in measuring devices and filtering techniques, even small amounts of measurement noise can result in significant parameter estimation errors.

A variant of the equation error method of least-squares parameter estimation, called the instrumental variable (IV) method, represents one promising approach to reducing the effect of measurement noise when estimating dynamic model parameters. P.C. Young gives a brief history of the IV method and notes that the first application of the IV method in the process identification field was by Joseph, Lewis, and Tou.[9] This group suggested an IV procedure for identifying the parameters of a process described by a difference equation model. Andeen and Shipley later suggested an updated version and applied it to the theoretical design of a digital adaptive flight control system for an aerospace vehicle. Shortly afterwards, Levadi described the mechanization of a purely analog IV method for identifying a linear dynamic process described by a differential equation model. Young used an IV approach to develop a digital recursive estimation algorithm for the real-time identification of linear models.

The IV method promises to alleviate, or at least reduce, the effect of signal noise

when estimating model parameters from measured data. The IV method has a basis in classical statistical estimation theory, but does not require *a priori* information on the signal noise statistics.

The IV method presented in this thesis is a non-recursive version of Young's recursive method. The basic philosophy of the approach developed herein is to solve the general least-squares estimation problem by choosing a set of instrumental variables that are uncorrelated with additive state noise. The anticipation is that if the input noise is relatively small, more accurate model parameter estimates can be made even if the vehicle state noise is relatively high. As will be shown, the least-squares (LS) solution is highly correlated with both the state and input noise. If the signal to noise ratio is low, then the LS solution may not predict accurate error parameters.

The need for more accurate, yet easily implementable, methods for simulation validation provided the motivation for this research. The goal of this work was to reveal the possibilities of using the IV method in identifying stability and control derivative errors in computer simulations given that actual flight test data is available. This goal was accomplished by using available simulation tools and computer software to setup the problem as realistically as possible. It is hoped that this strategy can be implemented in a variety of simulation environments and conditions not specifically studied in this work.

2.0 Methodology

The purpose of the methodology section is to develop the instrumental variable method employed in this thesis. Also, the differences between the instrumental variable method and the least-squares method will be shown and discussed.

The block diagram shown in Figure 1 illustrates the problem of simulation validation. This diagram is very important in understanding the problem that simulation engineers encounter. As shown in Figure 1, an aircraft receives input commands from the pilot (or autopilot), represented by vector u, and produces state and state derivative responses, x and $\dot{x}$. Unfortunately, the precise aircraft state-space model, inputs, and state and state derivative outputs cannot be measured. The devices that do measure the inputs and the state and state derivatives may not be calibrated to produce accurate values. The measurement calibration functions g(u), f(x), and $f_d(\dot{x})$ shown in Figure 1 may bias or scale the actual values of the inputs, states, and state derivatives if the measurement devices were not calibrated properly prior to the test flight. Also, the aircraft actuators and electronic devices may corrupt the u, x, and $\dot{x}$ signals with electronic and/or mechanical noise. Figure 1 shows the input noise, w, state noise, v, and state derivative noise, v_d that might be added to the calibrated signals u, x, and $\dot{x}$, respectively.

The known quantities that are recorded from test flights are the actual values that have been calibrated and corrupted with noise. These signals, shown in Figure 1, are u_m, x_m, and $\dot{x}_m$. Furthermore, the simulation block in Figure 1 represents the mathematically modeled aircraft. It will be assumed that this simulation block contains a state-space model which is generally predicted from wind tunnel experiments and mathematical equations. As shown in Figure 1, the simulation receives the *measured* control inputs, u_m, and produces *predicted* state and state derivatives, x and $\dot{x}_p$. The problem of simulation validation is to

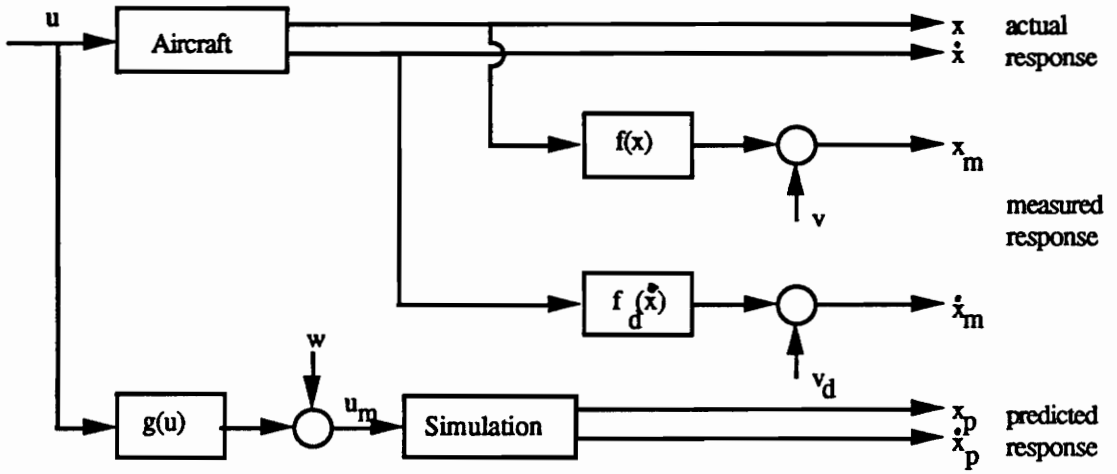

Figure 1: Simulation validation block diagram

insure that the predicted state and state derivative values are as close to the actual values as possible. Since the precise actual response is unattainable, the simulation engineer must resort to comparing the predicted values to the measured values.

For this analysis, it will be assumed that static tests can reveal bias and scale factors such that the following simplifications can be made:

$$f(x) = x \tag{1}$$

$$f_d(\dot{x}) = \dot{x} \tag{2}$$

and

$$g(u) = u \tag{3}$$

where, x and $\dot{x}$ are the state and state derivative vectors, respectively, and u are the control input vectors.

The dynamics of the aircraft are assumed to be adequately represented by the linear state-space model,

$$\dot{x} = Ax + Bu \tag{4}$$

while the simulation is represented by the state-space model,

$$\dot{x}_p = A_p x_p + B_p u_m \tag{5}.$$

The known (measured) variables are,

$$x_m = x + v \tag{6}$$

$$\dot{x}_m = \dot{x} + v_d \tag{7}$$

and

$$u_m = u + w \tag{8}$$

where v, v_d, and w are the noise vectors added respectively to the vehicle state, state derivative, and input vectors. Solving (6), (7), and (8) for x, $\dot{x}$, and u and substituting into (4) yields,

$$\dot{x}_m = Ax_m + Bu_m + \eta \tag{9}$$

where a new noise vector has been defined as,

$$\eta = v_d - Av - Bw \tag{10}.$$

The unknowns are matrices A, B, and noise vector η. Note that the noise vector η contains

all the noise sources, v_d, v, and w.

By subtracting (5) from (9), the following equation results,

$$\dot{x}_m - \dot{x}_p + A_p(x_p - x_m) = \Delta A x_m + \Delta B u_m + \eta \qquad (11)$$

where

$$\Delta A = A - A_p$$

and

$$\Delta B = B - B_p.$$

Let the equation error be denoted by the vector e where,

$$e = \dot{x}_m - \dot{x}_p + A_p(x_p - x_m),$$

and equation (11) becomes

$$e = \Delta A x_m + \Delta B u_m + \eta \qquad (12).$$

At this point, e, x_m, and u_m, which are time dependent, are available from flight test measurements or the predicted model. ΔA and ΔB represent the differences between the actual aircraft dynamics and the simulation dynamics.

To solve equation (12) row by row, let

$$e_i = i^{th} \text{ row of } e,$$

$$\eta_i = i^{th} \text{ row of } \eta,$$

and

$$\Delta A_i \, , \Delta B_i = i^{th} \text{ row of } \Delta A \, , \Delta B.$$

Equation (12) can then be written as

$$e_i = \begin{bmatrix} \Delta A_i & \Delta B_i \end{bmatrix} \begin{bmatrix} x_m \\ u_m \end{bmatrix} + \eta_i$$

for the i^{th} row. Or, since e_i and η are scalars,

$$e_i = \begin{bmatrix} x_m^T & u_m^T \end{bmatrix} \begin{bmatrix} \Delta A_i^T \\ \Delta B_i^T \end{bmatrix} + \eta_i \qquad (13).$$

This development is repeated for each time point, such that

$$\begin{bmatrix} e_i(t_1) \\ e_i(t_2) \\ . \\ . \\ e_i(t_N) \end{bmatrix} = \begin{bmatrix} x_m^T(t_1) & u_m^T(t_1) \\ x_m^T(t_2) & u_m^T(t_2) \\ . & . \\ x_m^T(t_N) & u_m^T(t_N) \end{bmatrix} \begin{bmatrix} \Delta A_i^T \\ \Delta B_i^T \end{bmatrix} + \begin{bmatrix} \eta_i(t_1) \\ \eta_i(t_2) \\ . \\ . \\ \eta_i(t_N) \end{bmatrix} \qquad (14).$$

Equation (14) leads to the standard form

$$y = Xp + \eta \qquad (15)$$

where,

y = an $N \times 1$ vector of known dependent error variables

X = an $N \times (n+m)$ matrix of known independent measured state and control variables

p = an $(n+m) \times 1$ vector of the unknown error dynamic parameters

η = an $N \times 1$ random noise vector .

The standard form equation assumes N data points, n states, and m control input variables.

To find the least-squares solution of equation (15), pre-multiply (15) by X^T to yield,

$$X^T y = X^T X p + X^T \eta \qquad (16).$$

Assume $(X^T X)^{-1}$ exists and multiply (16) by $(X^T X)^{-1}$ to yield,

$$(X^T X)^{-1} X^T y = p + (X^T X)^{-1} X^T \eta \qquad (17).$$

The LS parameter estimates are defined by ignoring the noise term in (17) and solving for p to obtain,

$$\hat{p}_{LS} = (X^T X)^{-1} X^T y \qquad (18).$$

The LS parameter error due to noise is obtained by comparing (17) and (18), to reveal,

$$\hat{p}_{LS} - p = (X^T X)^{-1} X^T \eta \qquad (19).$$

The LS parameter estimator is considered an unbiased estimator if $E[\hat{p}_{LS}] = p$. Taking expected values of (19) yields,

$$E[\hat{p}_{LS}] = p + E[(X^TX)^{-1}X^T\eta] \qquad (20).$$

If X and η were independent and η was a zero mean process, the least squares estimator is unbiased because the second term in (20) is then zero. In this case, X and η are not independent because X and η both contain contributions from the noise sources v, v_d, and w. Therefore, the least squares parameter estimates will be biased.

In an attempt to reduce the parameter bias of the least squares estimator, the IV solution is considered. To find the IV solution of equation (15), pre-multiply equation (15) by Z^T, where the matrix Z has the same size as X and are called the "instruments." The same procedure used to derive the LS parameter estimates is followed to yield the IV parameter estimates,

$$\hat{p}_{IV} = (Z^TX)^{-1}Z^Ty \qquad (21).$$

The IV parameter error due to noise is then,

$$\hat{p}_{IV} - p = (Z^TX)^{-1}Z^T\eta \qquad (22).$$

Equation (22) shows that the IV method also leads to biased estimates because,

$$E[\hat{p}_{IV}] = p + E[(Z^TX)^{-1}Z^T\eta] \qquad (23).$$

However, (23) demonstrates that by proper choice of the instruments, it is possible to reduce the parameter bias if $Z^T\eta$ is made small.

Because Z must be the same size as X, let

$$Z = \begin{bmatrix} \hat{x}^T(t_1) & \hat{u}^T(t_1) \\ \hat{x}^T(t_2) & \hat{u}^T(t_2) \\ \vdots & \vdots \\ \hat{x}^T(t_N) & \hat{u}^T(t_N) \end{bmatrix}$$

where Z is an N×(n+m) matrix, $\hat{x}$ is the same size as x_m, and $\hat{u}$ is the same size as u_m. The value of $Z^T\eta$ is then,

$$Z^T\eta = \begin{bmatrix} \hat{x}(t_1) & \hat{x}(t_2) & . & \hat{x}(t_N) \\ \hat{u}(t_1) & \hat{u}(t_2) & . & \hat{u}(t_N) \end{bmatrix} \begin{bmatrix} \eta_i(t_1) \\ \eta_i(t_2) \\ . \\ \eta_i(t_N) \end{bmatrix} = \begin{bmatrix} \sum_{j=1}^{N} \hat{x}(t_j)\eta_i(t_j) \\ \sum_{j=1}^{N} \hat{u}(t_j)\eta_i(t_j) \end{bmatrix} \quad (24)$$

where $Z^T\eta$ has dimension of (n+m)×1. Using the definition of η from equation (10), equation (24) becomes (25) for each row,

$$Z^T\eta = \begin{bmatrix} \sum_{j=1}^{N} \hat{x}(t_j)[v_{d_i}(t_j) - A_i v_i(t_j) - B_i w_i(t_j)] \\ \sum_{j=1}^{N} \hat{u}(t_j)[v_{d_i}(t_j) - A_i v_i(t_j) - B_i w_i(t_j)] \end{bmatrix} \quad (25).$$

If we can choose $\hat{x}$ and $\hat{u}$ such that $Z^T\eta = 0$, equation (23) reveals that the IV estimator will be unbiased. One way to make $Z^T\eta = 0$ for all rows of (25) is to meet the following conditions,

$$\sum_{j=1}^{N} \hat{x}(t_j)v_d^T(t_j) = 0 \quad (26)$$

$$\sum_{j=1}^{N} \hat{u}(t_j)v_d^T(t_j) = 0 \quad (27)$$

$$\sum_{j=1}^{N} \hat{x}(t_j)v^T(t_j)A^T = 0 \quad (28)$$

$$\sum_{j=1}^{N} \hat{u}(t_j)v^T(t_j)A^T = 0 \quad (29)$$

$$\sum_{j=1}^{N} \hat{x}(t_j)w^T(t_j)B^T = 0 \quad (30)$$

and

$$\sum_{j=1}^{N} \hat{u}(t_j)w^T(t_j)B^T = 0 \quad (31).$$

Note that equations (26)-(31) are obtained after considering (25) for each of the i=1, ..., n

rows of (12). Equations (26)-(31) can be met by proper choice of $\hat{x}$ and $\hat{u}$. For example, condition (26) will be met if $\hat{x}$ is not correlated with v_d. Therefore, equations (26) through (31) essentially mean we want to choose $\hat{x}$ and $\hat{u}$ such that they are not correlated with any of the noise sources v_d, v, or w.

For this research two choices of $\hat{x}$ and $\hat{u}$ will be considered. If $\hat{x} = x_m$ and $\hat{u} = u_m$ then Z = X and the least-squares solution results. With the least-squares solution, we can expect (28) and (31) not to be met because x_m is correlated with v and u_m is correlated with w. On the other hand, if $\hat{x} = x_p$ and $\hat{u} = u_m$, then we would expect all constraints to be met except (31) because u_m is correlated with w. So, constraint (28) is probably violated for the LS solution but will not be violated with the IV choice of $\hat{x} = x_p$. Note that many other choices are possible for $\hat{x}$ and $\hat{u}$, but only the LS solution and the choice of $\hat{x} = x_p$ and $\hat{u} = u_m$, herein called the IV solution, are explored in the sample studies to follow.

3.0 Results and Discussion

The following sections present the conditions under which the IV and LS methods were studied and the specific results obtained. The first section discusses the aircraft model employed and the input and noise variations studied. The second section presents the time response, eigenvalue, and identified stability derivative comparisons.

3.1 Case Study Description

3.1.1 Aircraft Model

A nonlinear simulation was used to generate states and inputs which will serve as the aircraft flight test data. Noise will be added to the nonlinear response so that realistic measurements are available. The simulation that was implemented, which will be called VTSim, is based on Brumbaugh's [11] aircraft control design challenge. The simulation code was obtained from NASA Ames-Dryden and a subroutine was added to provide for trimming.

VTSim models a generic, state-of-the-art, high-performance aircraft. It includes detailed, full-envelope, nonlinear aerodynamics, and a complete engine model. It models two afterburning turbofan engines, each capable of producing approximately 32,000 lb of thrust. A three-view of the aircraft is shown in Figure 2, including control surfaces and locations. The aircraft is shown along with a definition of the body axis coordinates (x_B, y_B, z_B). This coordinate system moves with the aircraft in the orientation shown. Also shown in Figure 2 are the five control surface actuators. The actuators are rate limited to 24 deg/sec and have a first-order response modeled by

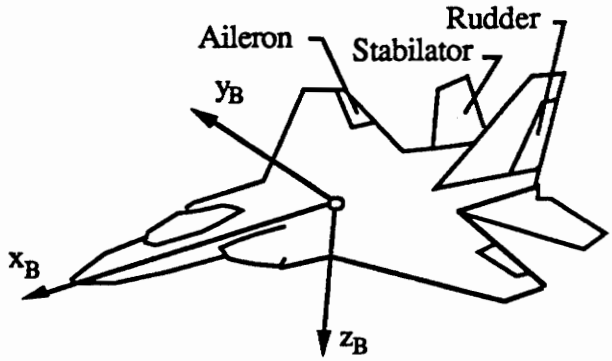

Figure 2: Three view of aircraft and control surfaces

$$G(s) = \frac{20}{s+20} \qquad (31).$$

The operational envelope for this vehicle, for trimmed straight-and-level, 1-g flight is shown in Figure 3 for the aircraft weight of 45,000 lb.

A FORTRAN subroutine was added to VTSim so that linearized models of the aircraft could be obtained numerically. The FORTRAN subroutine was developed by Brent York, who is also a graduate student at Virginia Tech. The subroutine essentially perturbs each of the states and inputs of the aircraft model and records the change in state derivatives and outputs. State-space models are then formed using the perturbation results.

MATLAB™ [12] by Mathworks, Inc. was then used to generate all identification results of this research. This software was used to add noise to the VTSim generated states, perform linear simulations using the state-space models, and calculate the LS and IV method results.

3.1.2 Input Variations

Two test simulations were performed to demonstrate the utility of the IV method in determining aircraft stability and control derivative error estimates. The first simulation was a second-order longitudinal axis example in which a simple elevator doublet was the control input. The actual surface deflection of the elevator is shown in Figure 4. The second case was a third-order lateral/directional axis example where two inputs were used simultaneously: an aileron doublet and an increasing sine frequency sweep. The surface deflections for the lateral/directional axis case are shown in Figure 5. This example was performed to observe the effect of two inputs on the parameter error estimates.

In both simulations, a steady level flight condition at an altitude of 10,000 feet and

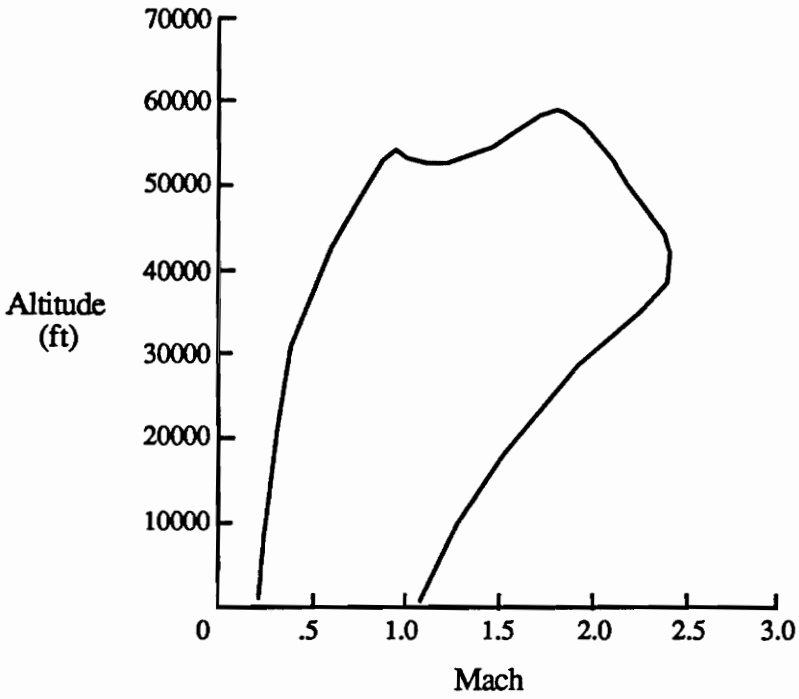

Figure 3: Vehicle operational envelope at 45,000 lb.

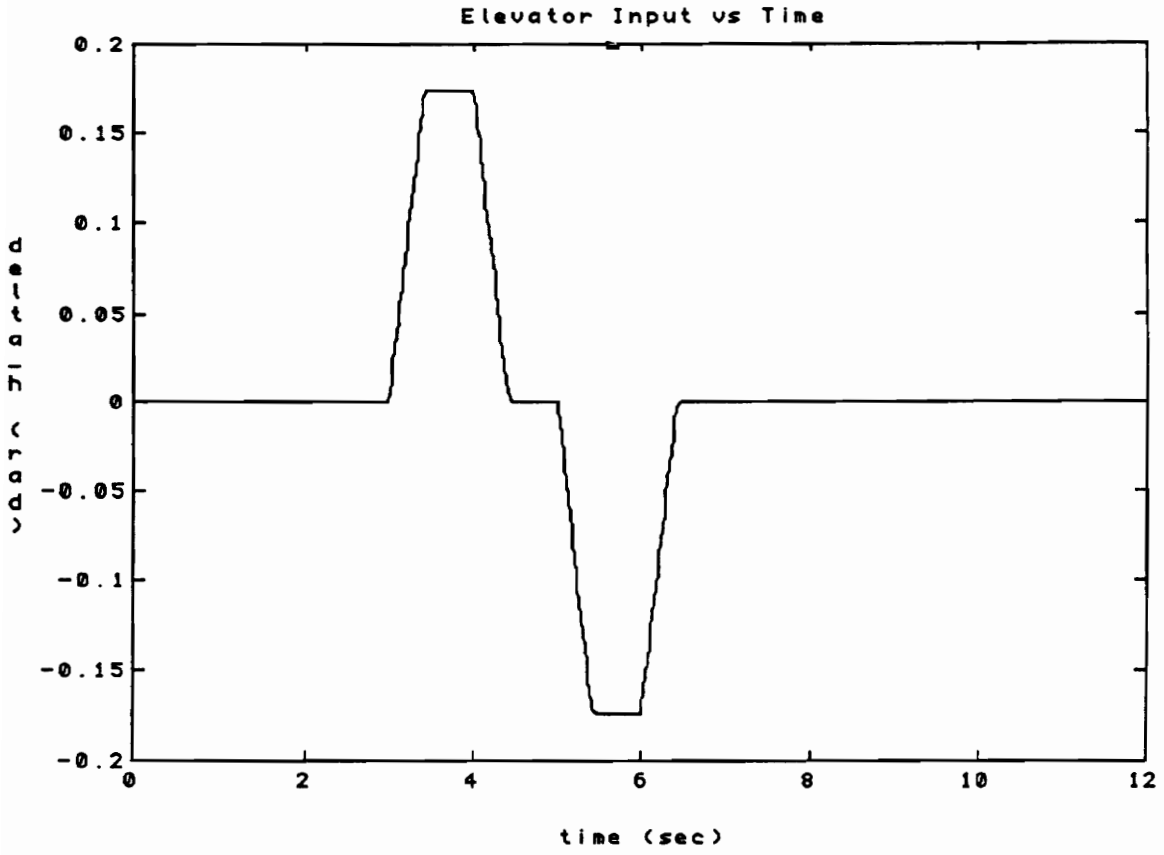

Figure 4: Elevator deflection shown without noise

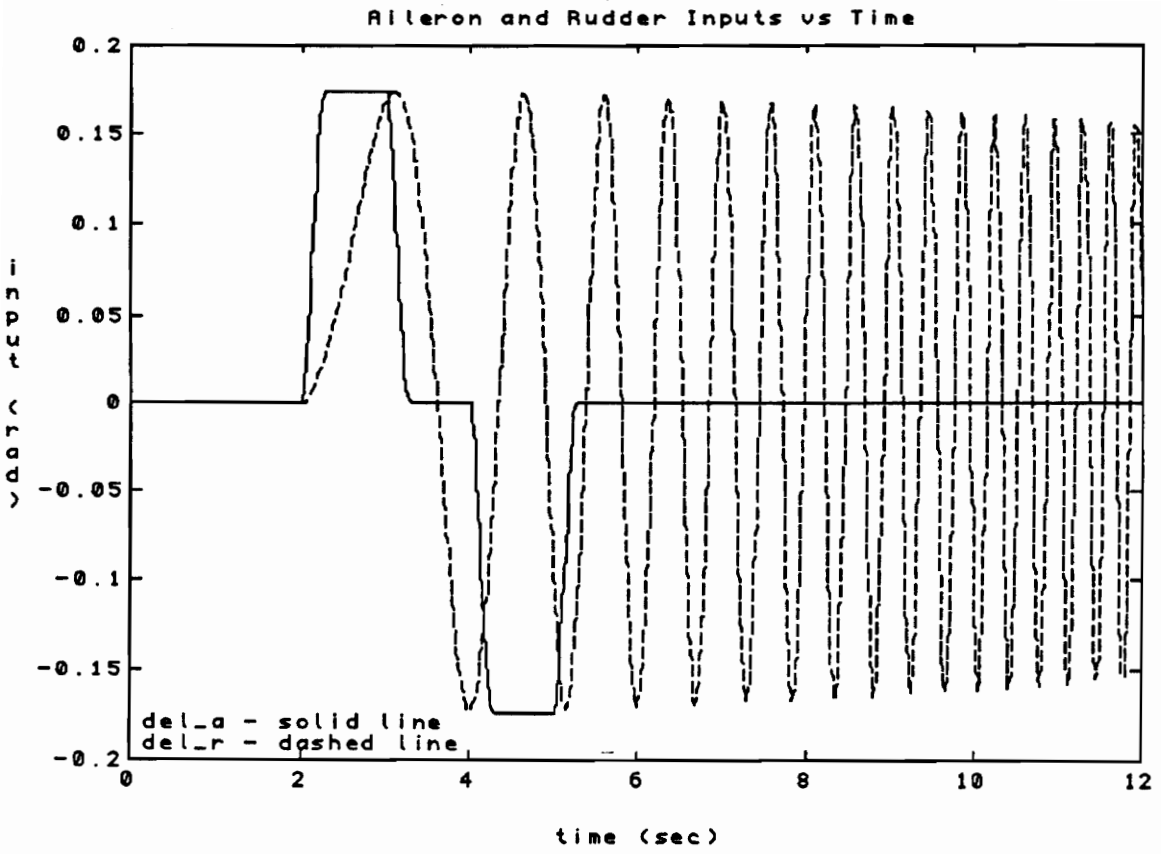

Figure 5: Lateral/directional deflections shown without noise

velocity equivalent to Mach 0.5 was considered. The trim value of each state and control was subtracted from the VTSim output so that small perturbation linear models could be studied.

Linear models of both longitudinal and lateral/directional examples were extracted from VTSim. The linear models derived numerically (using the linear model extraction subroutine), were used as the predicted models in (5). Pitch rate, q, and the change in angle-of-attack, $\Delta\alpha$, are the states of the longitudinal axis model. The following shows the state-space model of the longitudinal axis system [13]:

$$\begin{bmatrix} \dot{q} \\ \dot{\alpha} \end{bmatrix} = \begin{bmatrix} M_q & M_\alpha \\ L_q & L_\alpha \end{bmatrix} \begin{bmatrix} q \\ \Delta\alpha \end{bmatrix} + \begin{bmatrix} M_{\delta_h} \\ L_{\delta_h} \end{bmatrix} \Delta\delta_h \qquad (32).$$

Roll rate, p, yaw rate, r, and change in sideslip, $\Delta\beta$, are the states of the lateral/directional axis model. The following shows the state-space model of the lateral/directional axis system [13]:

$$\begin{bmatrix} \dot{p} \\ \dot{r} \\ \dot{\beta} \end{bmatrix} = \begin{bmatrix} L_p & L_r & L_\beta \\ N_p & N_r & N_\beta \\ Y_p & Y_r & Y_\beta \end{bmatrix} \begin{bmatrix} p \\ r \\ \Delta\beta \end{bmatrix} + \begin{bmatrix} L_{\delta_a} L_{\delta_r} \\ N_{\delta_a} N_{\delta_r} \\ Y_{\delta_a} Y_{\delta_r} \end{bmatrix} \begin{bmatrix} \Delta\delta_a \\ \Delta\delta_r \end{bmatrix} \qquad (33).$$

3.1.3 Noise Variations

The statistics of the state, state derivative, and input noise were varied in order to study the utility of the IV approach when compared to the LS approach. The root-mean-squared (RMS) values of noise used in this research were chosen similar to values used by Murphy [14]. The "nominal" RMS values chosen were the following:

- angles (α, β): σ = .01 rad
- angular rates (q, p, r): σ = .01 rad/sec

• inputs (δ_h, δ_r, δ_a): σ = .01 rad .

Using these as the baseline values, seven studies of noise variations were set up for the state noise, v, state rate noise, v_d, and input noise, w. Table 1 shows each case and the corresponding RMS factor, which represents a multiple of the baseline RMS noise. For example, Case 2 has RMS values of σ = .02 rad for angles and σ = .02 rad/sec for rates. The "zero" case was chosen to obviously represent the case with zero RMS factors or no noise.

The noise variation study is of critical importance in support of the results of this thesis. Although Cases 3, 4, 6, and 7 have relatively large RMS noise values which may not occur in actual measured data, they are important in establishing the error trends. These cases were considered in order to study the theoretical correlation of the states and inputs with noise. Recall that high noise values were expected to greatly influence the LS solution while having a lower effect when instruments are chosen from simulation predictions.

3.2 Case Study Results

This section presents the results of the longitudinal and lateral/directional axis studies with comparisons of the LS and IV solutions. Three types of comparisons are made for each selected noise case: time response, eigenvalue, and stability derivative comparisons. Since this research was performed for a particular aircraft at a particular point in its flight envelope, the exact results shown should not necessarily be extrapolated to other flight vehicles at other flight conditions.

When presenting time response comparisons, the VTSim states are *shown* without noise in each comparison graph. Noise is not included in the graph so that a visual

Table 1: Baseline RMS noise factors

Case	v, v_d RMS factor	w RMS factor
0	0	0
1	1	1
2	2	2
3	4	4
4	6	6
5	2	1
6	4	1
7	6	1

comparison of each method is not distorted by the presence of noise. For example, Figure 6 shows the pitch rate with Case 1 measurement noise σ =.01 rad/sec added while Figure 7 shows the pitch rate with Case 7 noise σ =.06 rad/sec added. Noise was added to the VTSim states for analysis and parameter identification but the noise was left out on the plots for clarity. In all test simulations, plots comparing the VTSim states without noise, the

predicted response using the IV solution, and the predicted response using the LS solution were made for noise cases listed in Table 1. Results of all cases are shown in the Appendix.

Eigenvalue plots were also made to show the effect of noise in the system stability. Plots were made for the case combinations of 0, 1, 2, 3, 4 and 0, 1, 5, 6, 7. The combination of 0, 1, 2, 3, 4 shows the trend when both state and input noise values were increased while the combination of 0, 1, 5, 6, 7 reveals the trend when only the state noise values were increased above the baseline value. Short period mode eigenvalues of the longitudinal axis system are shown while the roll and Dutch Roll eigenvalues are presented for the lateral/directional axis case.

Identified parameters were also determined for comparison of each stability and control derivative error with respect to the zero noise value. For example, del_Mq is the absolute value of the identified change in Mq with respect to the zero noise identified error value. Parameters were computed for each stability and control derivative and bar graphs were made for each derivative for comparison. It should be noted that the parameter error estimates that were generated for each case were the result of an *average* of ten independent simulations. Note that for the identified stability derivative results, comparisons of Cases 2 through 7 are made with respect to Case 1 (which used the baseline noise values).

The following sections present the results of the two simulation case studies.

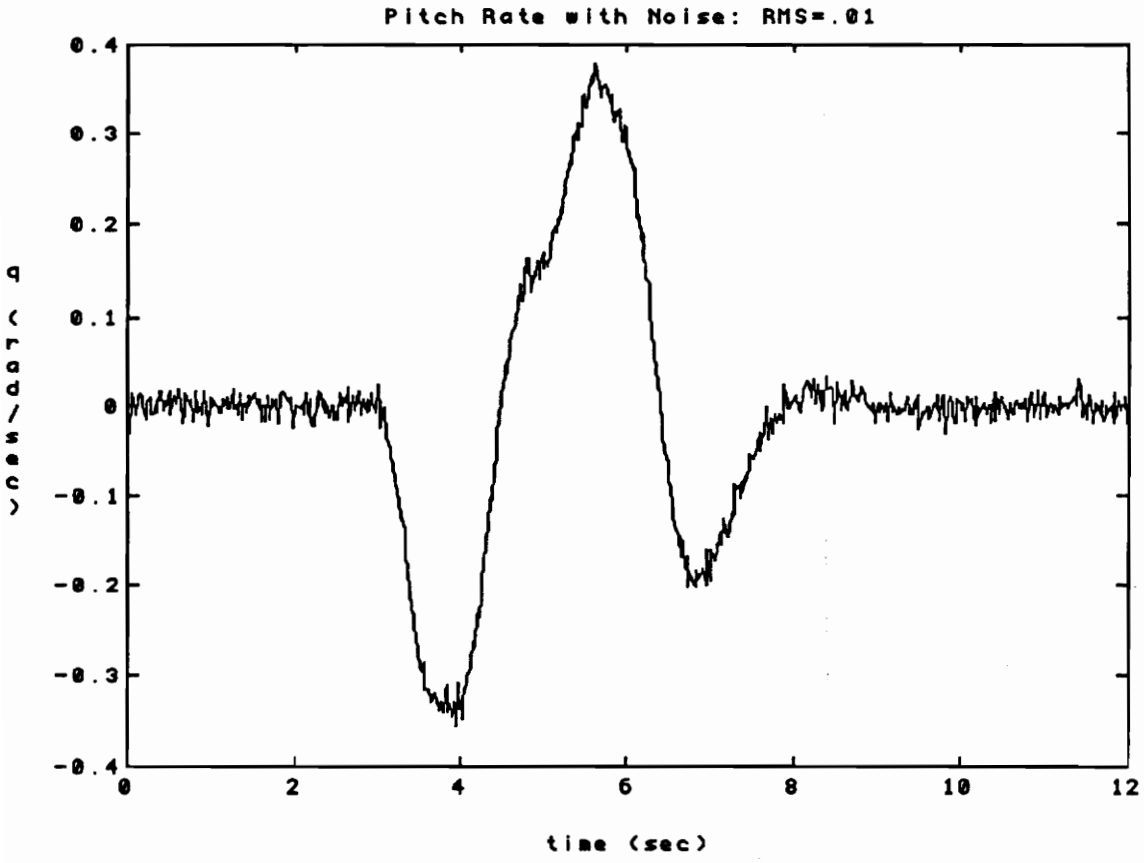

Figure 6: Pitch rate shown with noise --- RMS = .01

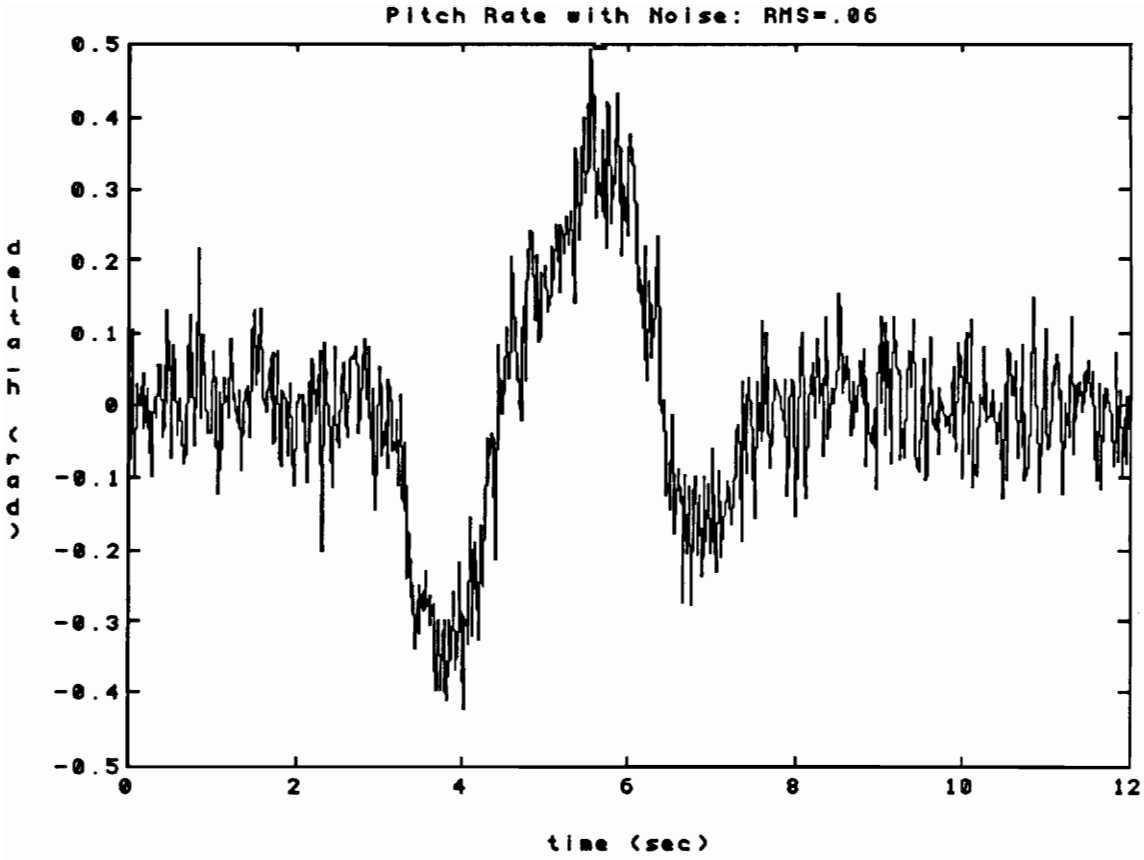

Figure 7: Pitch rate shown with noise --- RMS = .06

3.2.1 Longitudinal Axis Example

3.2.1.1 Time Response Comparisons

The time responses for the longitudinal axis example verify the expected trend of the IV method with the input noise factor and trend of the LS method with both state and input noise factors. Figures 8 and 9 show q and $\Delta\alpha$ when the identified error with zero noise is added to the predicted simulation state-space model. As can be observed, both the IV and LS methods follow the VTSim time responses closely. However, when noise is added to the system, differences in the IV and LS method time responses appear. In Case 4, for example, Figures 10 and 11 reveal large deviations by both solutions, with the LS identified model responses varying from the nonlinear VTSim responses somewhat more than the IV identified model results. Furthermore, Case 7 results, shown in Figures 12 and 13, reveal only small differences between the IV identified model and VTSim responses, but distinct deviations between the LS identified model and VTSim responses. Case 7 dramatically supports the conclusion that the LS method is correlated with both state and input noise while the IV solution is relatively unaffected by the high state RMS noise values.

3.2.1.2 Eigenvalue Comparisons

Figure 14 shows the state-space model eigenvalues for Cases 0, 1, 2, 3, and 4 of the longitudinal axis system. This comparison is made to reveal the system stability trend when increasing both the state and input noise values by the same factor (see Table 1). With each increase in noise factor, both the IV and LS identified systems become less

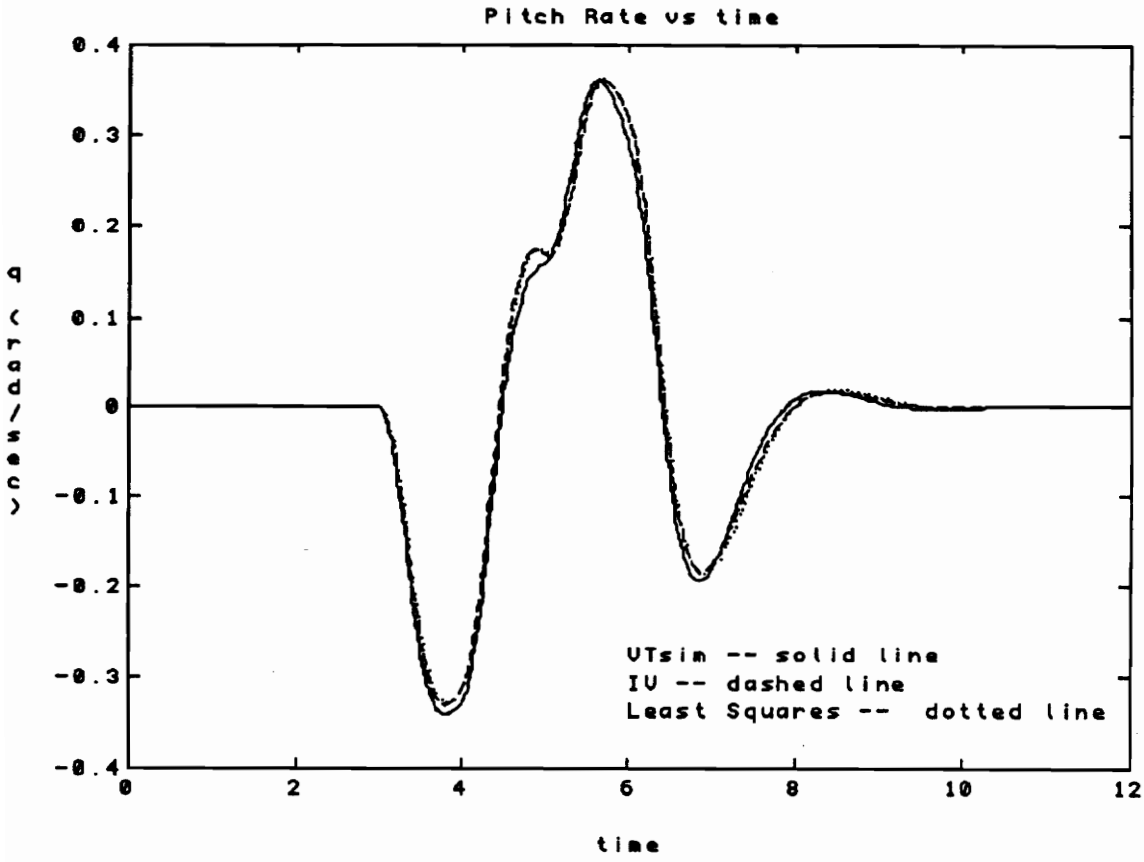

Figure 8: Pitch rate without added noise; Case 0

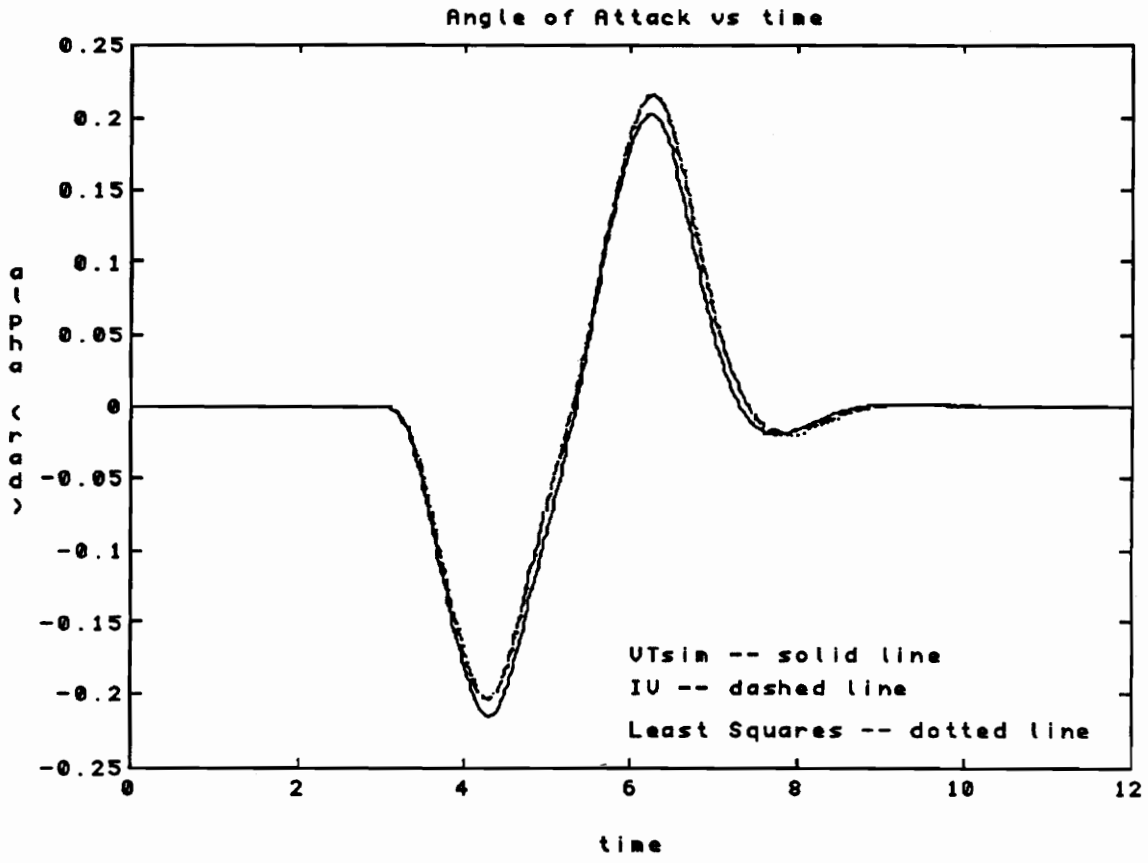

Figure 9: Angle of attack without added noise; Case 0

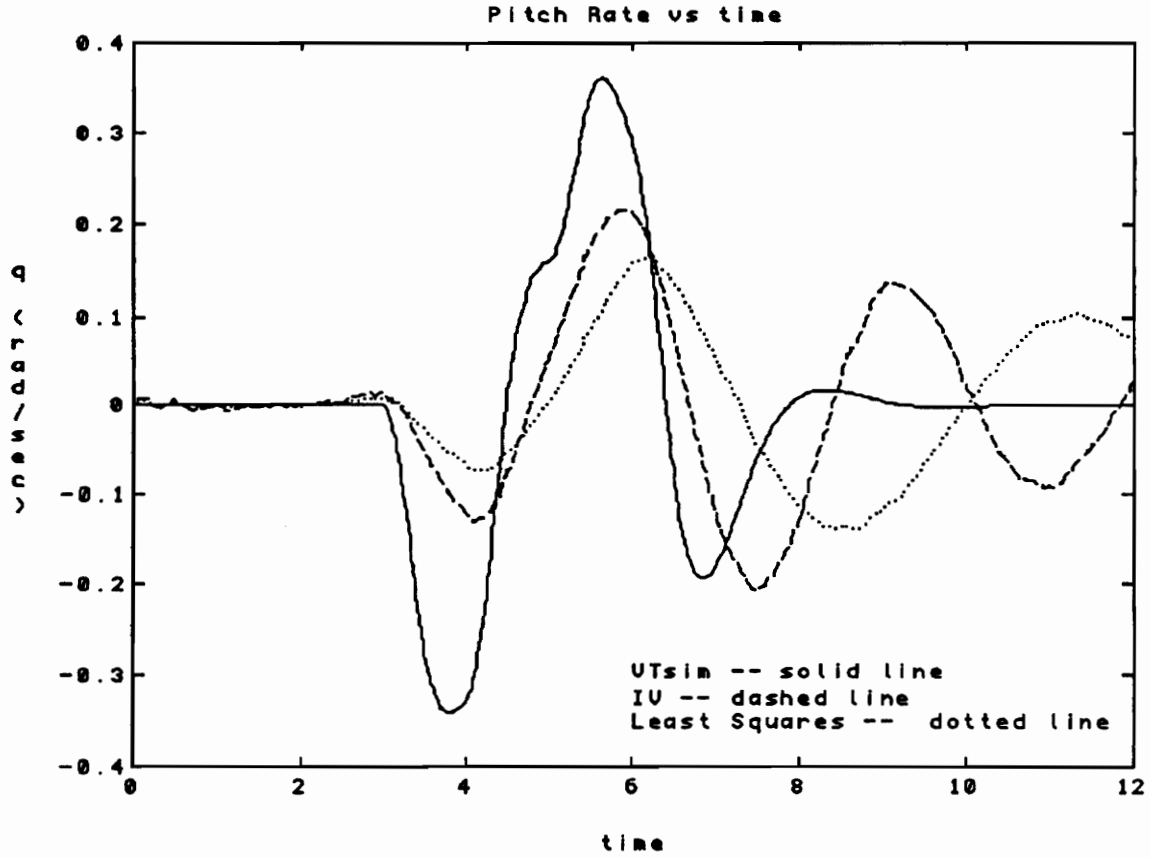

Figure 10: Pitch rate; Case 4

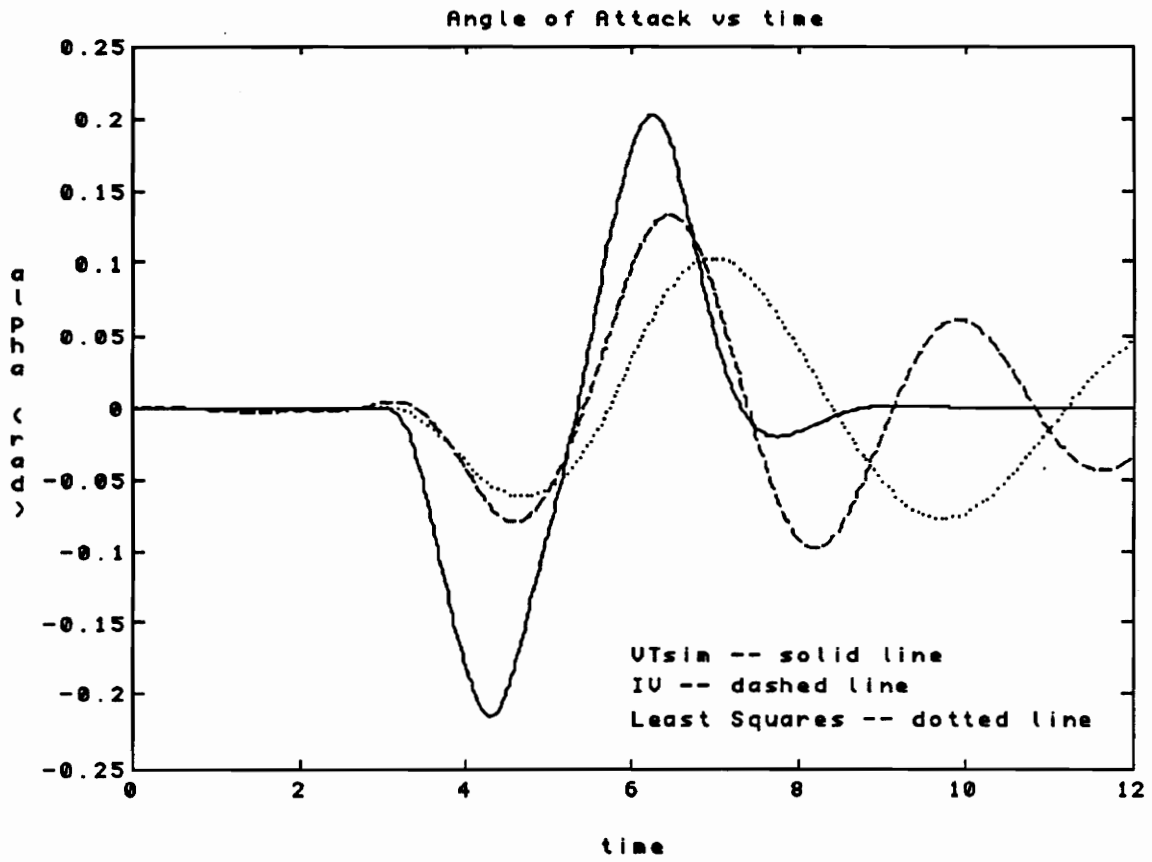

Figure 11: Angle of attack; Case 4

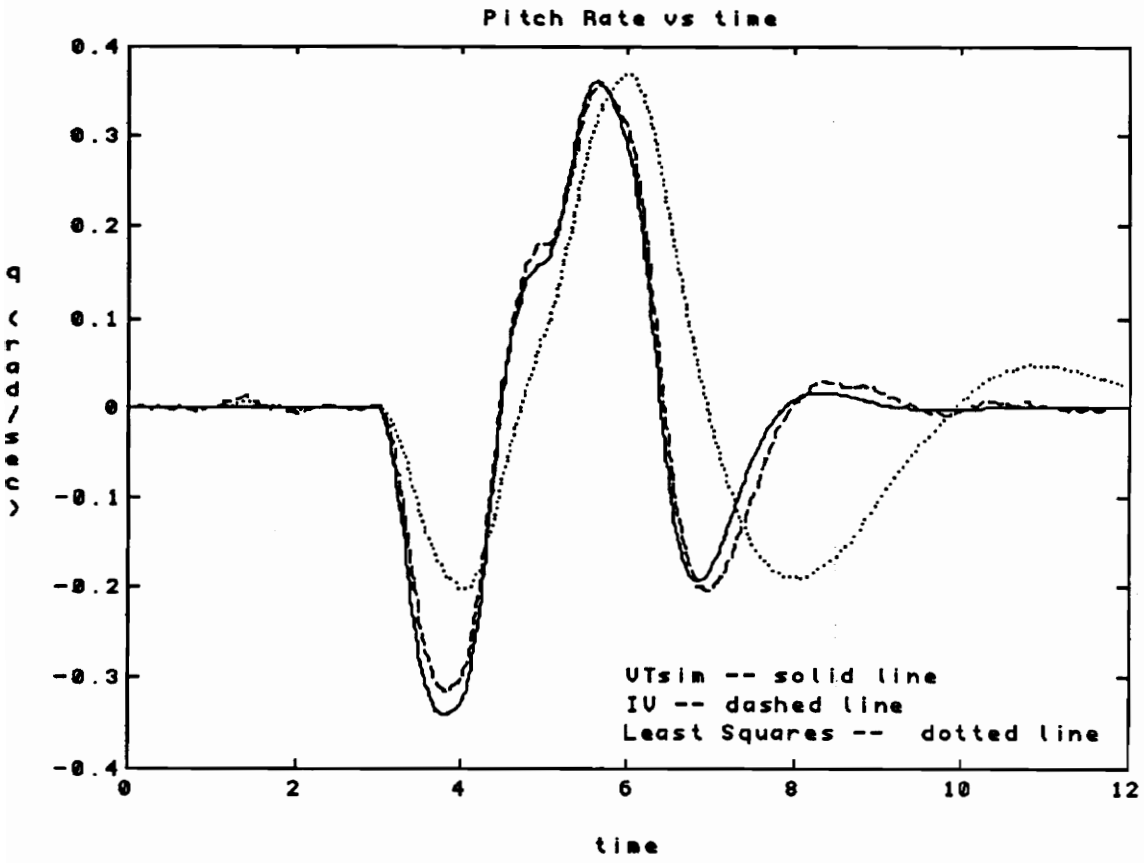

Figure 12: Pitch rate; Case 7

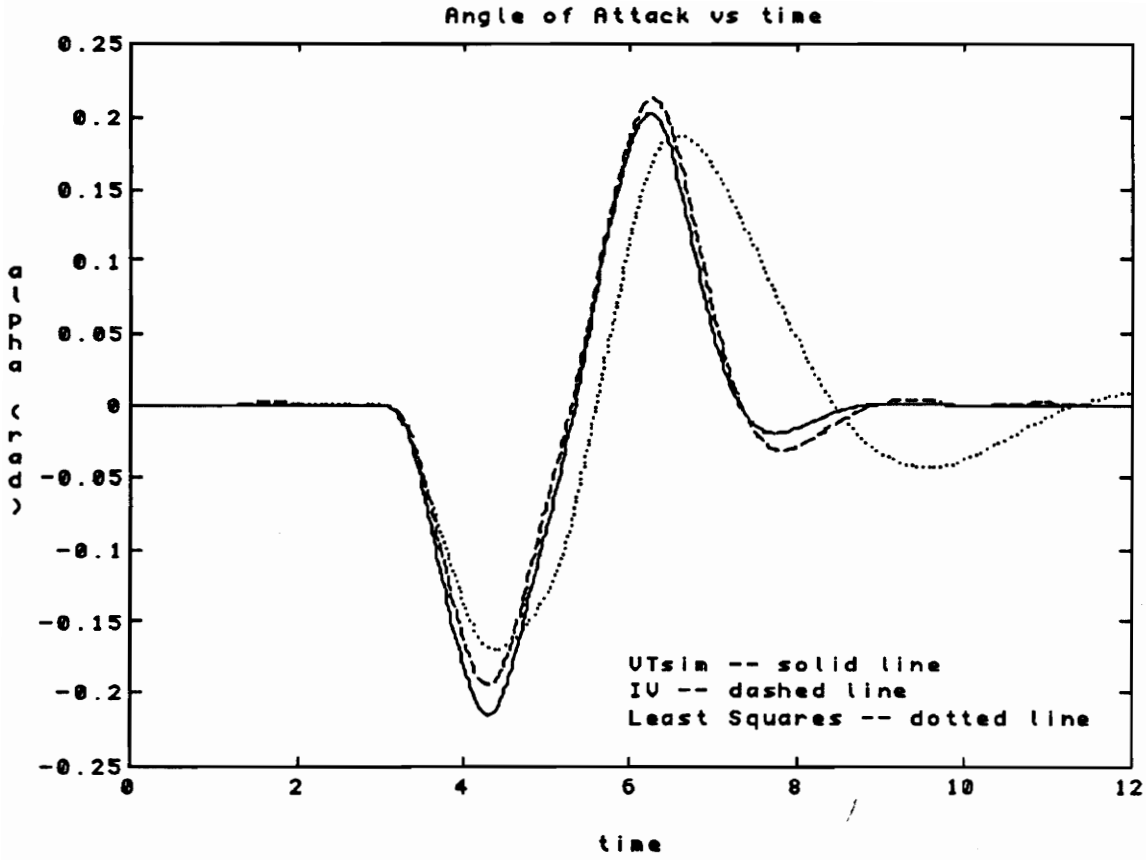

Figure 13: Angle of attack; Case 7

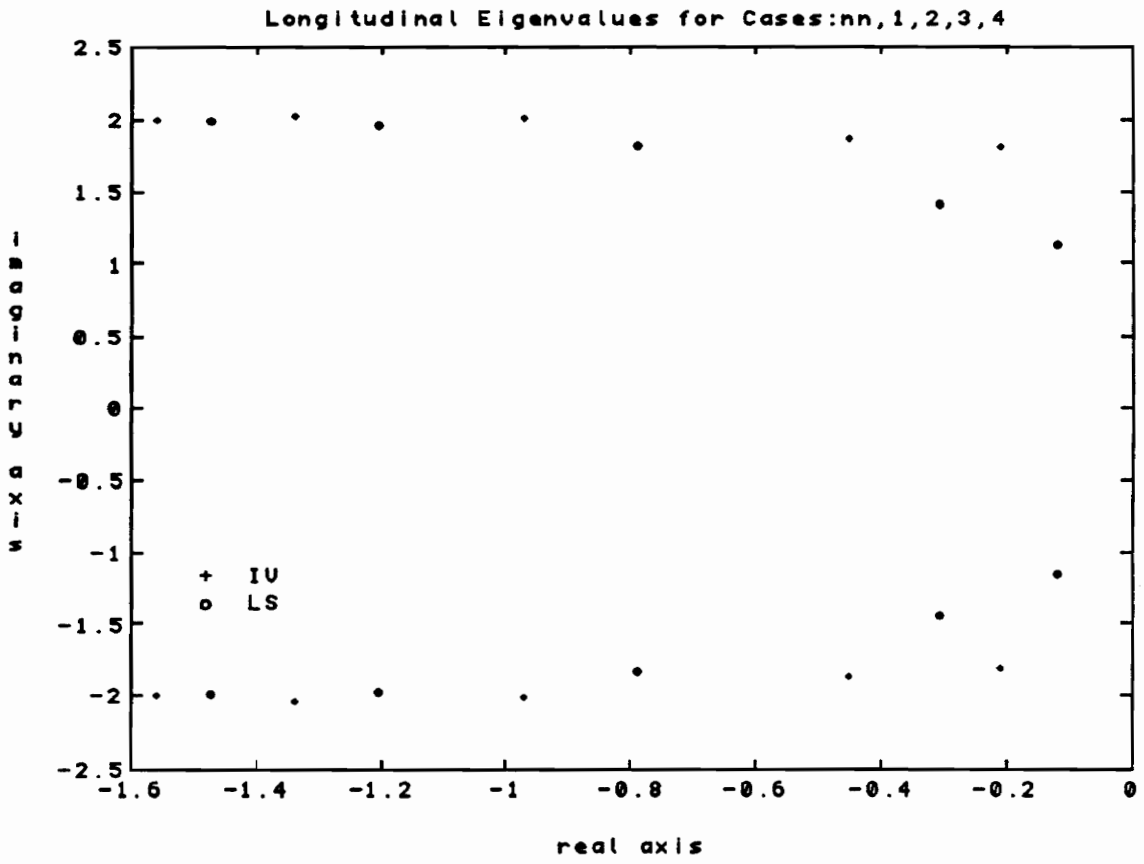

Figure 14: Longitudinal modified A matrix eigenvalue plot for Cases: 0, 1, 2, 3, 4

stable. For example, the IV identified model eigenvalues for Case 0 are -1.56 ± 2.00j and LS identified model eigenvalues are -1.48 ± 1.99j. The Case 4 IV identified model eigenvalues are -0.21 ± 1.58j and LS identified model eigenvalues are -.12 ± 1.20j. For this series, there is not a great difference in the stability change between the two methods.

Figure 15 shows the model eigenvalues of Cases 0, 1, 5, 6, and 7. This comparison is made to reveal the system stability trend when increasing only the state noise value while keeping the input noise, w, at the nominal value of 0.1 rad. The eigenvalue plot shows a distinct difference in the stability change between the two solutions. As can be seen, the real parts of the IV identified model eigenvalues never become greater than -1.28 and the imaginary parts remain at approximately ± 2.00j. The LS identified models, however, become less stable with each successive case; the Case 7 values are -.48 ± 1.10j. Also, the short period damping ratio, ζ, decreases with each successive case for the LS identified model eigenvalues. For example, Case 0 $\zeta = 0.6$ while Case 7 $\zeta = 0.4$. The IV identified model damping ratio decreases from only $\zeta = 0.6$ to $\zeta = .54$.

3.2.1.3 Identified Stability Derivative Comparisons

For the longitudinal axis example, the pitching moment errors are affected similarly for both methods for Cases 1 through 4. For example, the del_Mq values in Figure 16 increase approximately 400% from the Case 1 values of both the IV and LS identified model solutions. However, for Cases 1, 5, 6, and 7, the IV identified model errors are basically unaffected while the trend for the LS identified model errors reveals an increase of up to 220% from the LS identified model value of Case 1.

The lift force stability derivative errors are almost all negligible for the IV identified model while they are affected greatly in the LS identified model. For example, the del_Lq

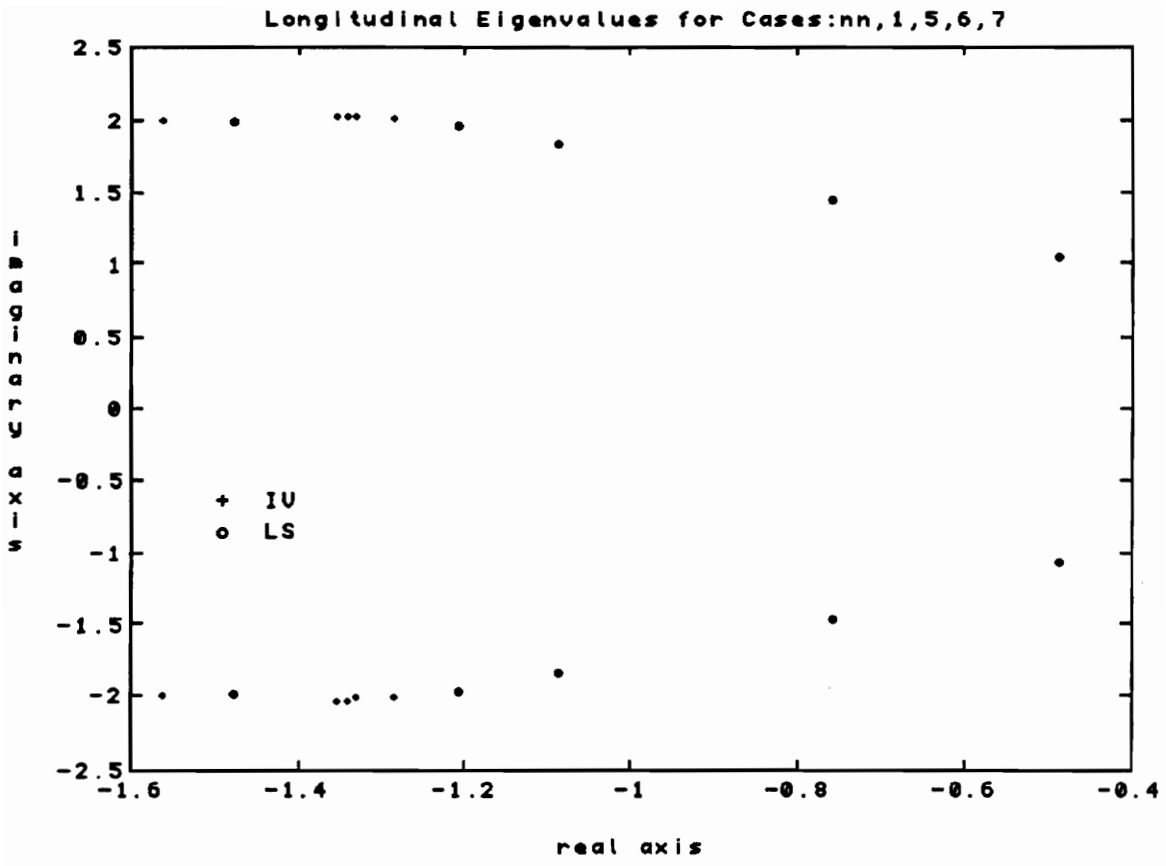

Figure 15: Longitudinal modified A matrix eigenvalue plot for Cases: 0, 1, 5, 6, 7

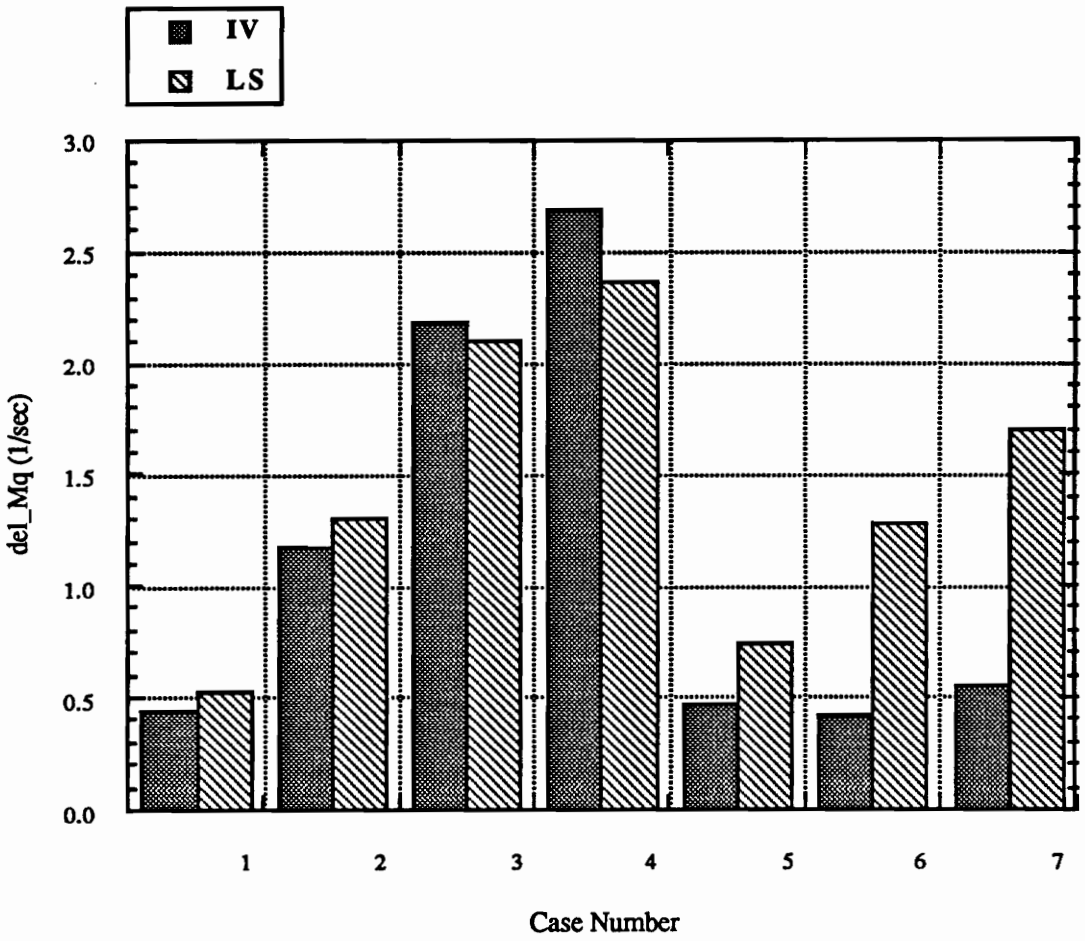

Figure 16: Absolute value of change in Mq from zero noise identified error value

values shown in Figure 17 for Cases 1 through 4 reveal an increase of over 1000% for the LS identified model while the IV identified model error remains insignificant. For Cases 1, 5, 6, and 7, the IV identified model error again remains low while the LS identified model error increases to well over 2000% from the Case 1 value.

3.2.2 Lateral/directional Example

3.2.2.1 Time Response Comparisons

The time responses for the lateral/directional example show dramatic differences between the IV and LS techniques, especially for Cases 5, 6, and 7. As will be shown, the IV method produces time responses that follow the VTSim responses closely even when the input noise is extremely high. The LS method produces responses that appear marginally stable or perhaps even unstable. This result will be discussed in the next section. The lateral/directional axis example further supports the expected trend of the IV method with the input noise and the trend of the LS method with both state and input noise.

Figures 18, 19 and 20 show p, r, and $\Delta\beta$ when the identified error model with zero noise is added to the predicted simulation state-space model. Similar to the longitudinal case, both the IV and LS solutions follow the VTSim output closely. However, when noise is added to the system, differences in the IV and LS results appear. For example, Figures 21, 22 and 23 show the results of Case 1. Both the IV and LS identified model responses deviate somewhat from the VTSim responses, but the LS identified model responses exhibit the largest variations. Case 4 Figures 24, 25 and 26, however, reveal larger deviations by both solutions, with the LS identified model response deteriorating much more than the IV identified model response, especially for roll rate, p, and sideslip, β.

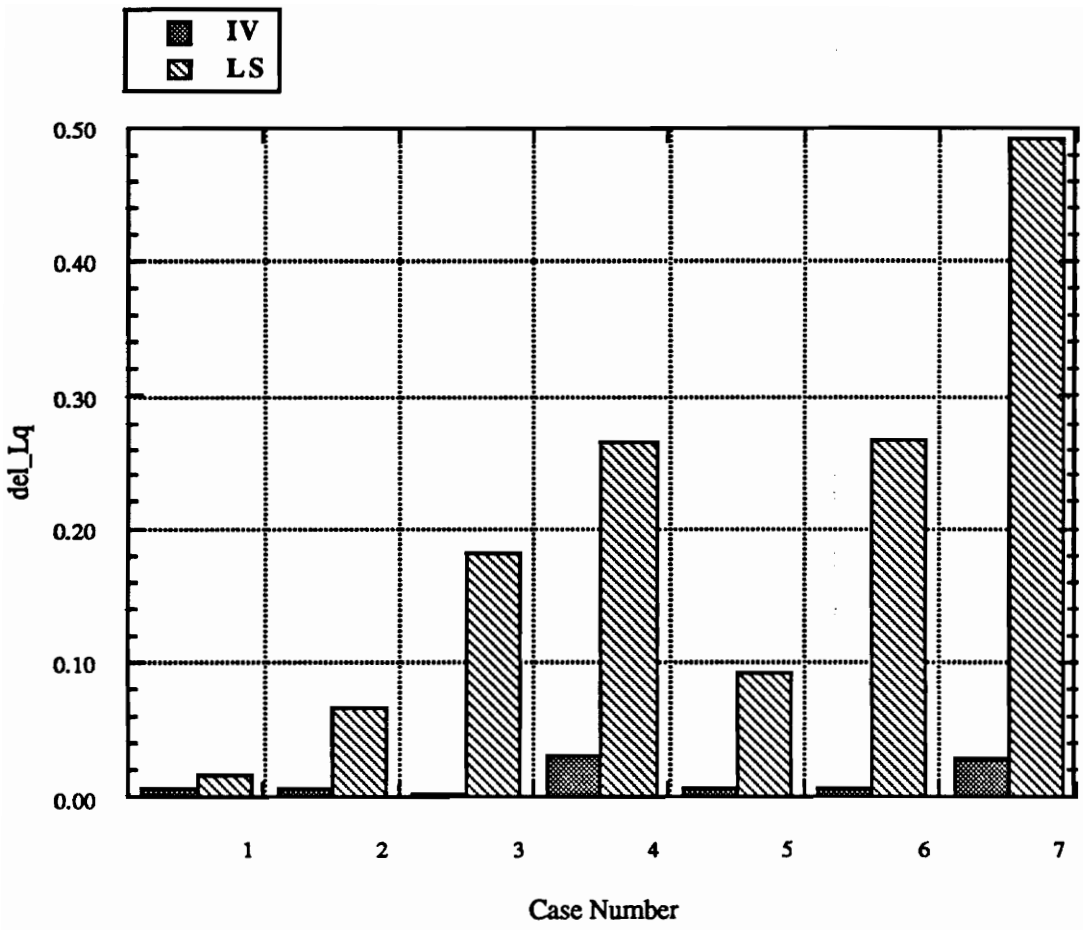

Figure 17: Absolute value of change in Lq from zero noise identified error value

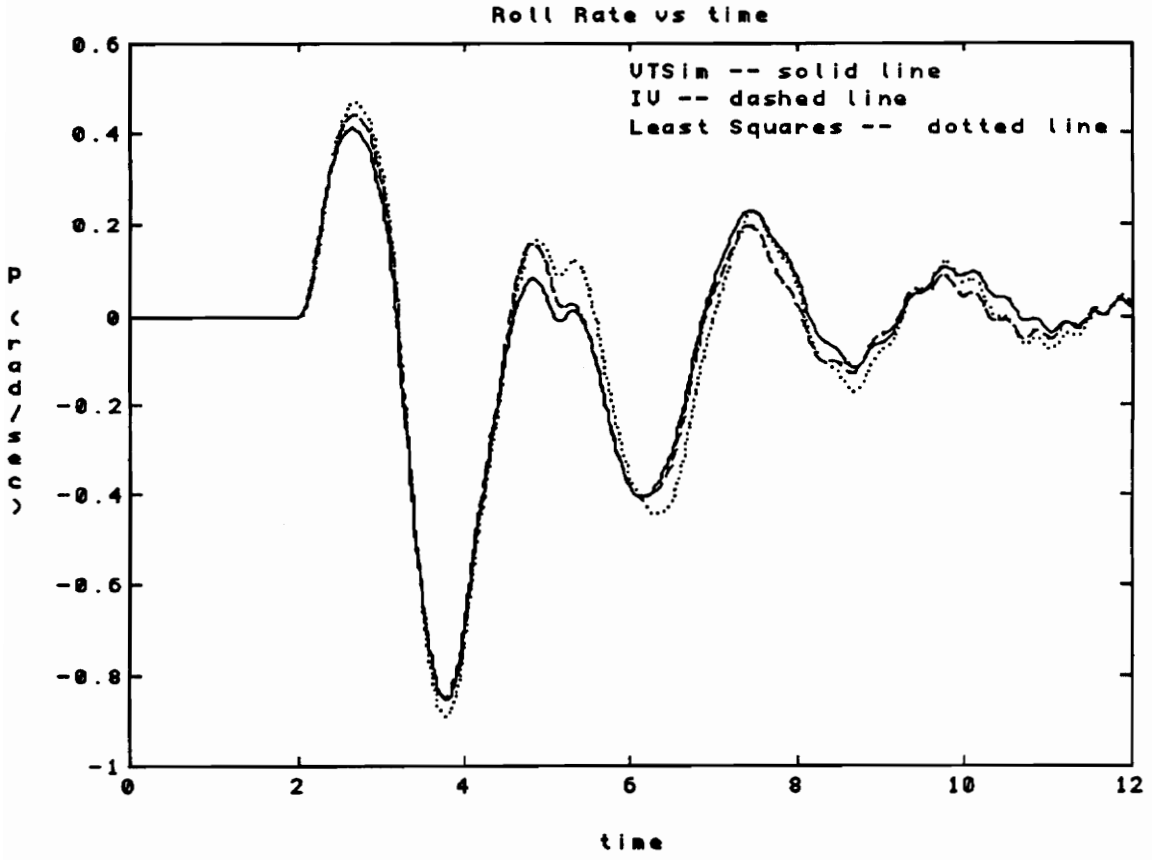

Figure 18: Roll rate without added noise; Case 0

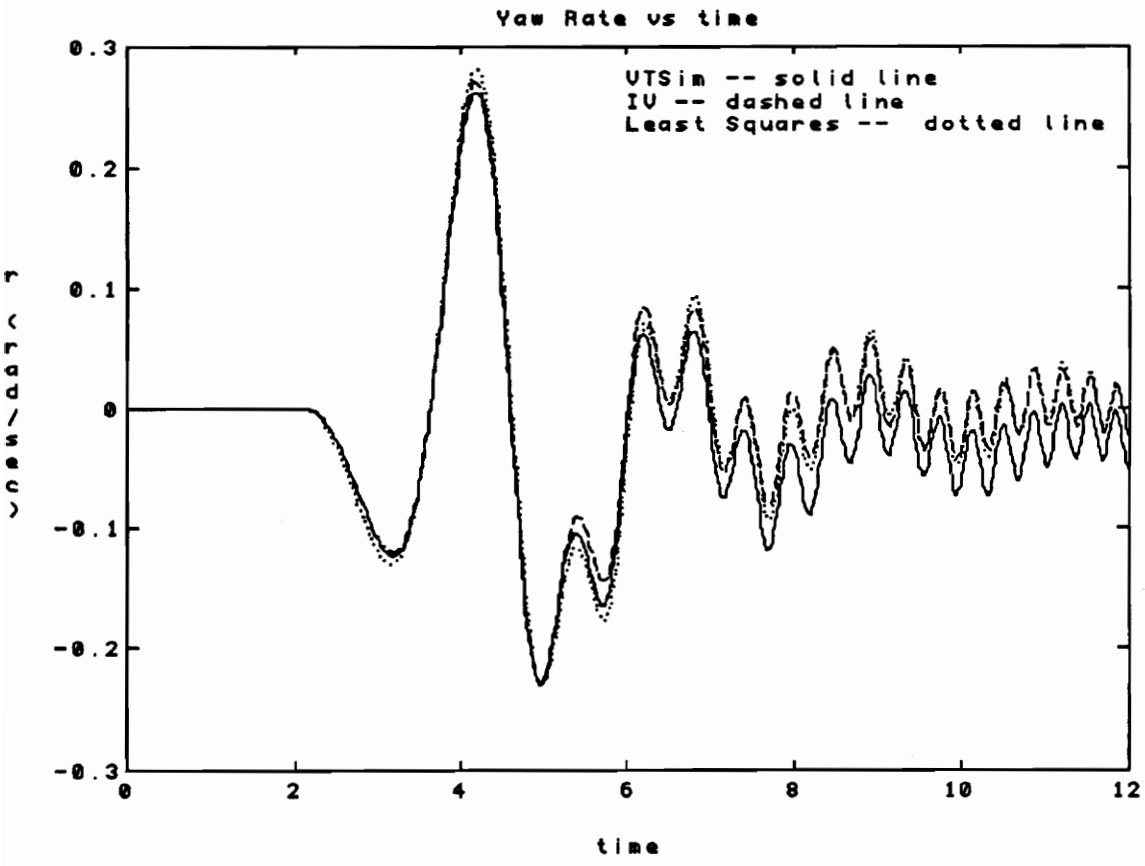

Figure 19: Yaw rate without added noise; Case 0

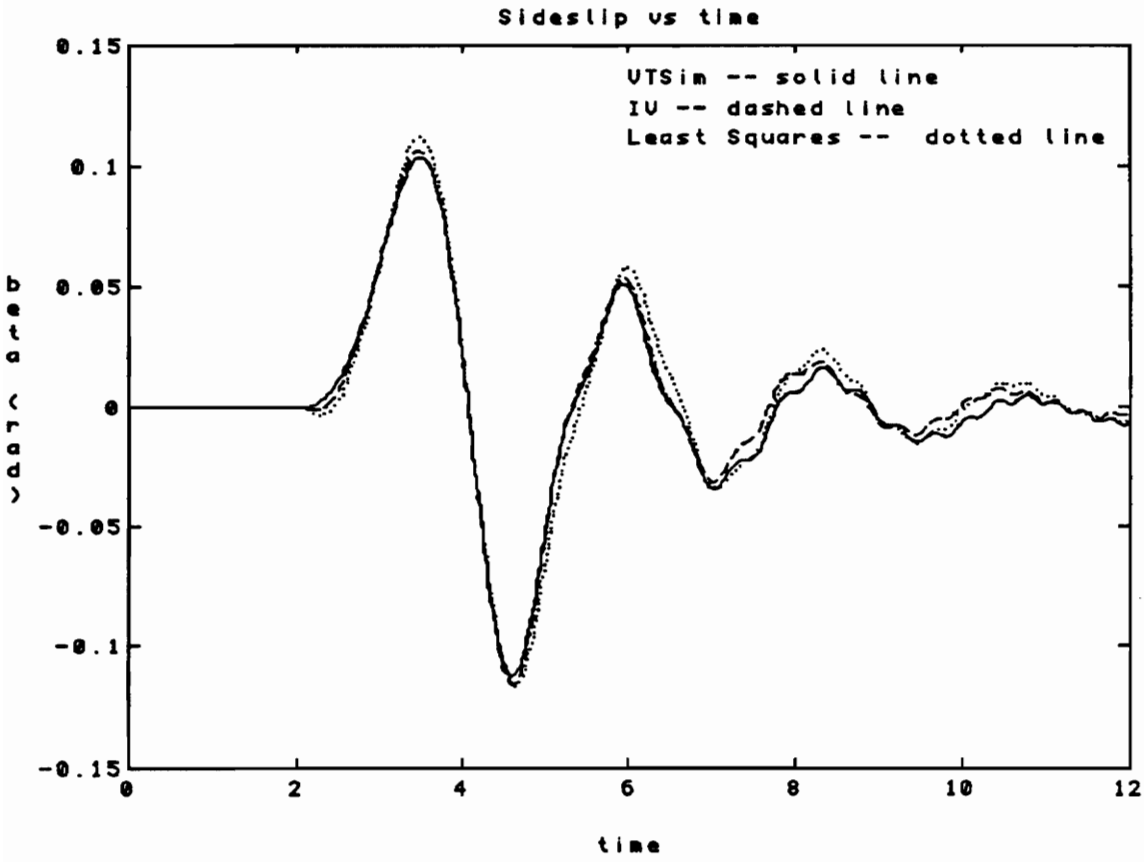

Figure 20 : Sideslip without added noise; Case 0

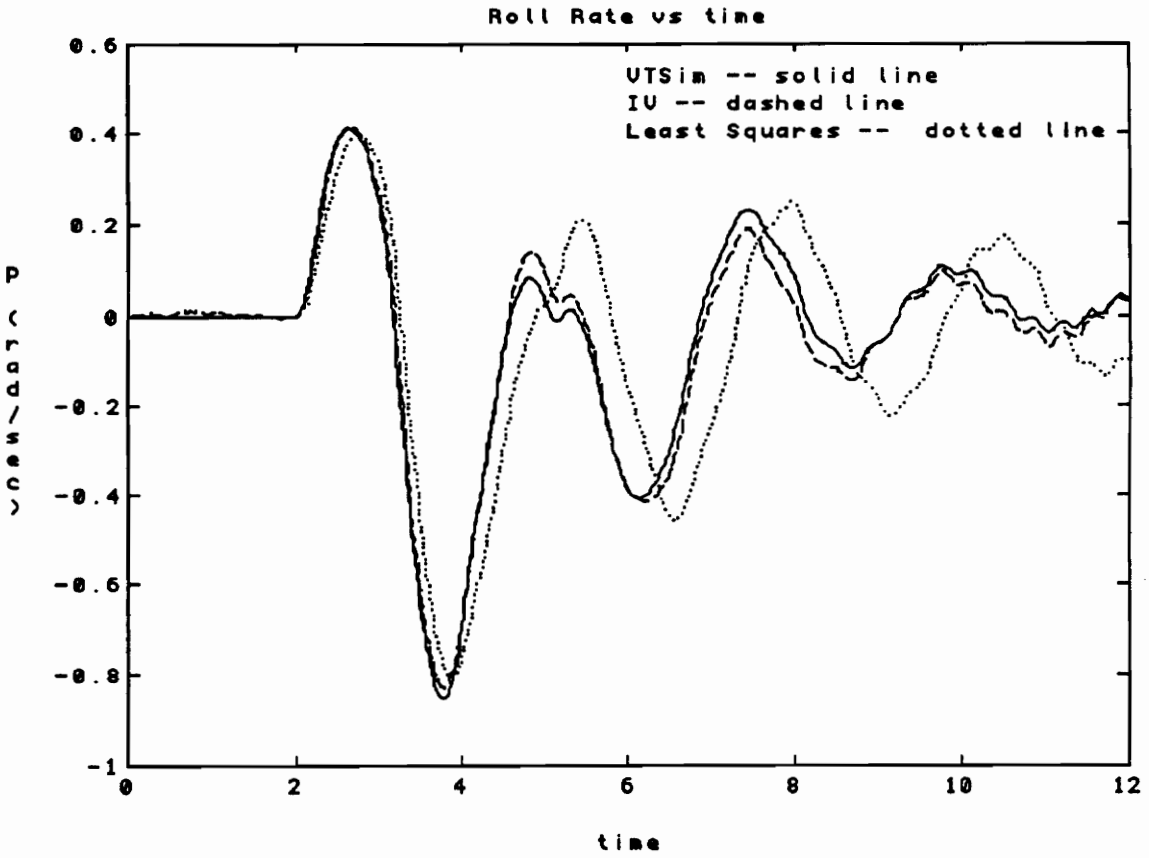

Figure 21: Roll rate; Case 1

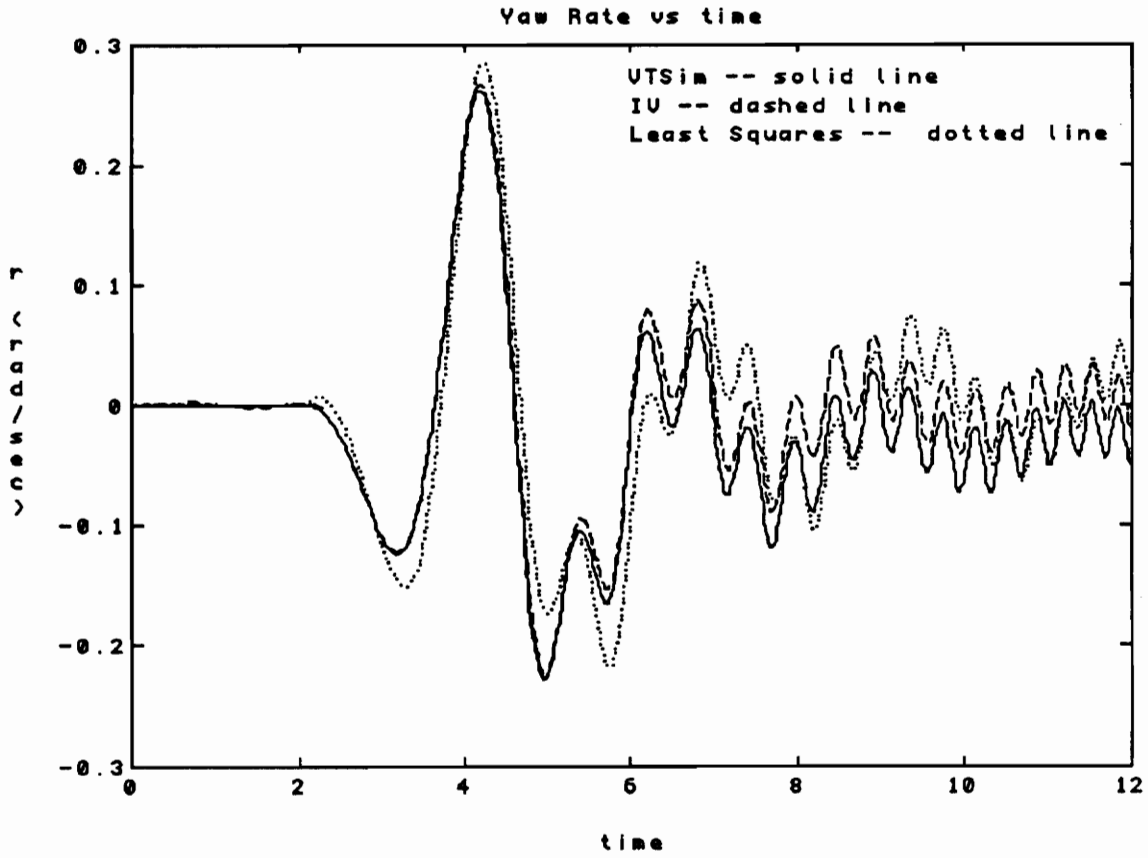

Figure 22: Yaw rate; Case 1

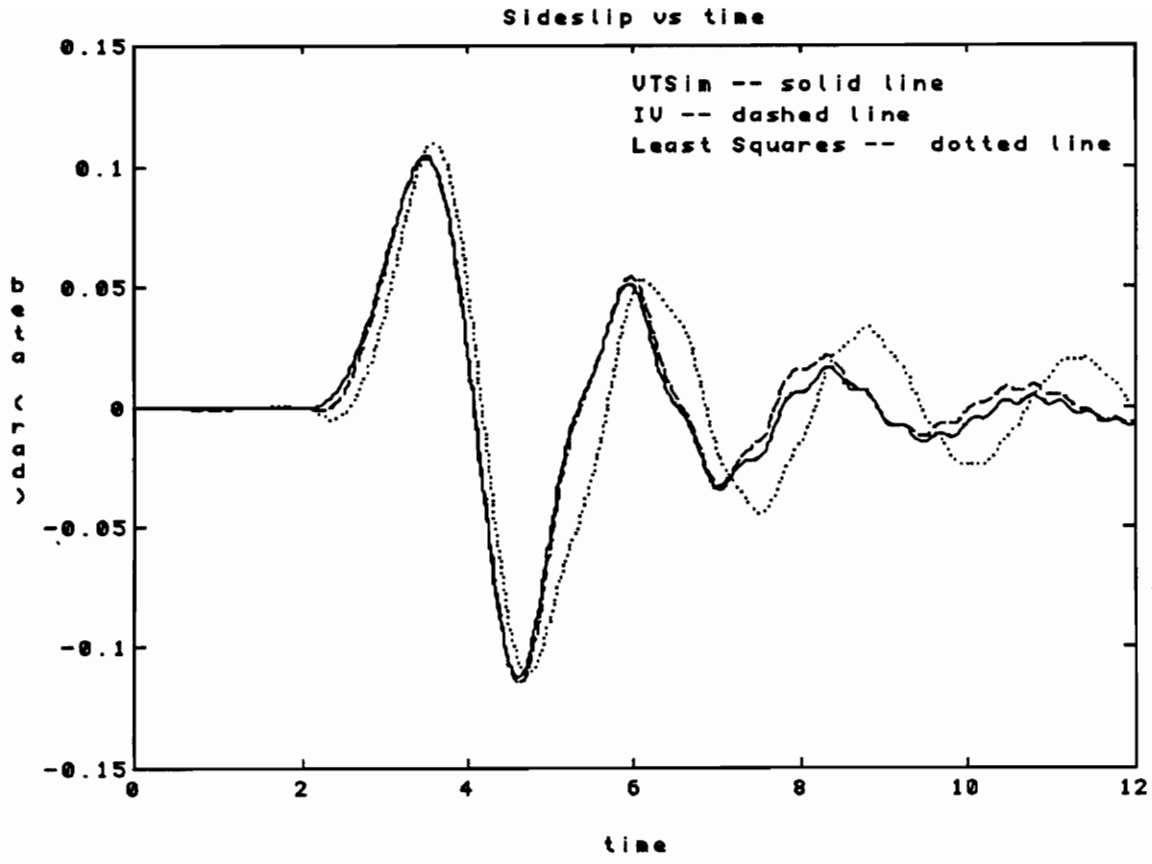

Figure 23: Sideslip; Case 1

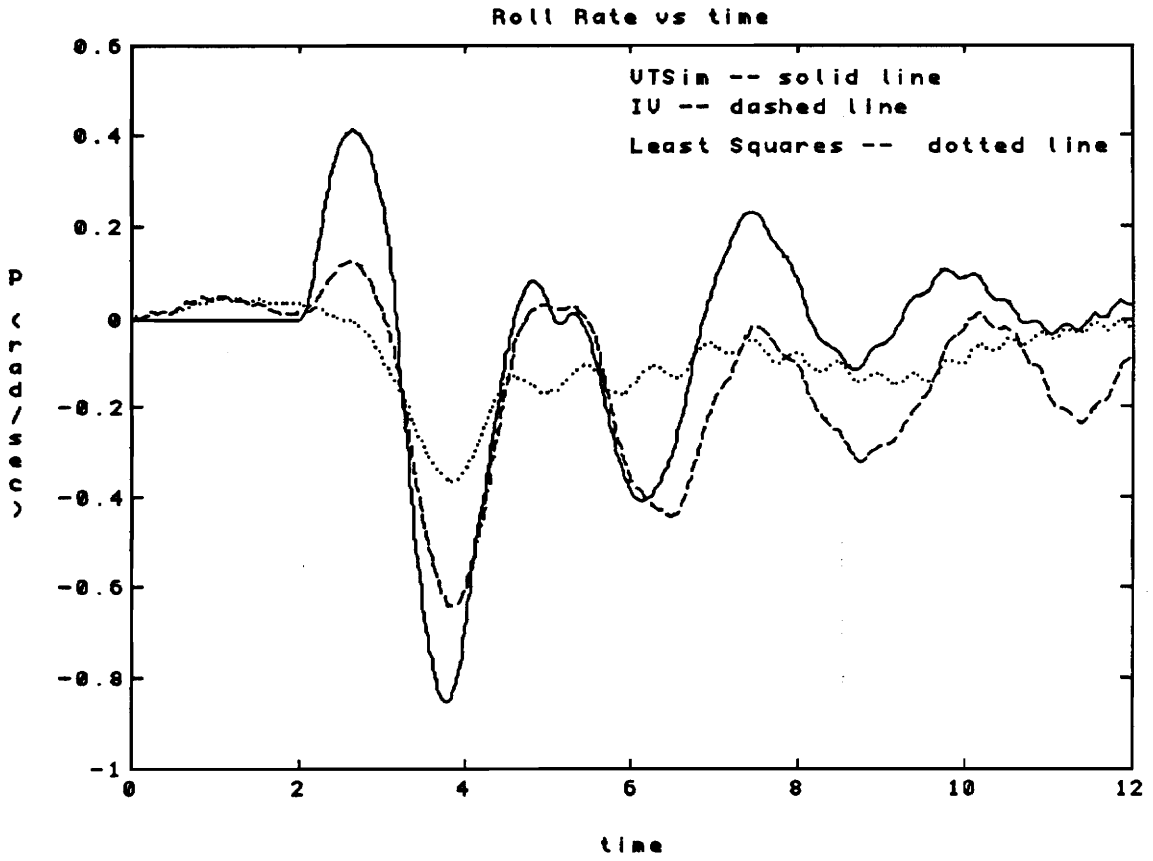

Figure 24: Roll rate; Case 4

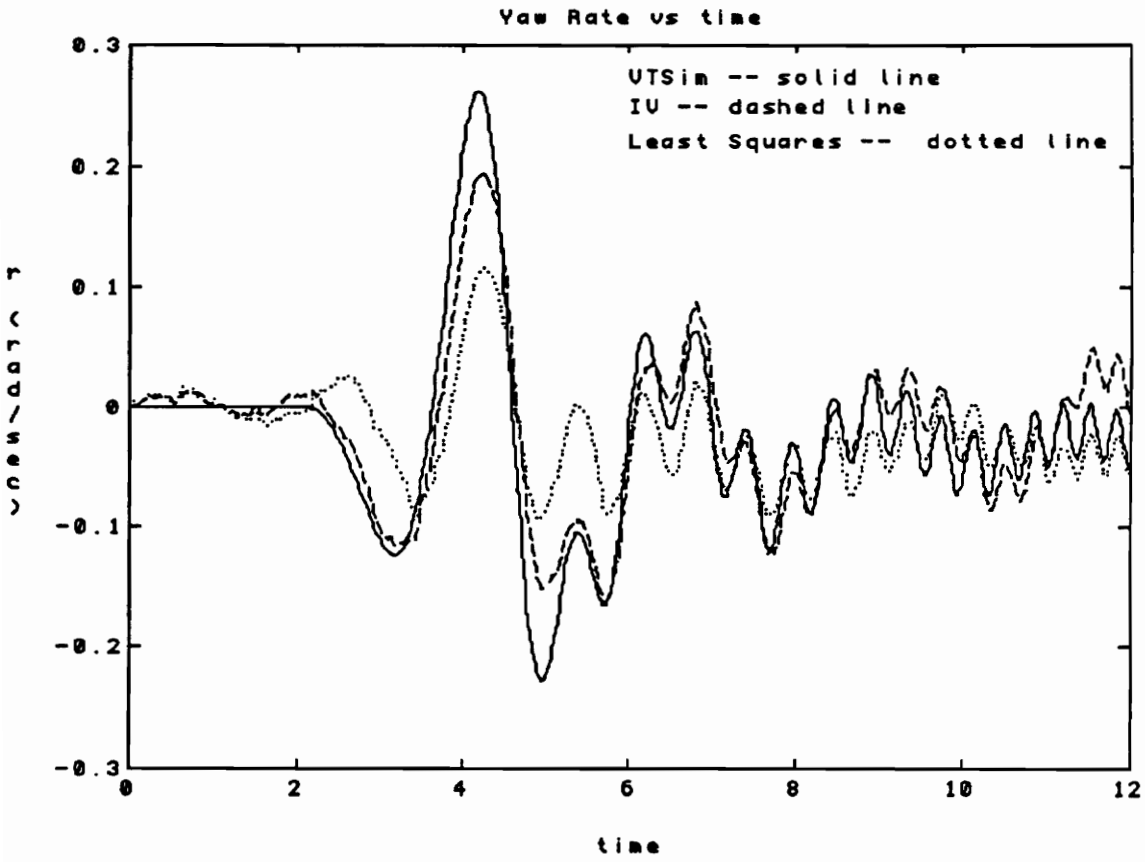

Figure 25: Yaw rate; Case 4

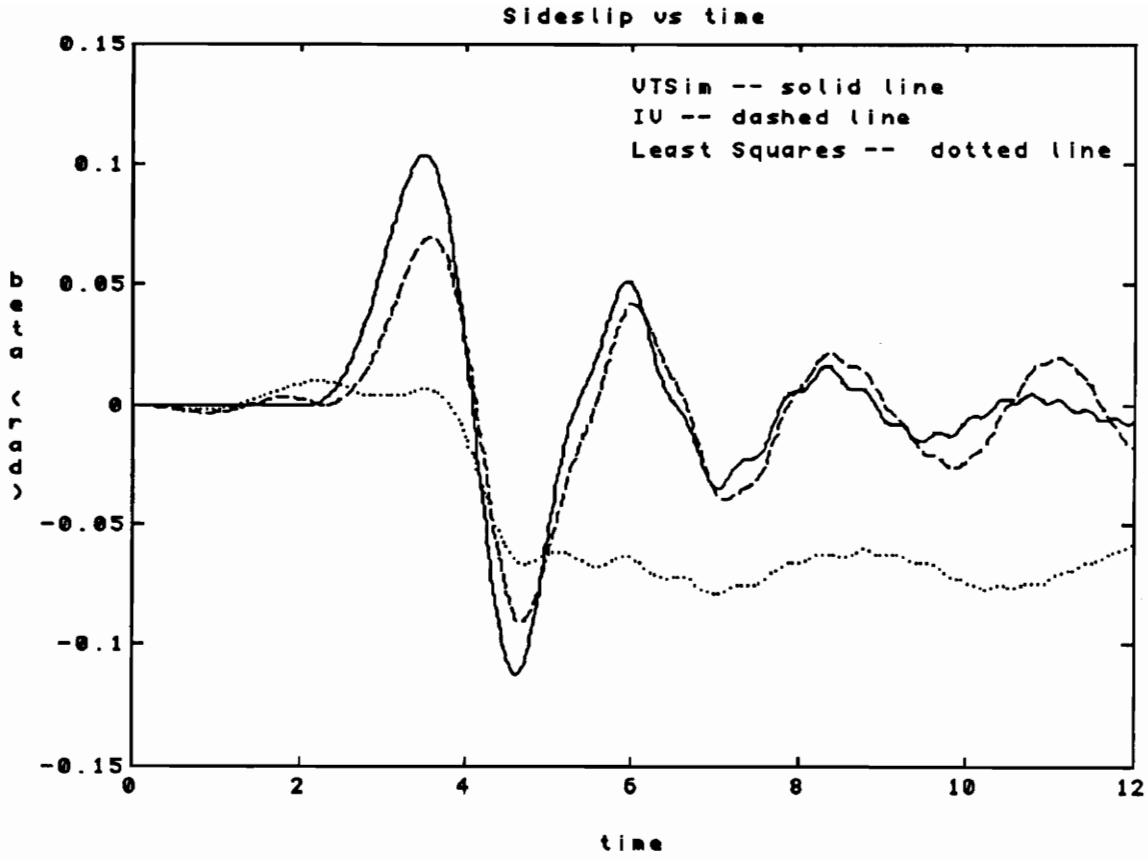

Figure 26: Sideslip; Case 4

Finally, Case 7 Figures 27, 28 and 29 show the vast difference between the two method results when the input noise is held relatively small and the state noise is large. For all three states, the IV method produces results similar to the VTSim responses. The LS identified model solution, on the contrary, produces a model that is seemingly only marginally stable or even unstable. This destabilizing behavior will be confirmed by the eigenvalue comparison shown in the next section. Case 7 reveals that the LS method results are greatly affected by the state noise whereas the IV solution results are relatively unaffected by the high state noise values.

3.2.2.2 Eigenvalue Comparisons

Figure 30 shows the model eigenvalues for Cases 0, 1, 2, 3, and 4. As in the longitudinal axis example, this comparison is made to reveal the system stability trend when increasing both the state and input noise values by the same factor (see Table 1). With each increase in noise level, both the IV and LS identified models become less stable. For the roll mode eigenvalues, the LS identified model is slightly less stable than the IV identified model. For example, the Case 0 IV identified model eigenvalue is -1.57 and the LS identified model eigenvalue is -1.36 while the Case 4 IV identified model eigenvalue is -0.22 and the LS identified model eigenvalue is -.09. For the "Dutch Roll" mode, the LS identified models become less stable and more lightly damped than the IV identified models. For example, the IV identified model eigenvalues vary from $-.41 \pm 2.70j$ for Case 0 to $-.23 \pm 2.50j$ for Case 4, while the LS identified model eigenvalues vary from $-.35 \pm 2.70j$ for Case 0 to $-.01 \pm 1.30j$ for Case 4. Also, the damping ratio, ζ, decreases from .13 to .01 for the LS method from Case 0 to Case 4, but only from .15 to .10 for the IV method from Case 0 to Case 4.

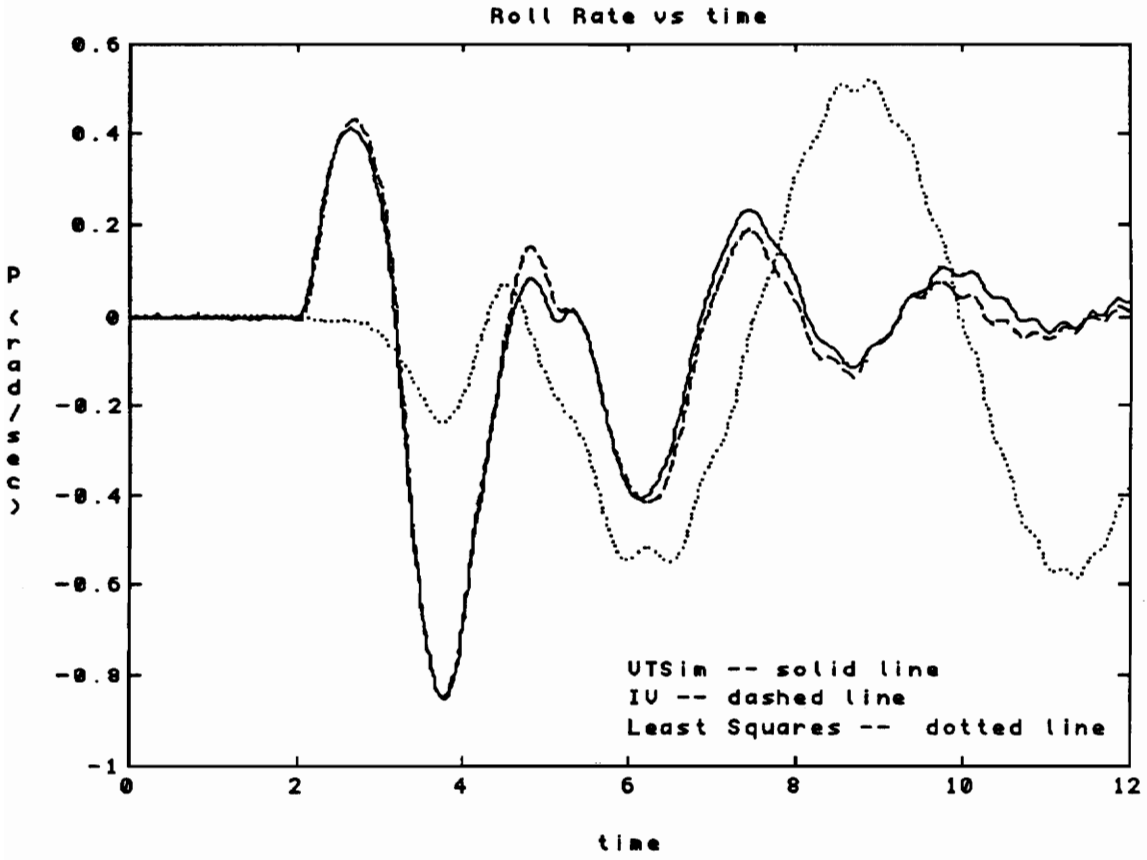

Figure 27: Roll rate; Case 7

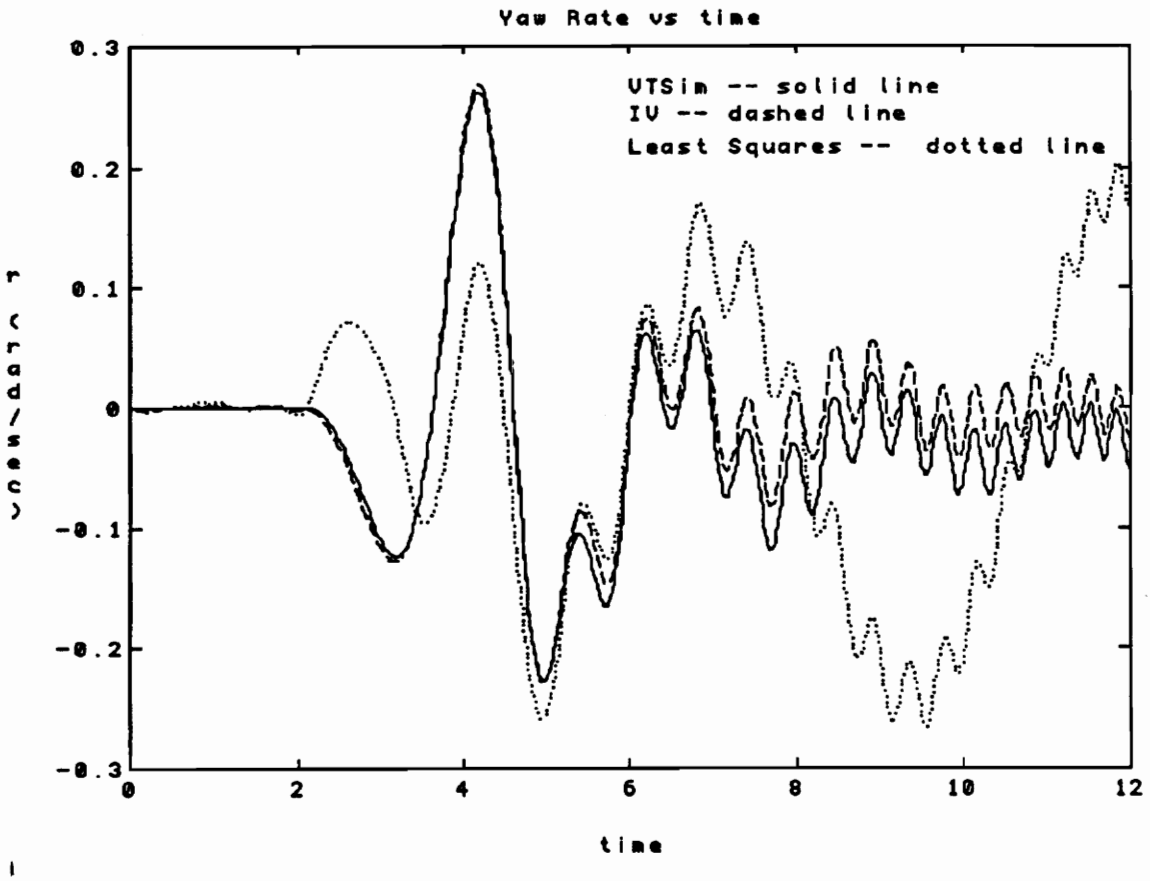

Figure 28: Yaw rate; Case 7

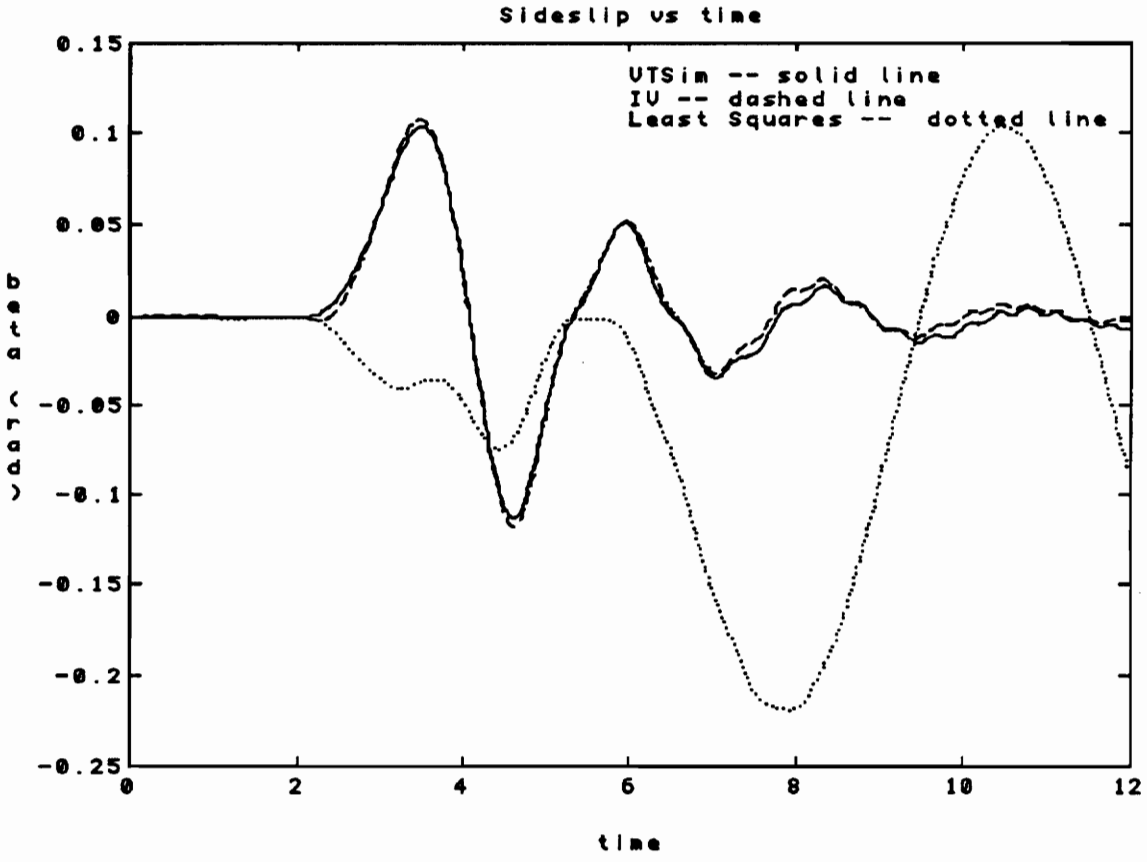

Figure 29: Sideslip; Case 7

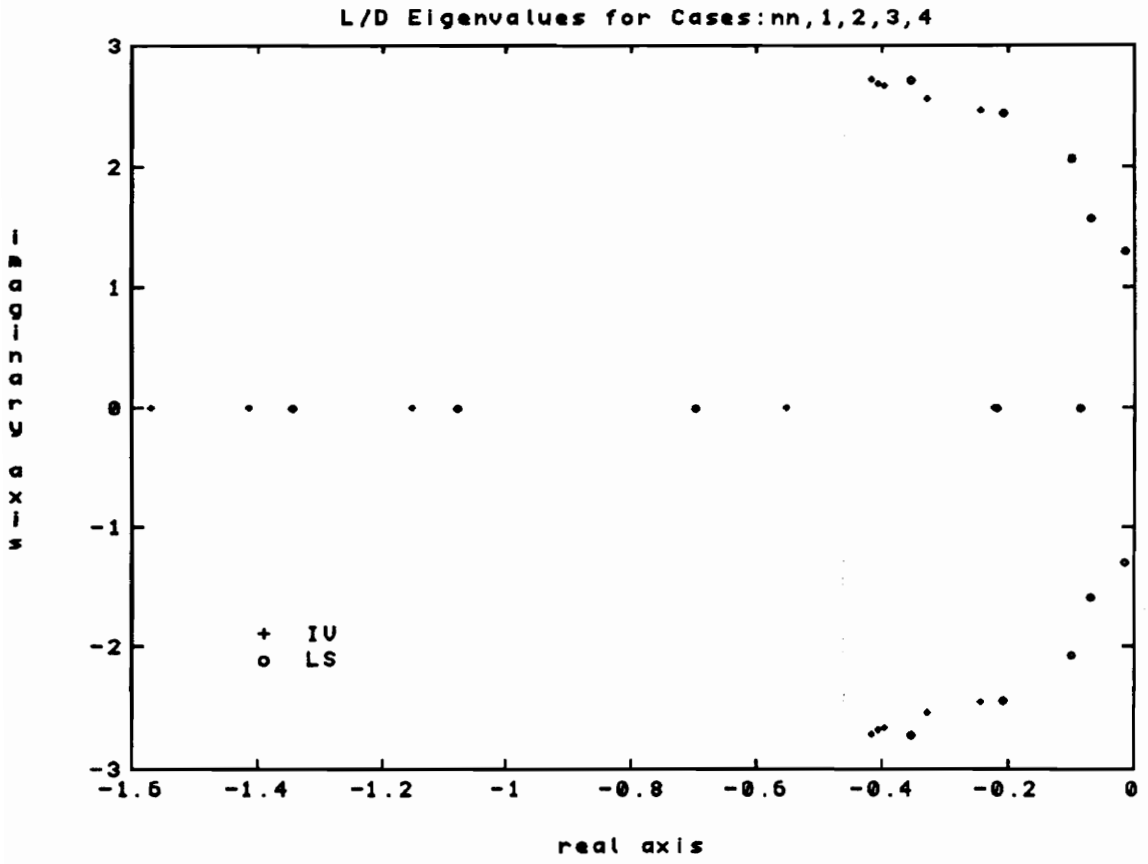

Figure 30: Lateral/directional modified A matrix eigenvalue plot for Cases: 0, 1, 2, 3, 4

Figure 31 shows the model eigenvalues for Cases 0, 1, 5, 6, and 7. From Figure 31, one can see the difference in the stability trend between the two solutions. The rolling convergence IV identified model eigenvalue never become greater than -1.40 while the LS identified models become less stable with each successive case; the Case 7 eigenvalue is -.21. For the "Dutch Roll" mode, the IV identified model eigenvalues remain relatively unchanged at approximately $-.42 \pm 2.70j$ while the LS identified model actually becomes unstable for Case 7 where the eigenvalues are $+.01 \pm 1.30j$. Also, the damping ratio, ζ, decreases from .13 to -.01 for the LS solution from Case 0 to Case 7, but remains about .15 for the IV solution from Case 0 to Case 7. This case shows that the LS method does produce more lightly damped models than the IV method.

3.2.2.3 Identified Stability Derivative Comparisons

For the lateral/directional axis example, the rolling moment derivative errors are affected similarly for both methods in Cases 1 through 4, although IV identified model errors produced are typically smaller. For example, in Figure 32 the del_Lp IV identified model value increases up to a larger percentage (770%) from its Case 1 value than does the LS identified model value (180%), but each IV identified model value is smaller than the LS identified model value. For Cases 1, 5, 6, and 7, the IV identified model errors are basically unaffected while the LS identified model errors are relatively high. Figure 32 shows an increase of up to 190% in the LS identified model values for del_Lp, while the IV identified model values remain small. The noticeable exception of this rolling moment error trend is for Case 7 of stability derivative error del_Ldel_r shown in Figure 33 where the IV solution yields a larger error than the LS solution.

For the yawing moment derivatives, most cases show large LS identified model

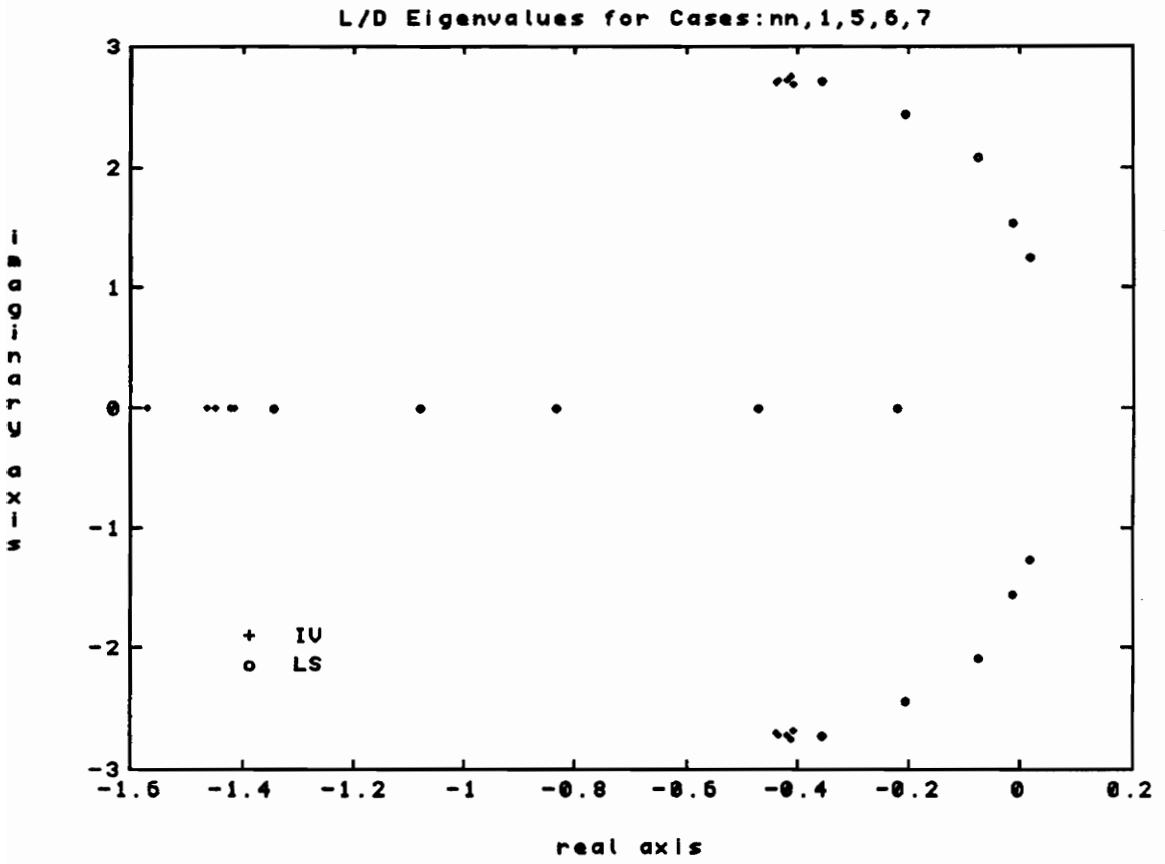

Figure 31: Lateral/directional modified A matrix eigenvalue plot for Cases: 0, 1, 5, 6, 7

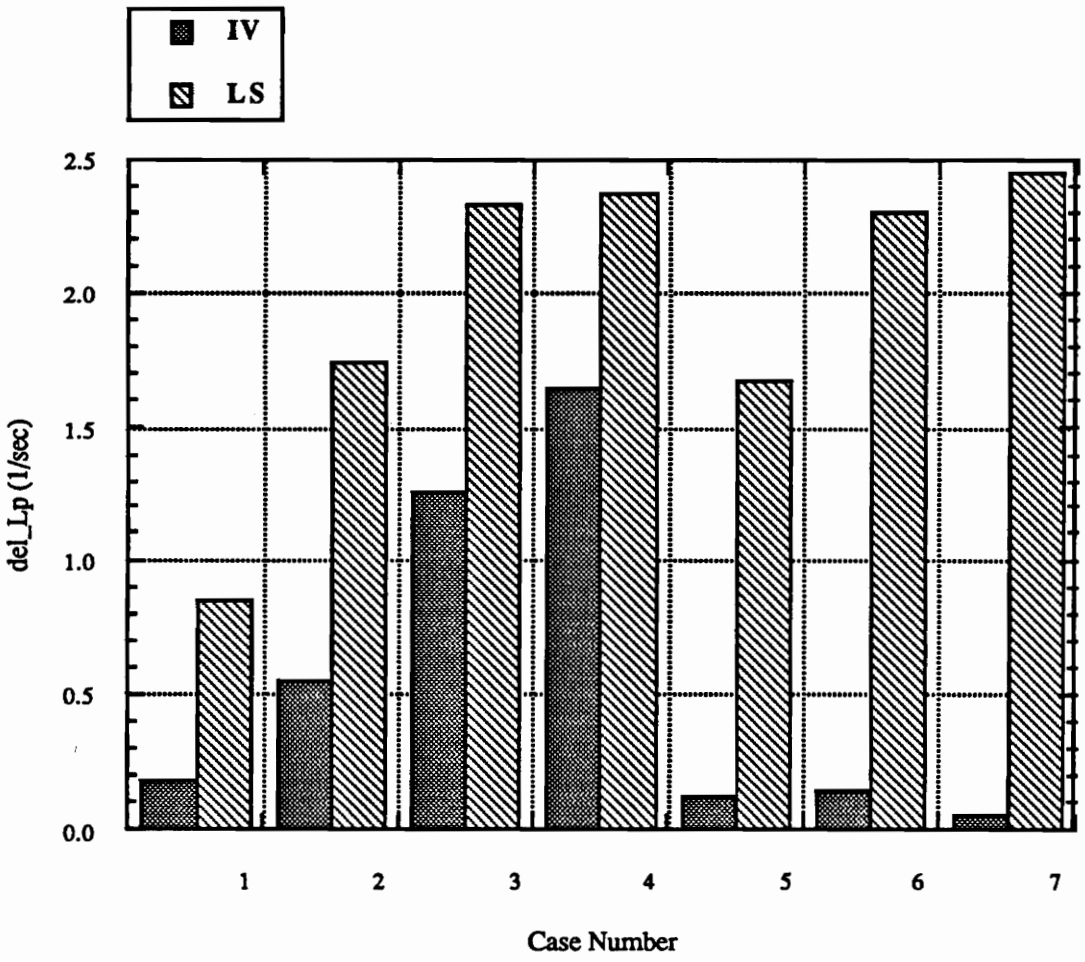

Figure 32: Absolute value of change in Lp from zero noise identified error value

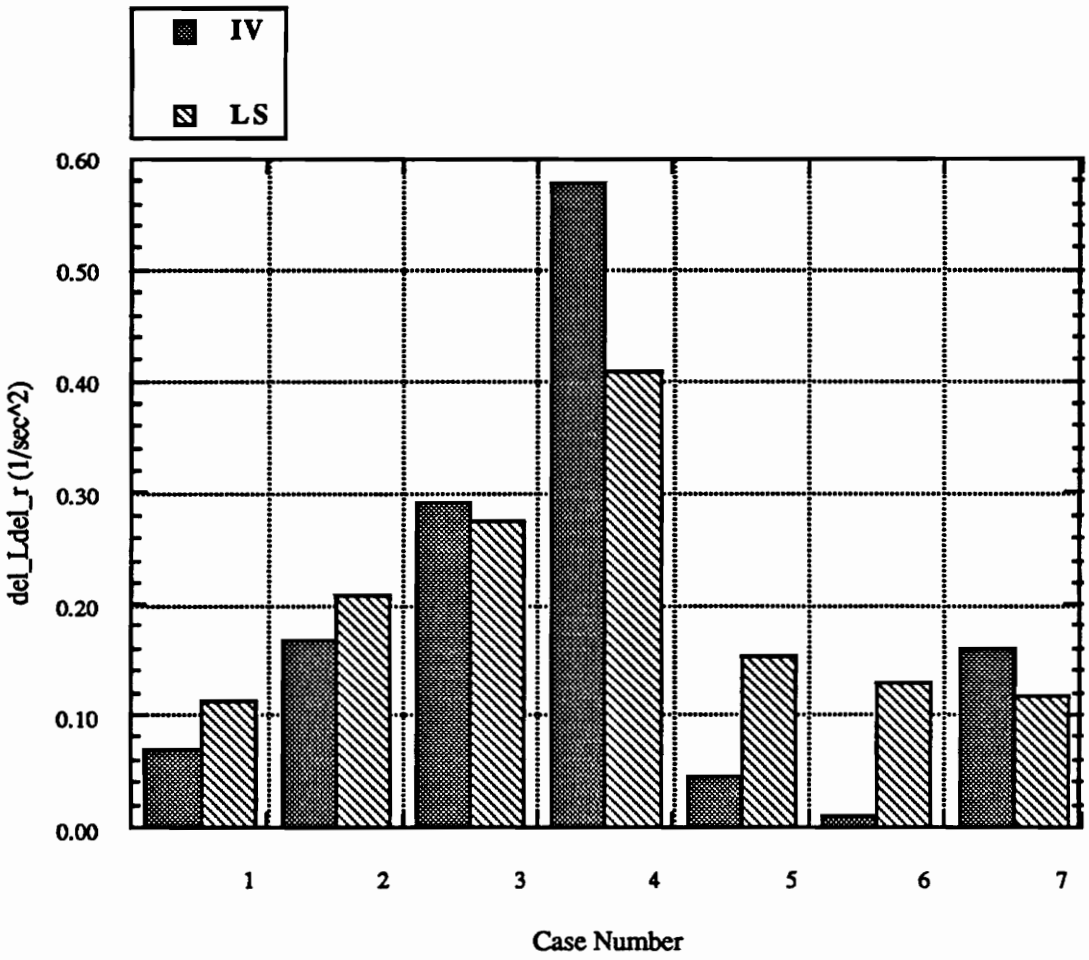

Figure 33: Absolute value of change in L_delta_r from zero noise identified error value

errors and relatively small IV identified model errors. Only Cases 1 through 4 of the derivatives del_Nr and del_Ndel_r have large errors for the IV identified model solution. For example, for the del_Np results shown in Figure 34, the values for Cases 1 through 4 reveal an increase in error of up to 160% from the Case 1 value for the LS identified model. On the contrary, the IV identified model error remains very low. For Cases 1, 5, 6, and 7, the IV identified model error again remains low but the LS identified model error increases over 200% from the Case 1 value.

The del_Nr values, shown in Figure 35, increase up to 800% from the Case 1 value for the IV identified model for Cases 1 through 4. The LS identified model error for Case 2 is about 200% of the Case 1 value. However, Case 3 and 4 errors increase only slightly from the Case 1 error. For Cases 1, 5, 6, the trend reveals an increase of up to 130% in error using the LS identified model. The Case 7 LS identified model error, however, unexpectedly decreases to below its Case 1 value. The del_Nr IV identified model values remain very low for Cases 1, 5, 6, and 7.

The side force derivative errors increase in both case trends 1-4 and 1, 5, 6, and 7 for the LS identified model but they are typically significant only in Cases 1 through 4 for the IV identified model. For example, for the del_Ybeta derivative shown in Figure 36, the values for Cases 1 through 4 show an increase in error of up to 210% form the Case 1 value for the LS identified model. On the other hand, the IV identified model error increases somewhat but remains low compared to the LS results. For Cases 1, 5, 6, and 7, the IV identified model error again remains low while the LS identified model error increases over 200% from the Case 1 value.

The results shown for the longitudinal axis and lateral/directional axis examples reveal that both state and input noise affect identified parameters. Also, the eigenvalue comparisons reveal that noise can actually lead to unstable models, particularly for the LS identified solution. Finally, the case studies confirm the theoretical prediction that the IV

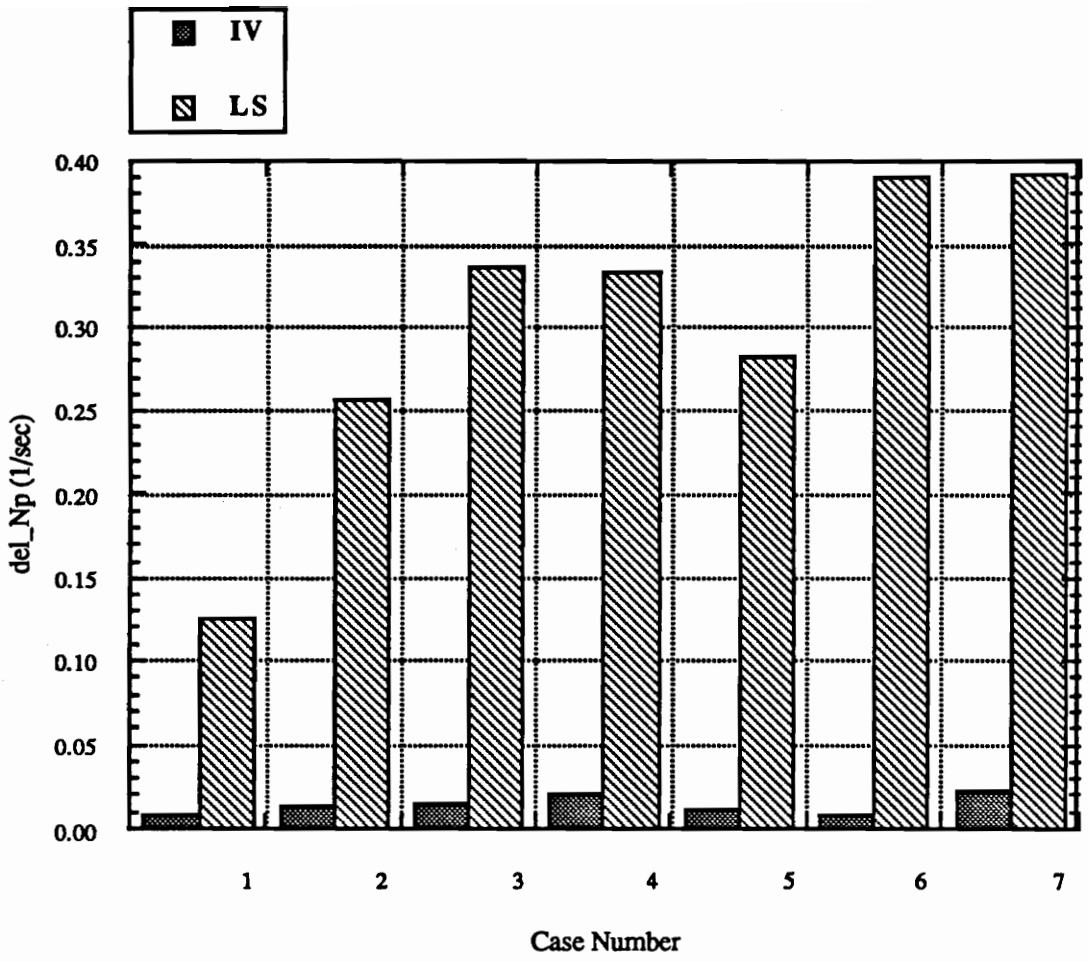

Figure 34: Absolute value of change in Np from zero noise identified error value

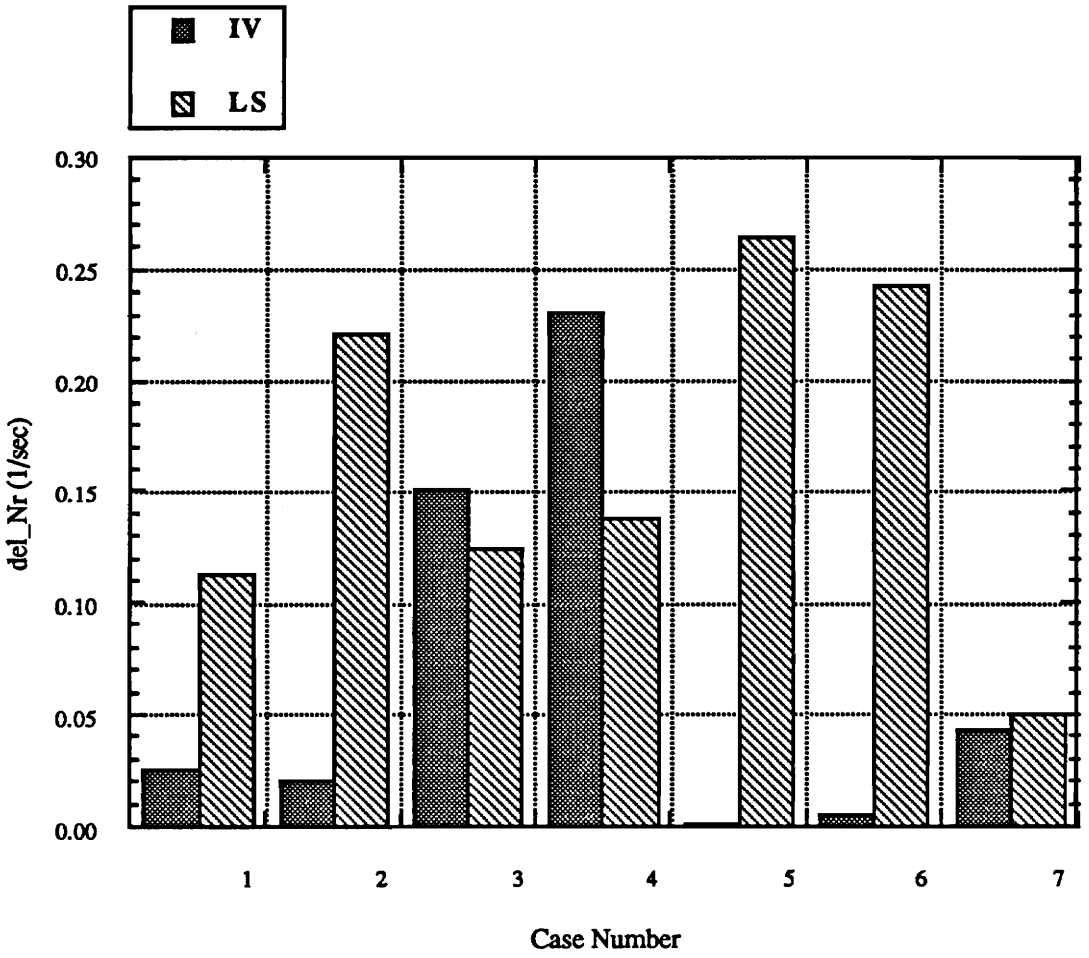

Figure 35: Absolute value of change in Nr from zero noise identified error value

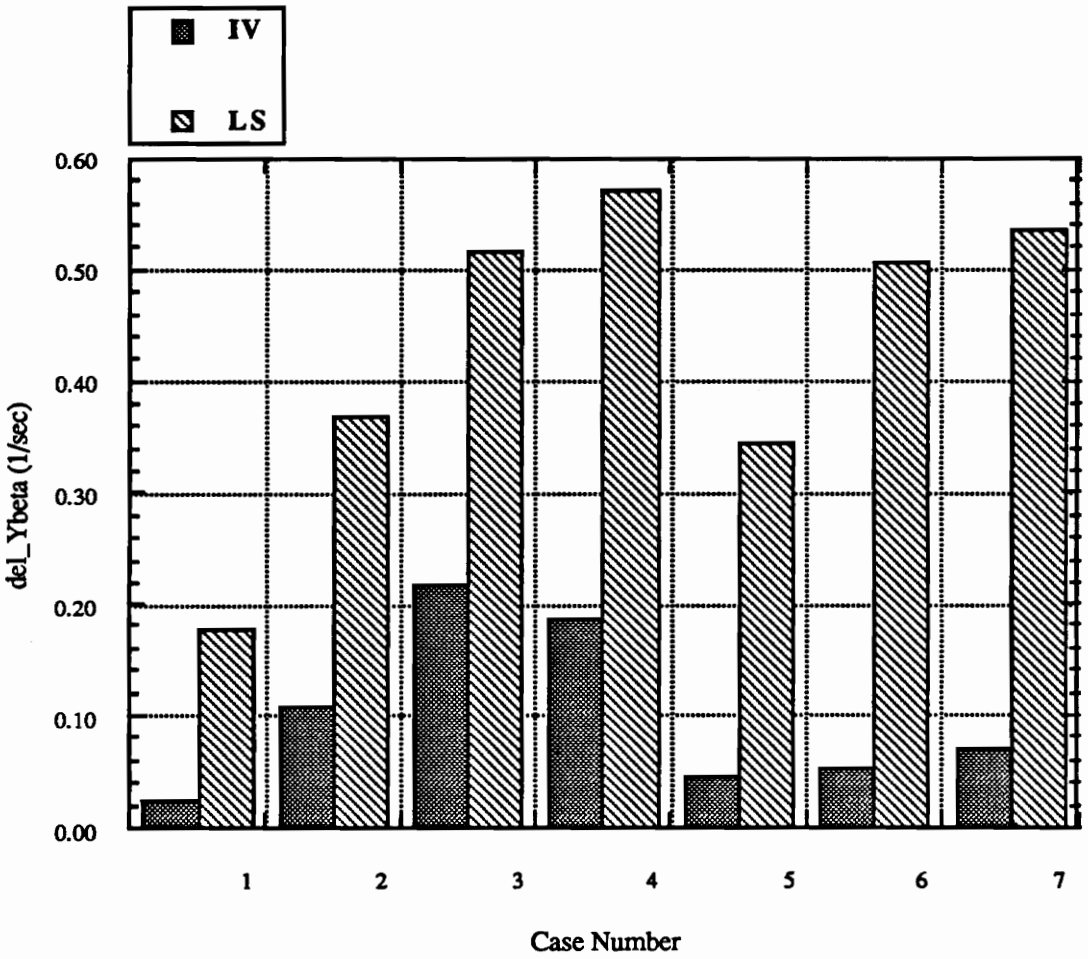

Figure 36: Absolute value of change in Ybeta from zero noise identified error value

method is less sensitive to state noise.

4.0 Conclusions

The main conclusions to be drawn from this study are:

1.) The error parameters identified by the instrumental variable solution appear to be of greater accuracy than the least-squares method when state noise is high relative to its baseline value and the input noise remains at its baseline value. This result substantiates the theoretical development which reveals that the IV method is correlated with only the input noise and the LS approach is correlated with both the state and input noise.

2.) The IV approach performs marginally better than the LS method when both the state and input noise are increased, by the same amount, to at least twice their "nominal" value.

3.) The least-squares identification process generally predicts less stable and more lightly damped systems than the instrumental variable technique.

4.) High state and input noise levels tend to cause the models identified using both methods to become less stable.

5.) Both the instrumental method and the least-squares method perform better for the simpler, single input, longitudinal case as opposed to the more complicated two-input lateral/directional axis case.

The instrumental variable technique used in this thesis performed well for the specific conditions studied. However, further study may be useful to study the effects of varying flight conditions, inputs, noise types, and noise levels.

5.0 References

[1] Ballin, M.G., and Dalang-Secretan, M., "Validation of Dynamic Response of a Blade-Element UH-60 Simulation Model in Hovering Flight", *Journal of the American Helicopter Society*, Oct. 1990, pp. 77-88.

[2] Tischler, M.B., "Frequency-Response Identification of XV-15 Tiltrotor Aircraft Dynamics", NASA-TM-89428, 1982.

[3] Friedrich, H., "Determination of Stability Derivatives from Flight Test Results by Means of the Regression Analysis", AGARD CP-172, *Methods for Aircraft State and Parameter Identification*, Nov. 1974, pp. 20-1 to 20-8.

[4] Klein, V., "Two Biased Estimation Techniques in Linear Regression - Application to Aircraft", NASA-TM-100649, 1988.

[5] Klein, V., "Aerodynamic Parameters of High-Angle-of-Attack Research Vehicle (HARV) Estimated from Flight Data", NASA-TM-102692, August 1990.

[6] Klein, V., "Aerodynamic Parameters of the X-31 Drop Model Estimated from Flight Data at High Angles of Attack", AIAA 92-4357, AIAA Atmospheric Flight Mechanics Conference, Hilton Head, SC, 1992.

[7] Hess, R.A., Stanka, B.H., and Purdy, M.B., "A Methodology for Simulation Validation Using Optimal Time History Matching", AIAA-88-4617-CP, 1988.

[8] Hess, R.A., and Ly, P.L., "Use of a Simplified Estimation Scheme for Simulation Validation and Improvement", AIAA-89-3262-CP, 1989.

[9] Young, P.C., "An Instrumental Variable Method for Real-time Identification of a Noisy Process", *Automatica*, Vol. 6, Pergamon Press, 1970, pp. 271-287.

[10] Mode, E.B., Elements of Probability and Statistics, Prentice-Hall, Inc., Englewood Cliffs, N.J., 1966.

[11] Brumbaugh, R.W., "An Aircraft Model for the AIAA Controls Design Challenge", AIAA 91-2631, AIAA Guidance, Navigation, and Control Conference, New Orleans, LA., August 1991.

[12] MATLAB - The Mathworks, Inc., Cochituate Place, 24 Prime Park Way, Natick, MA 01760.

[13] Etkin, B., Dynamics of Atmospheric Flight, John Wiley & Sons, New York, 1972.

[14] Murphy, P.C., "A Methodology for Airplane Parameter Estimation and Confidence Interval Determination in Nonlinear Estimation Problems", NASA-RP-1153, 1986.

[15] Eykhoff, P., System Identification, John Wiley & Sons, New York, 1974.

6.0 Appendix

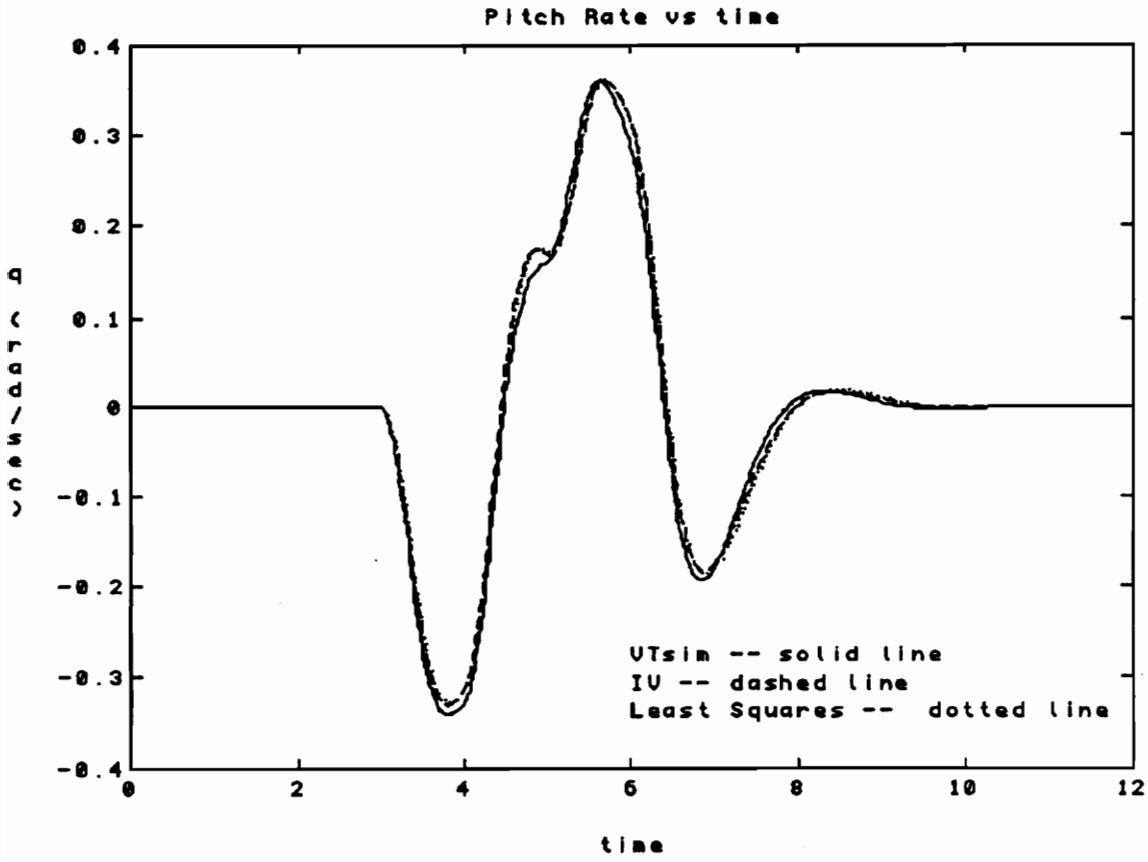

Figure A1: Pitch rate without added noise; Case 0

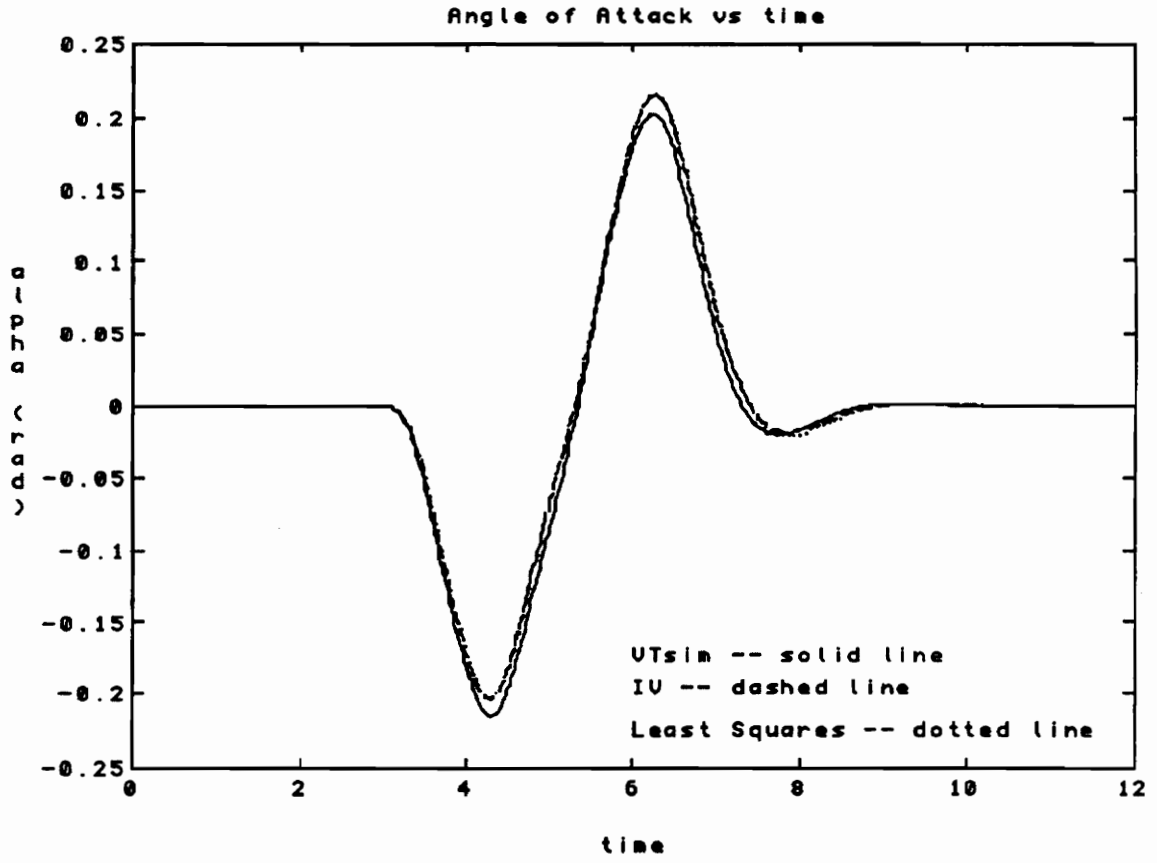

Figure A2: Angle of attack without added noise; Case 0

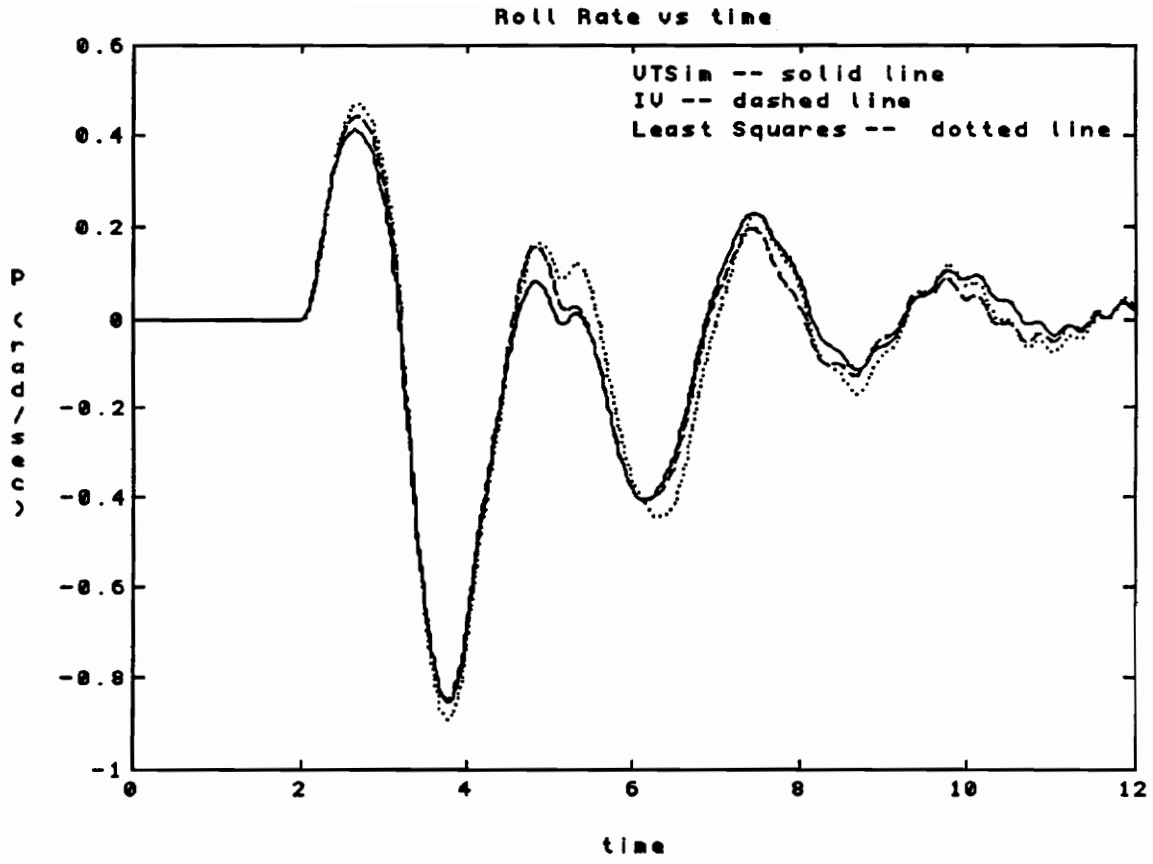

Figure A3: Roll rate without added noise; Case 0

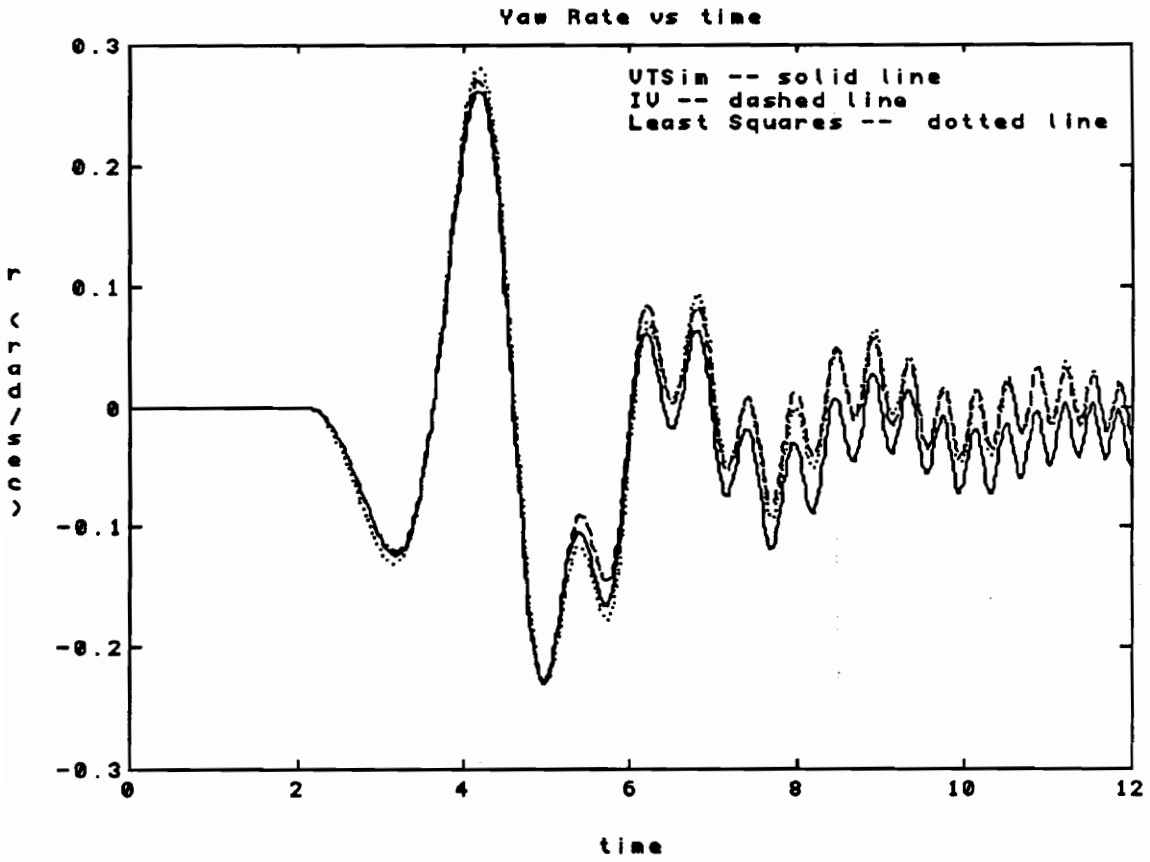

Figure A4: Yaw rate without added noise; Case 0

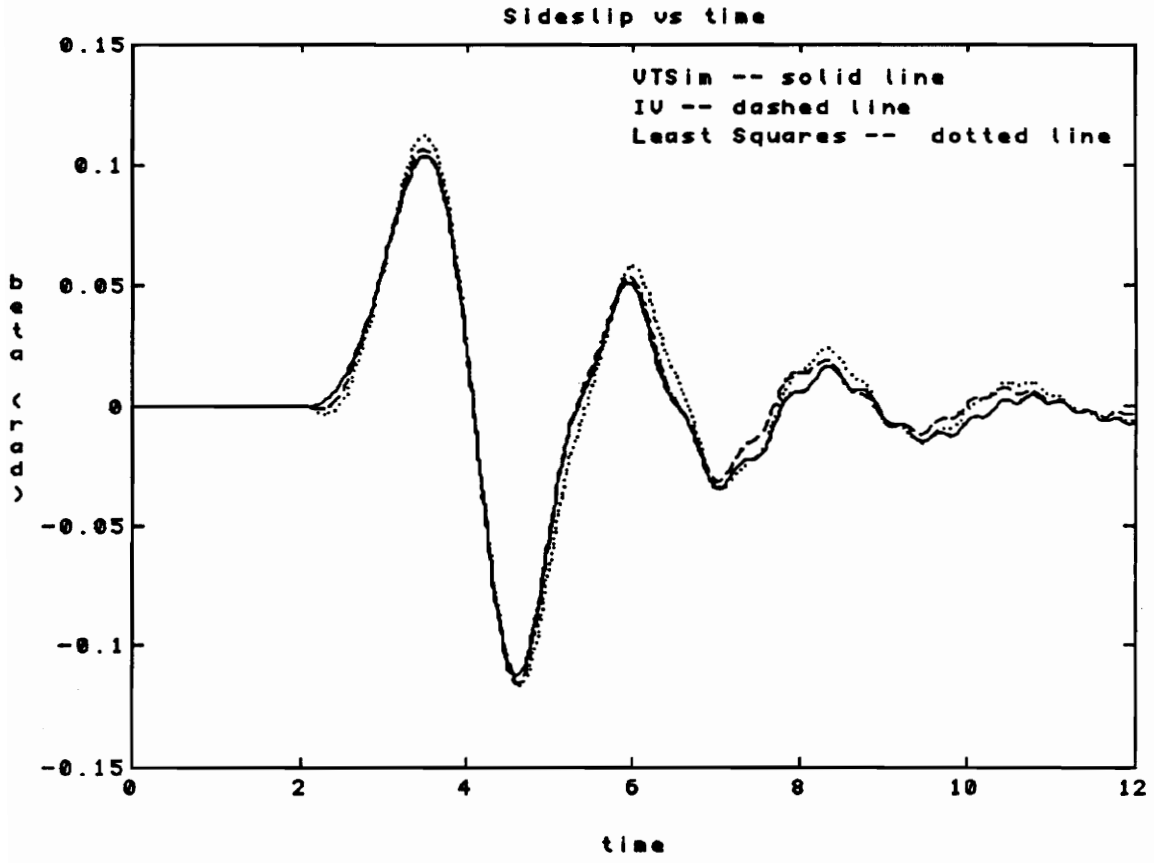

Figure A5 : Sideslip without added noise; Case 0

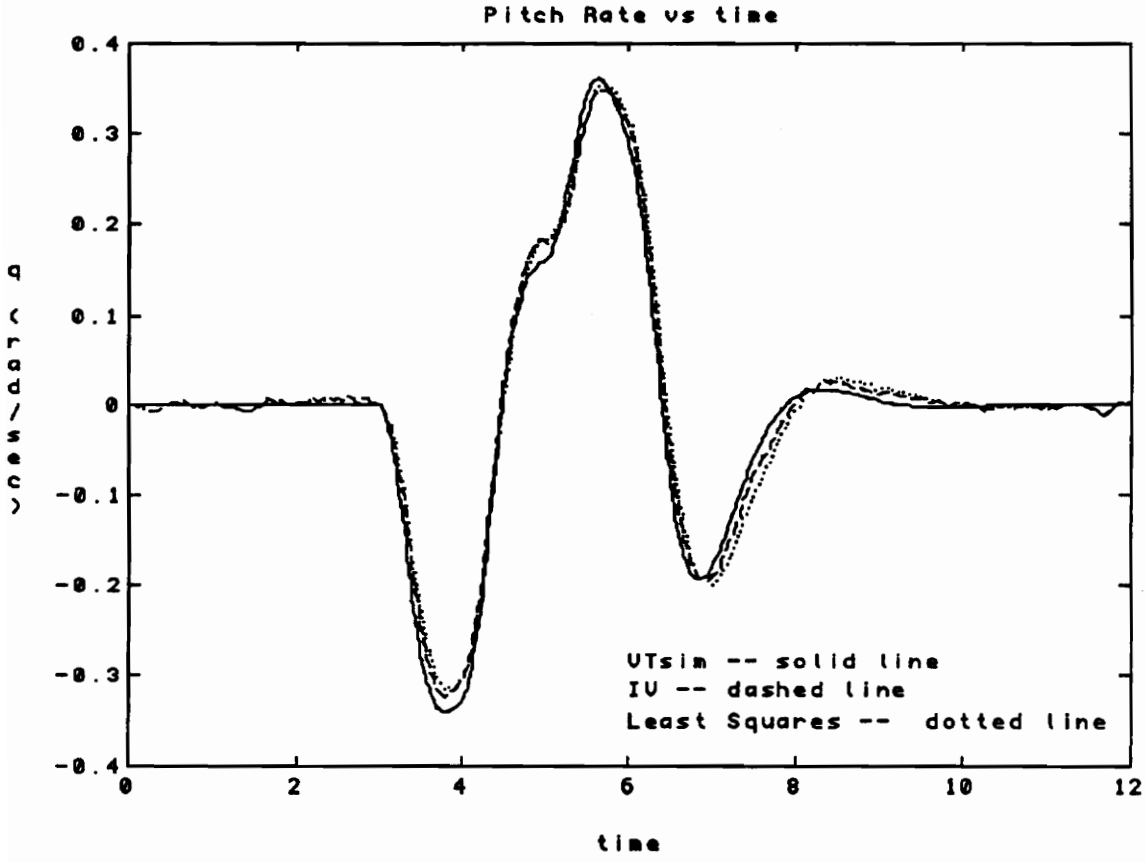

Figure A6: Pitch rate; Case 1

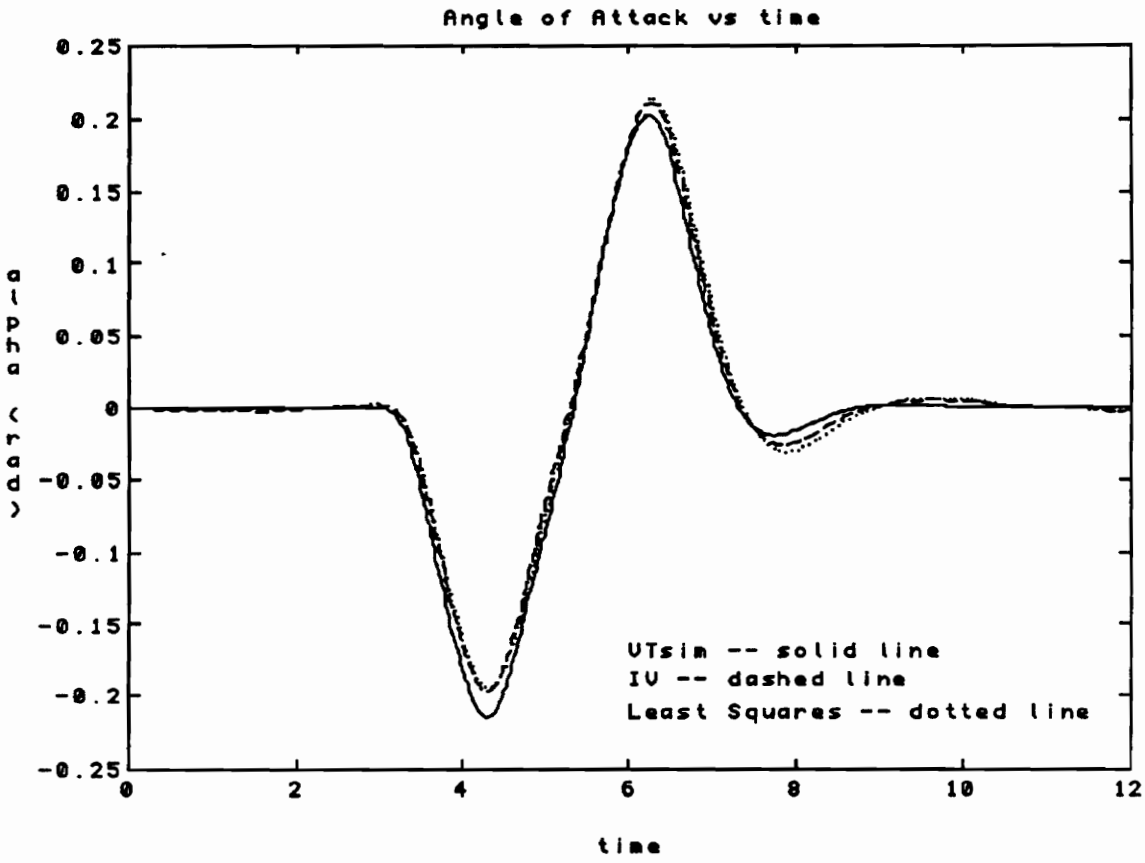

Figure A7: Angle of attack; Case 1

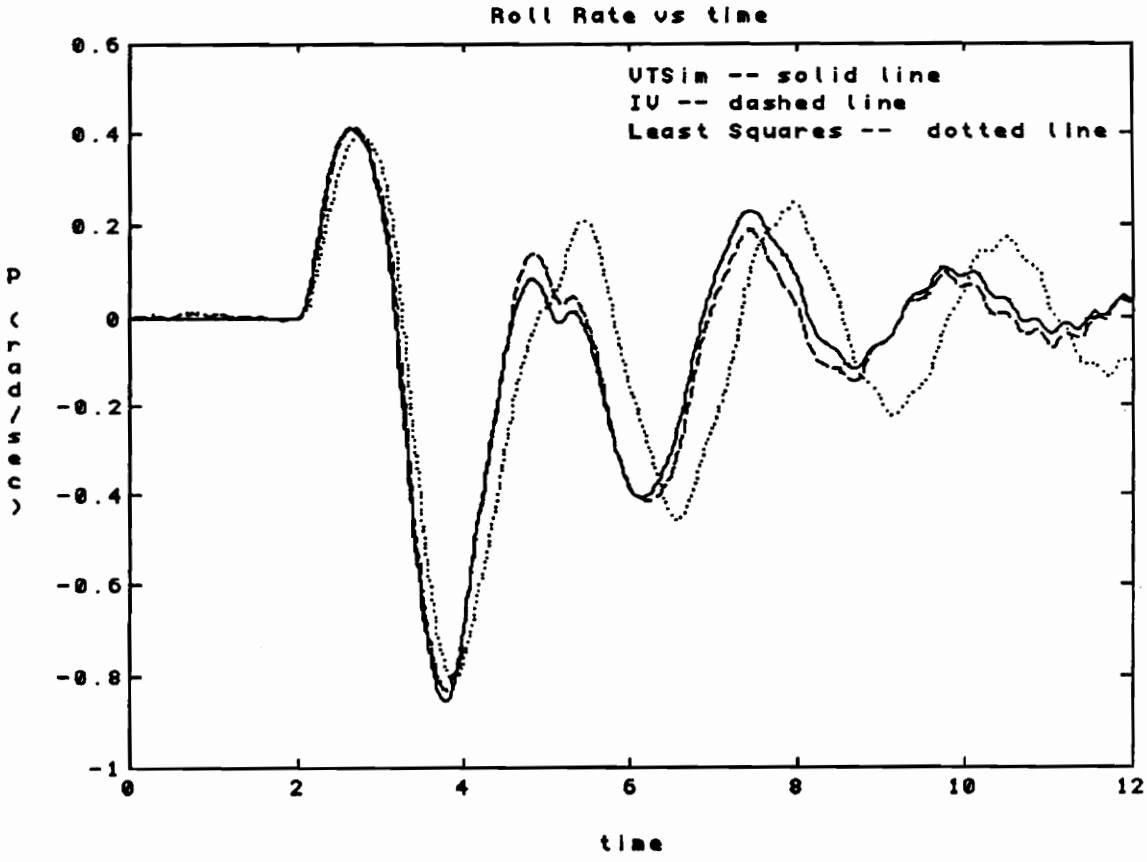

Figure A8: Roll rate; Case 1

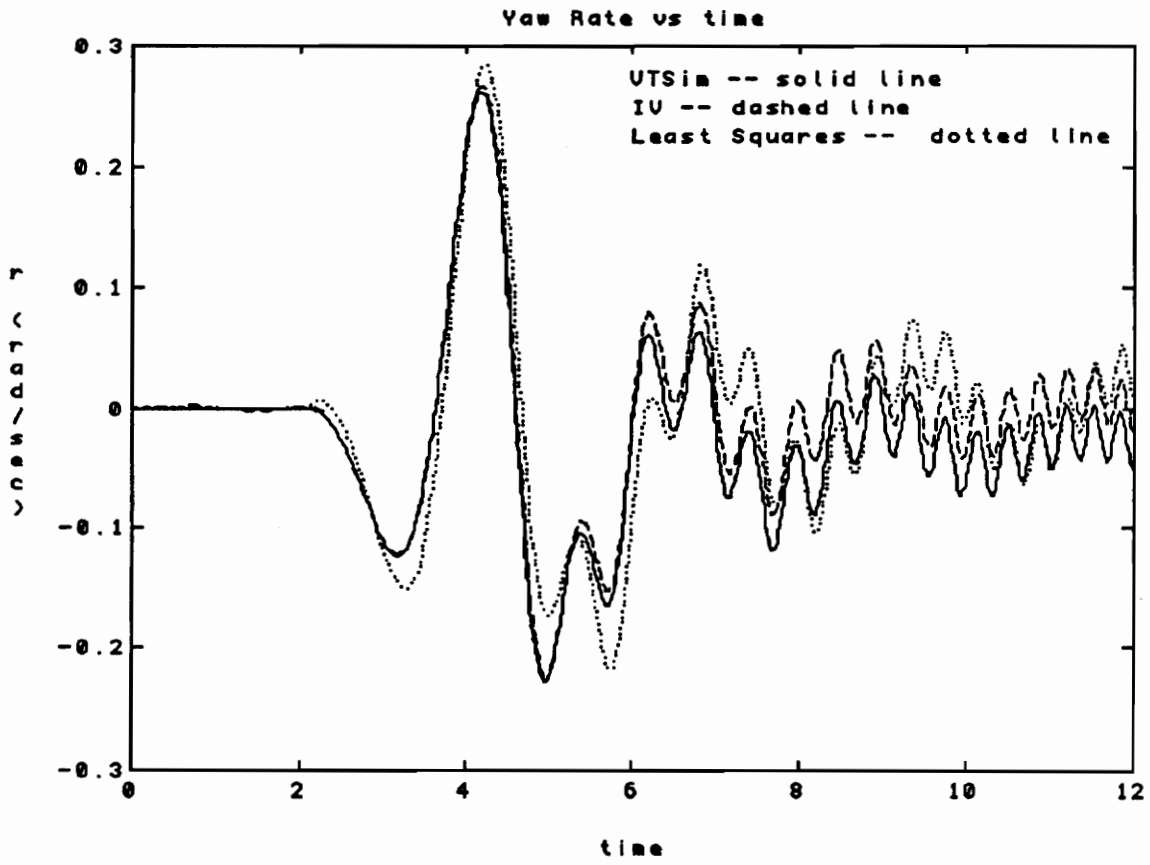

Figure A9: Yaw rate; Case 1

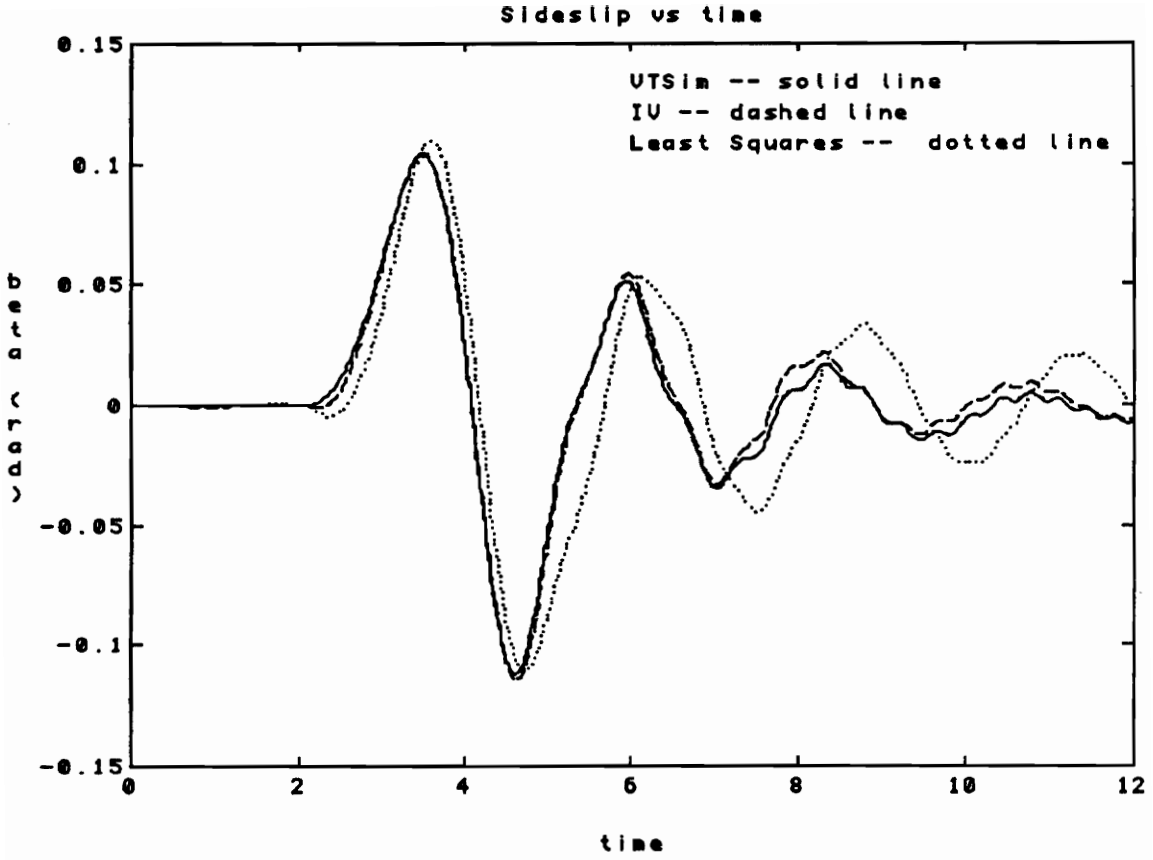

Figure A10: Sideslip; Case 1

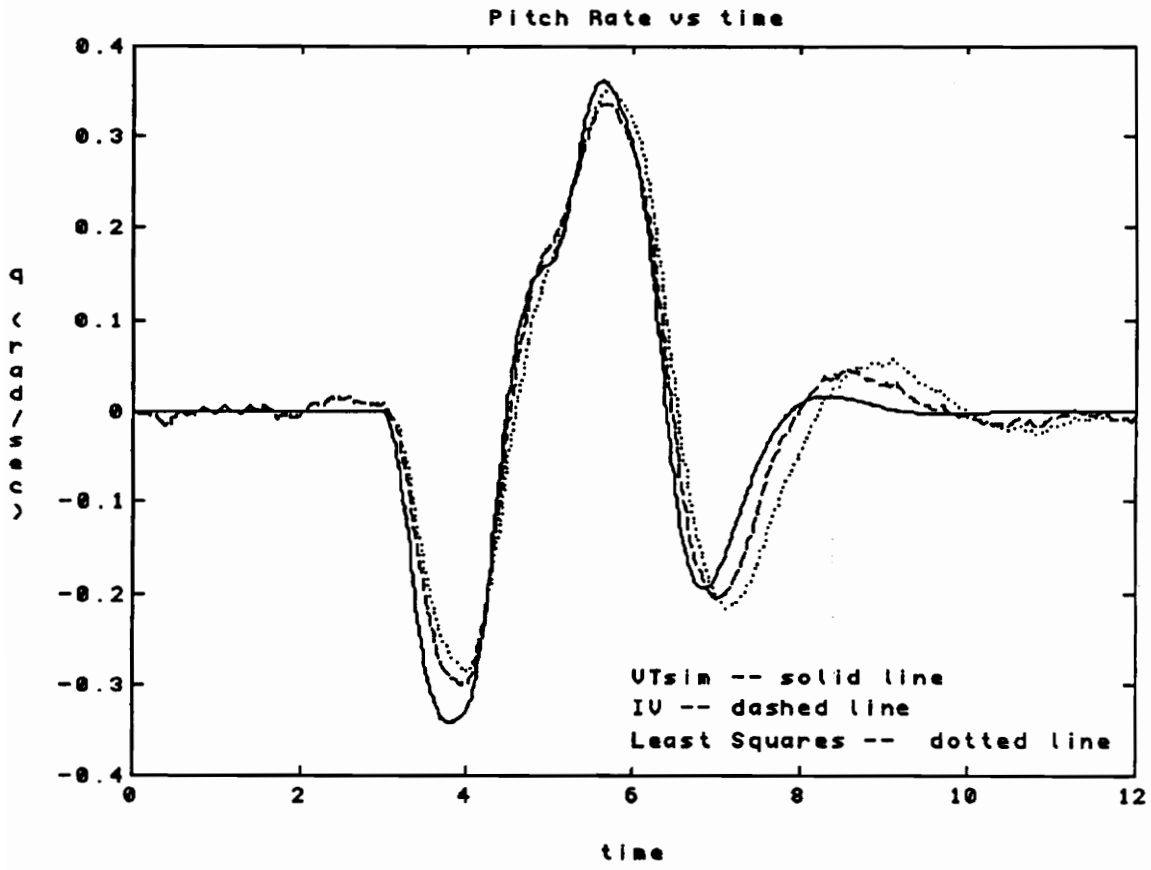

Figure A11: Pitch rate; Case 2

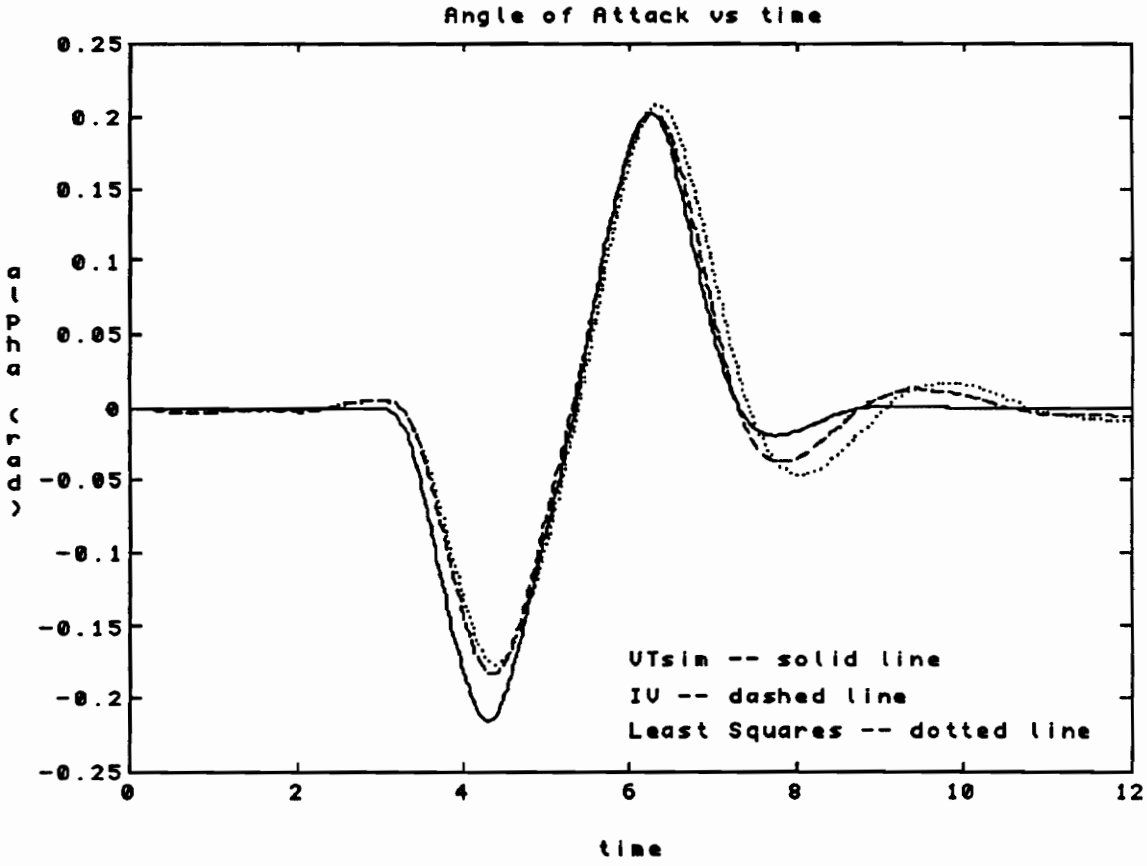

Figure A12: Angle of attack; Case 2

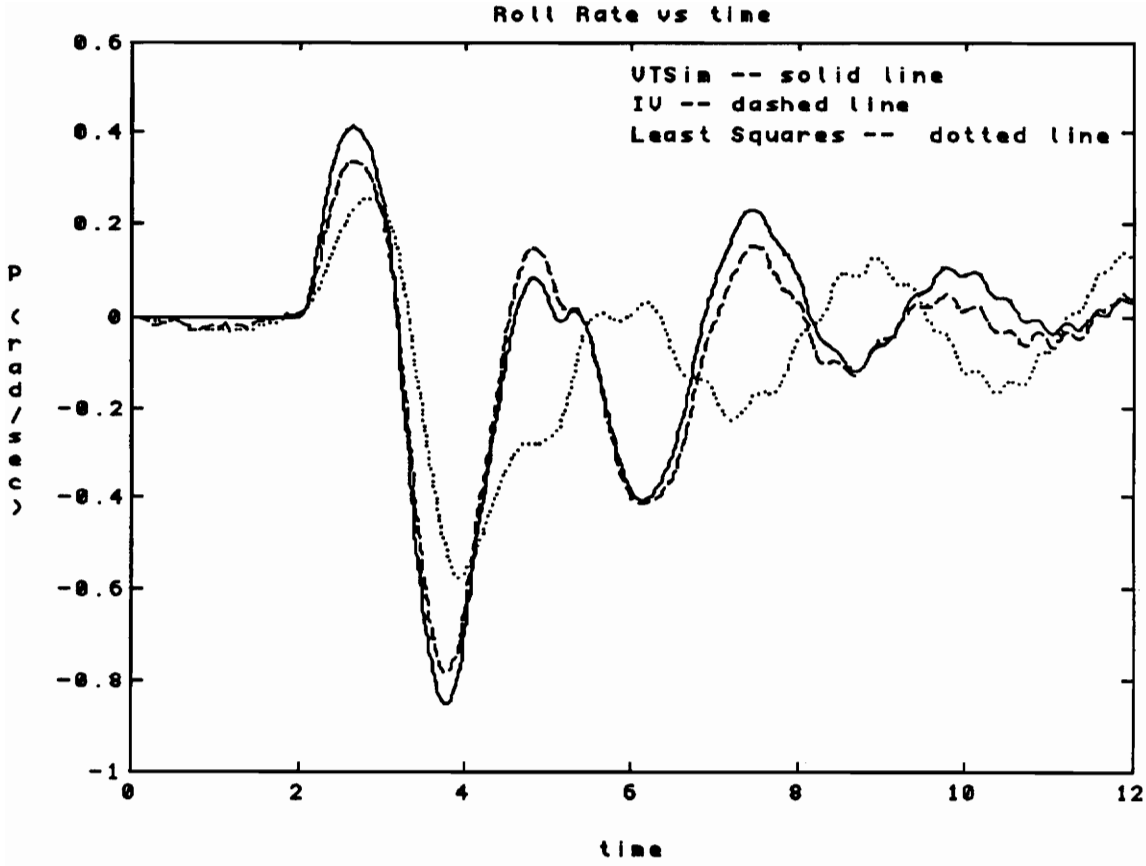

Figure A13: Roll rate; Case 2

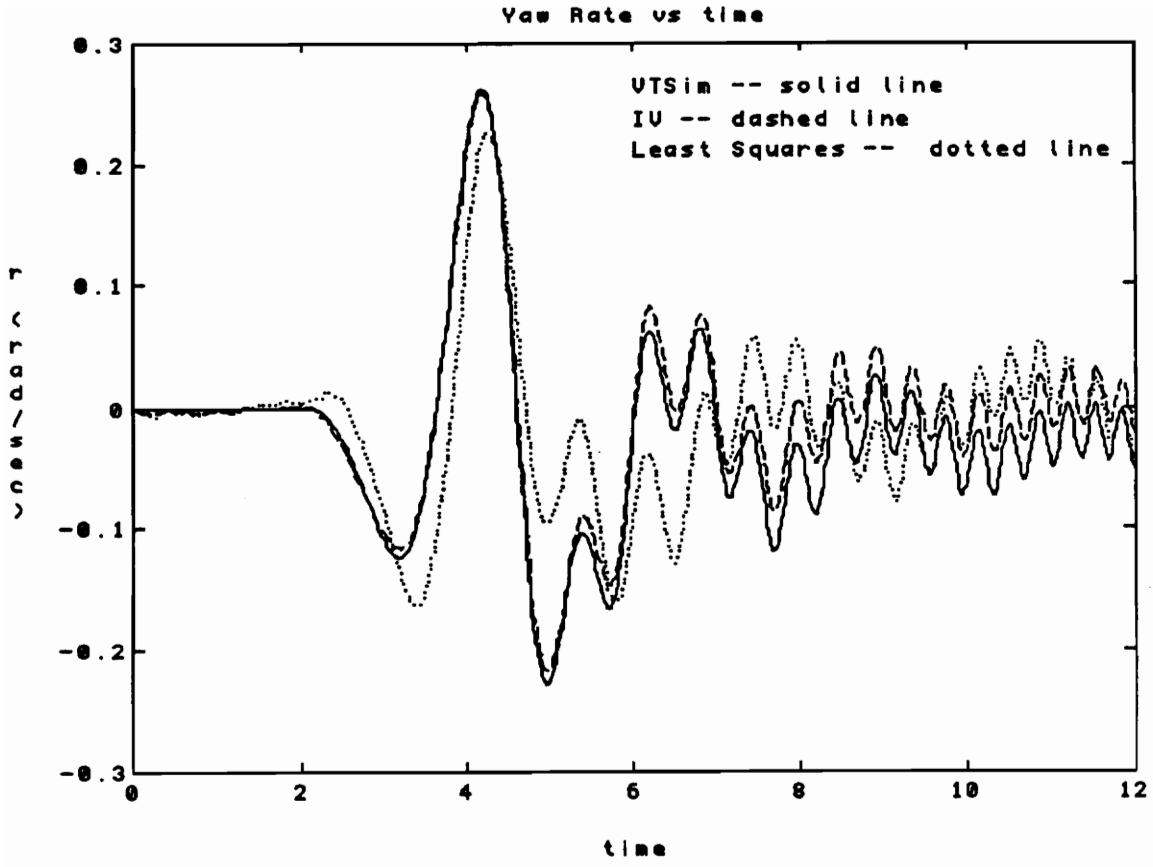

Figure A14: Yaw rate; Case 2

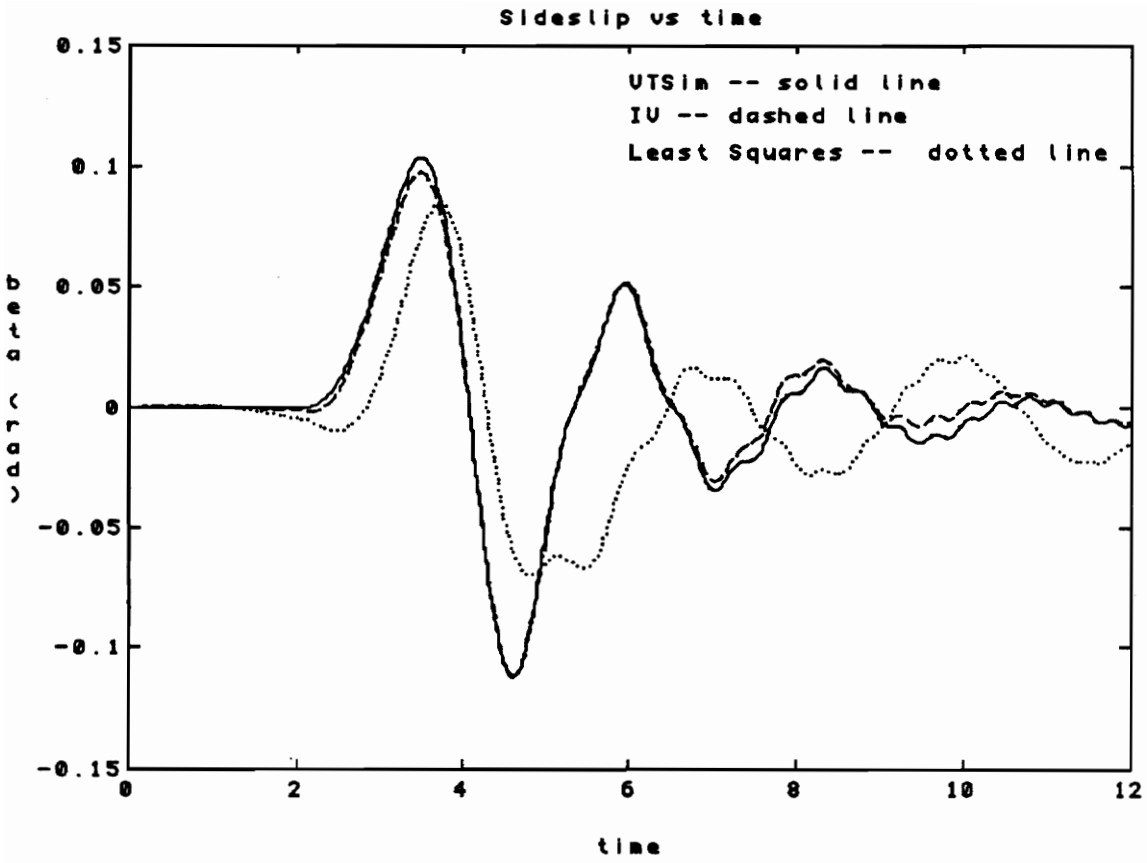

Figure A15: Sideslip; Case 2

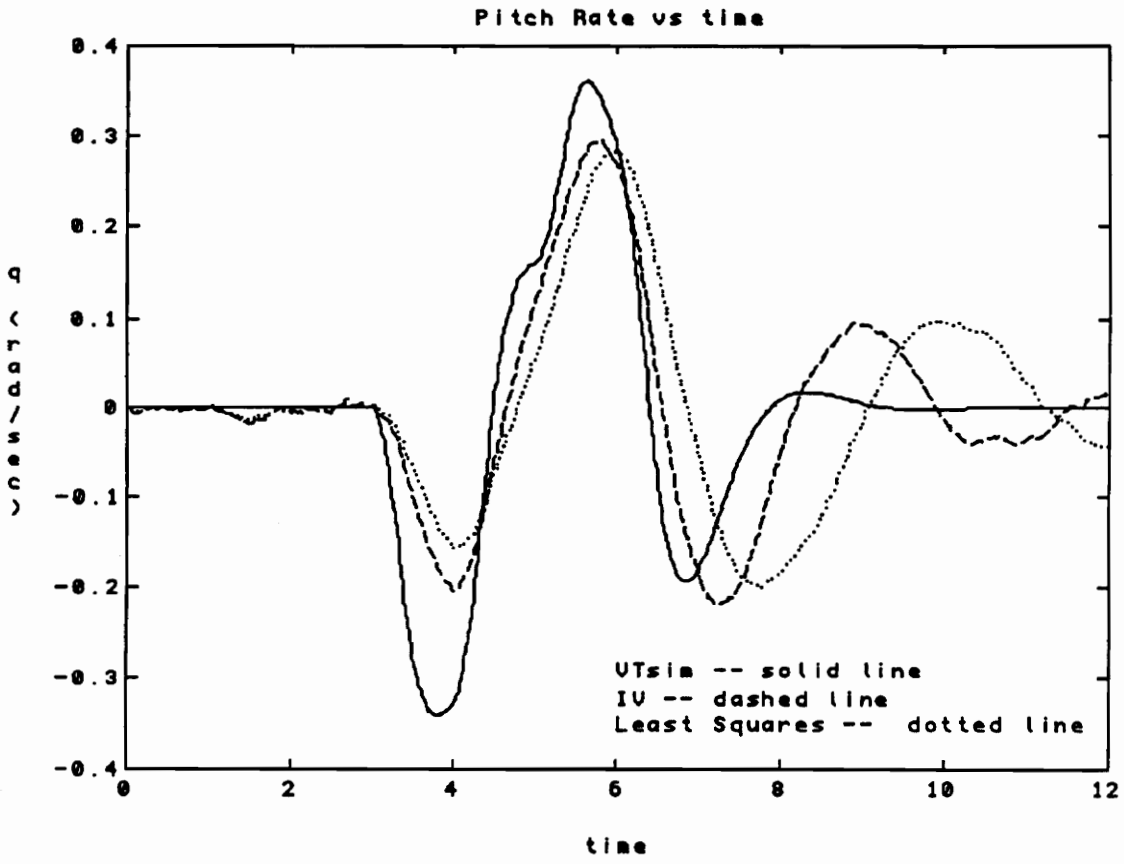

Figure A16: Pitch rate; Case 3

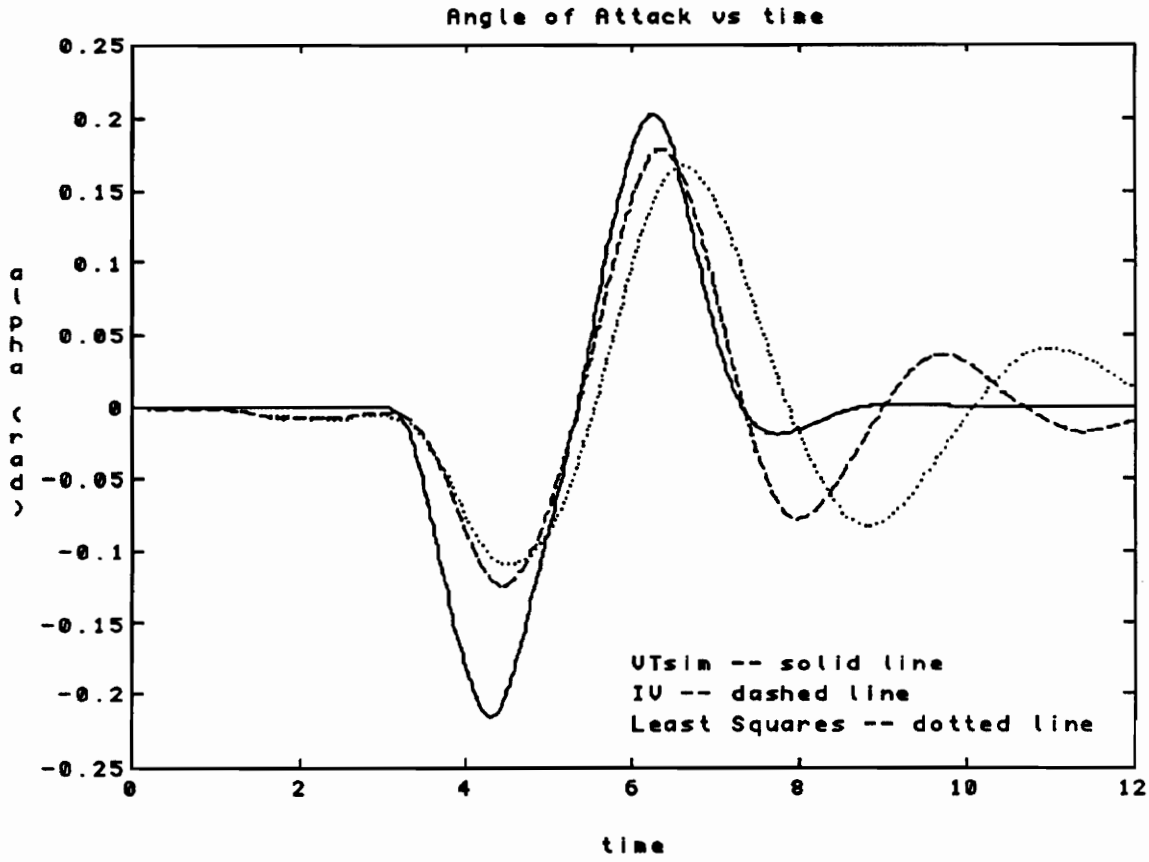

Figure A17: Angle of attack; Case 3

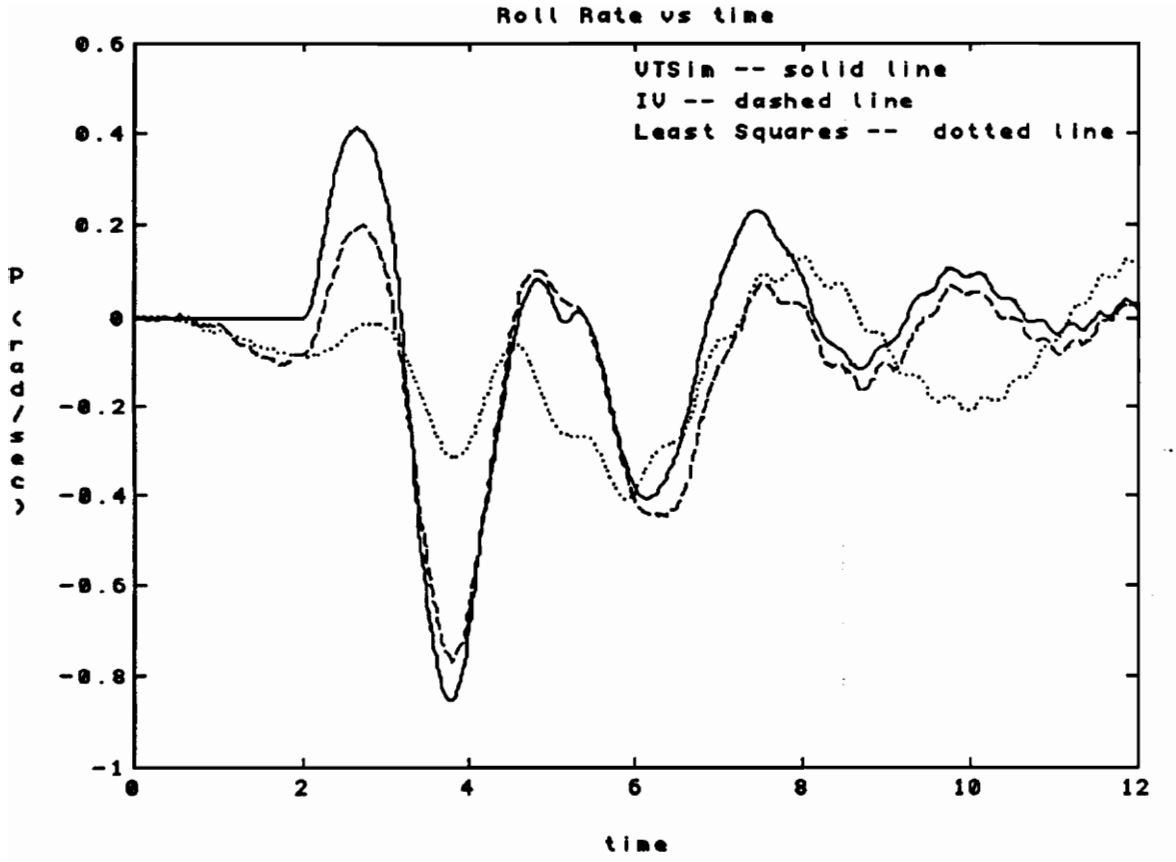

Figure A18: Roll rate; Case 3

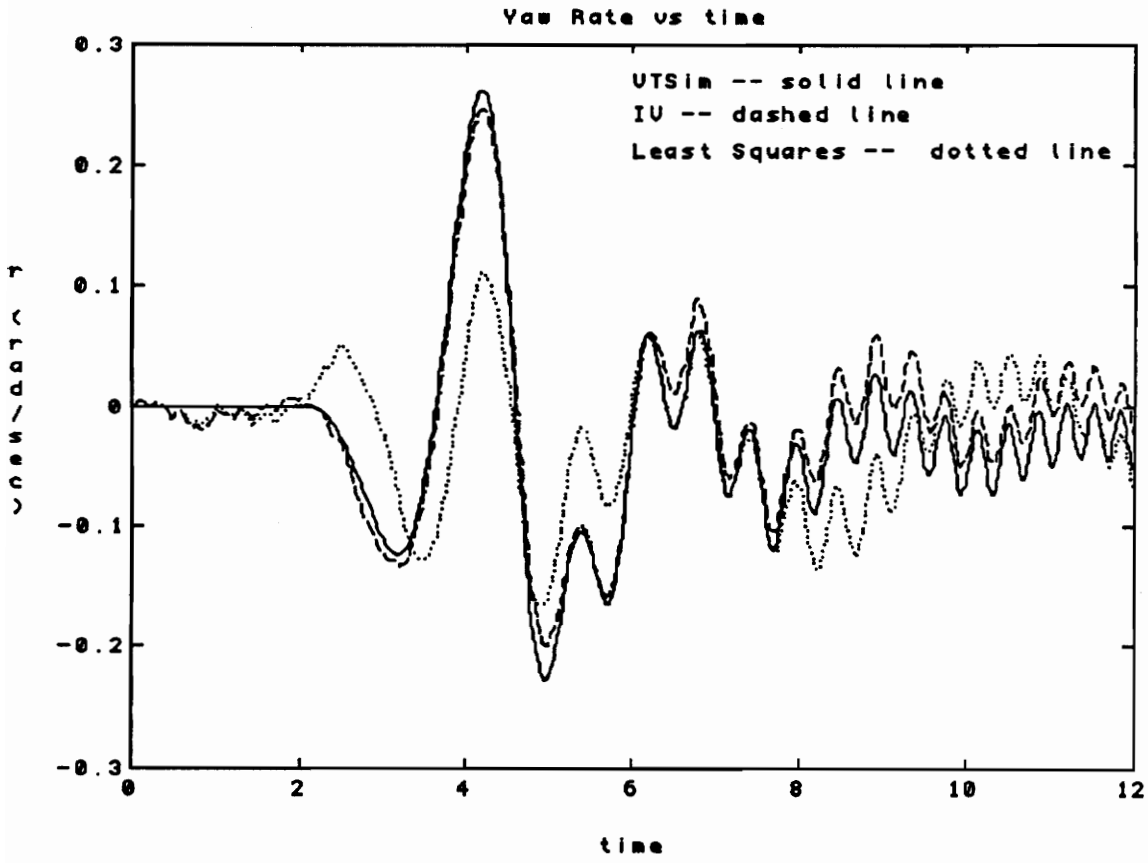

Figure A19: Yaw rate; Case 3

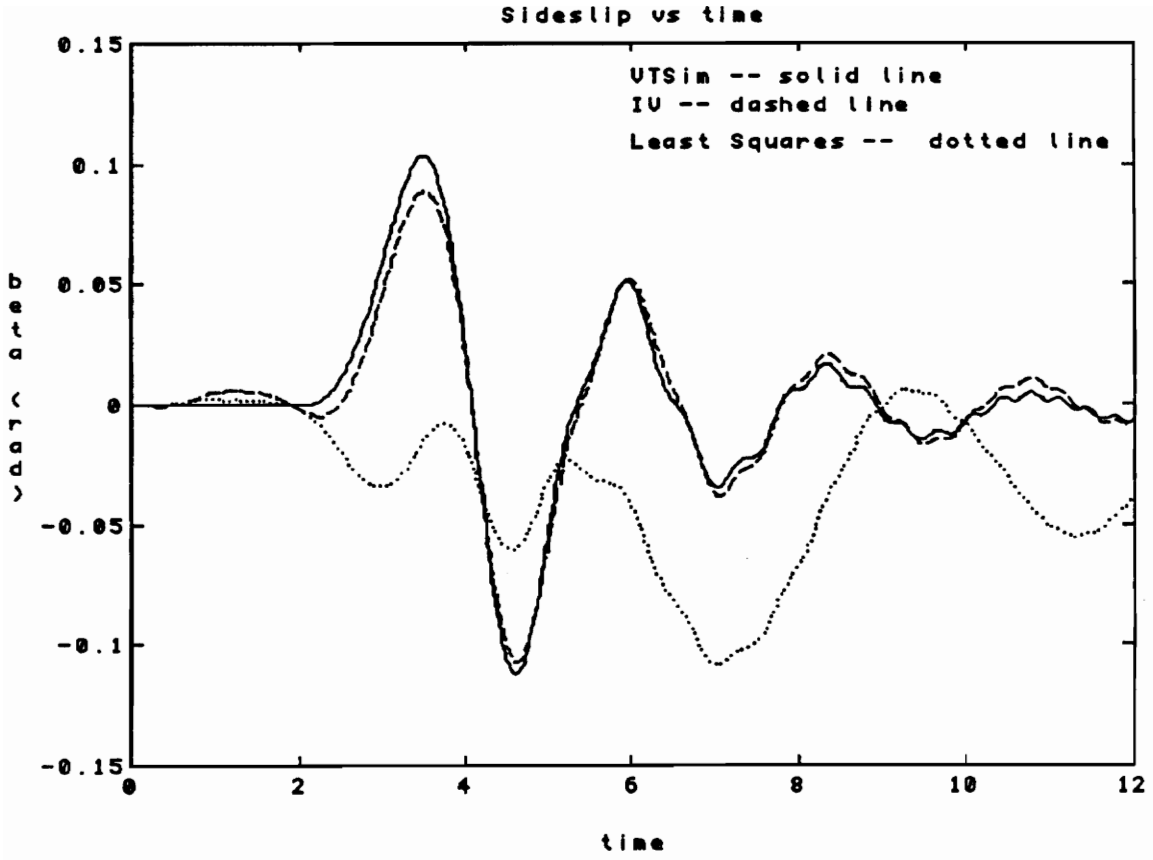

Figure A20: Sideslip; Case 3

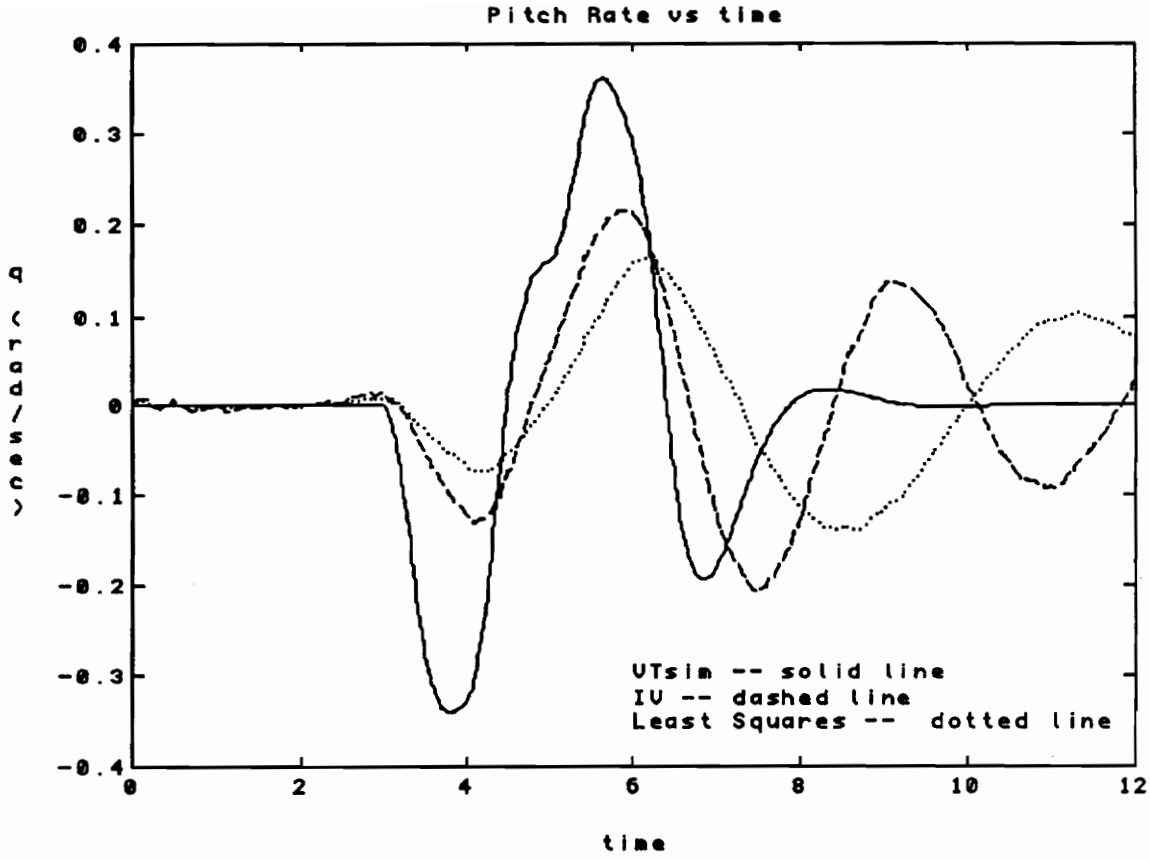

Figure A21: Pitch rate; Case 4

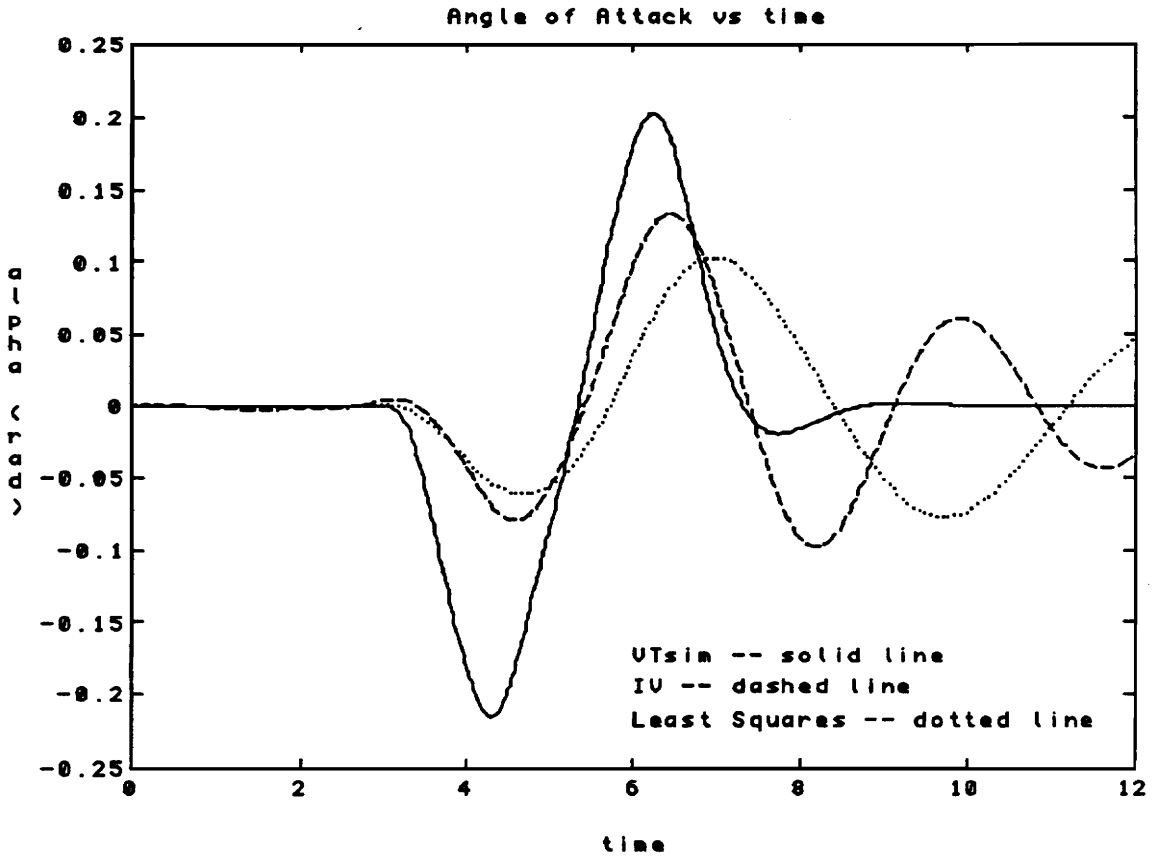

Figure A22: Angle of attack; Case 4

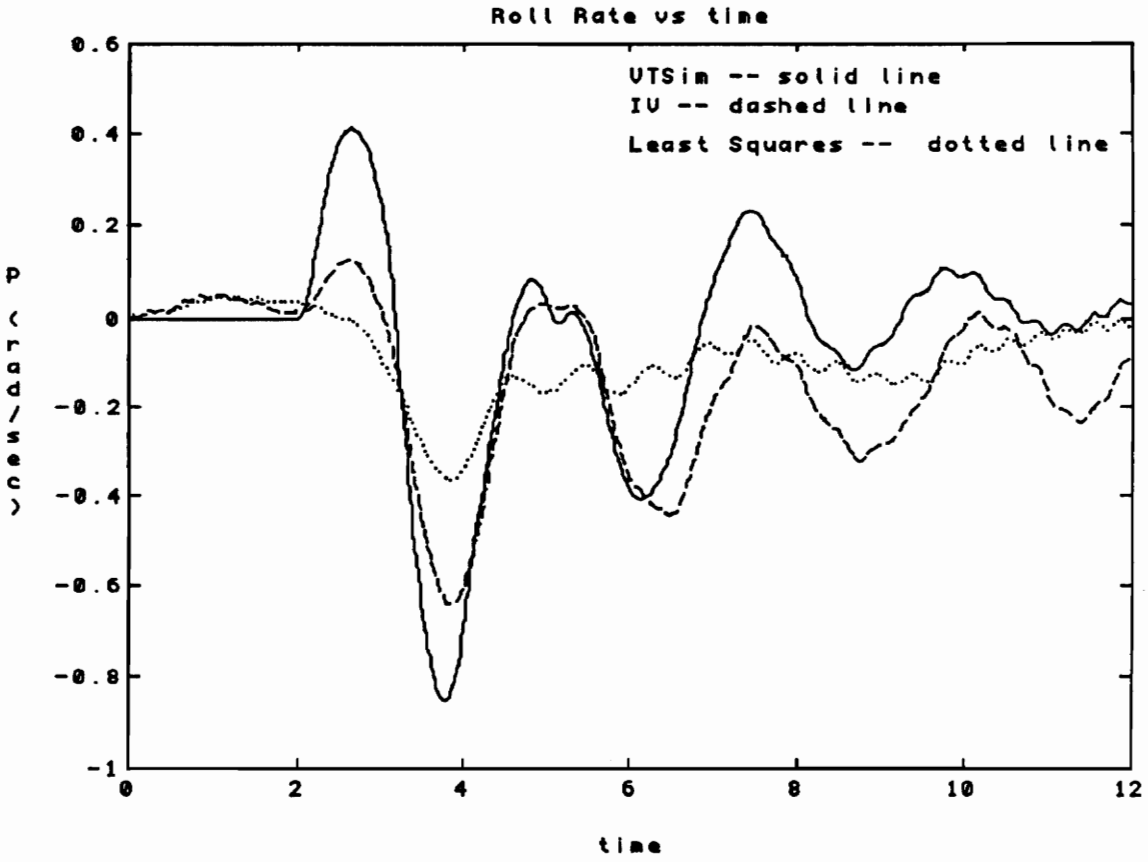

Figure A23: Roll rate; Case 4

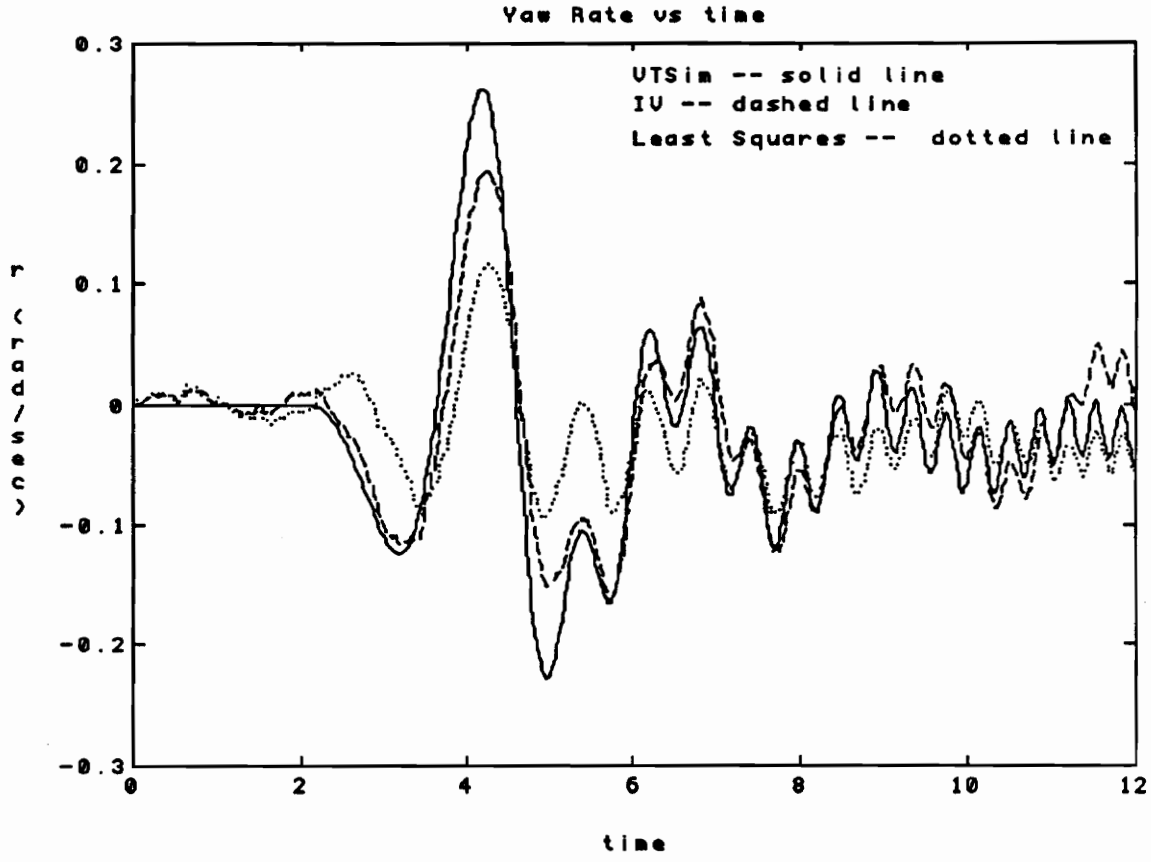

Figure A24: Yaw rate; Case 4

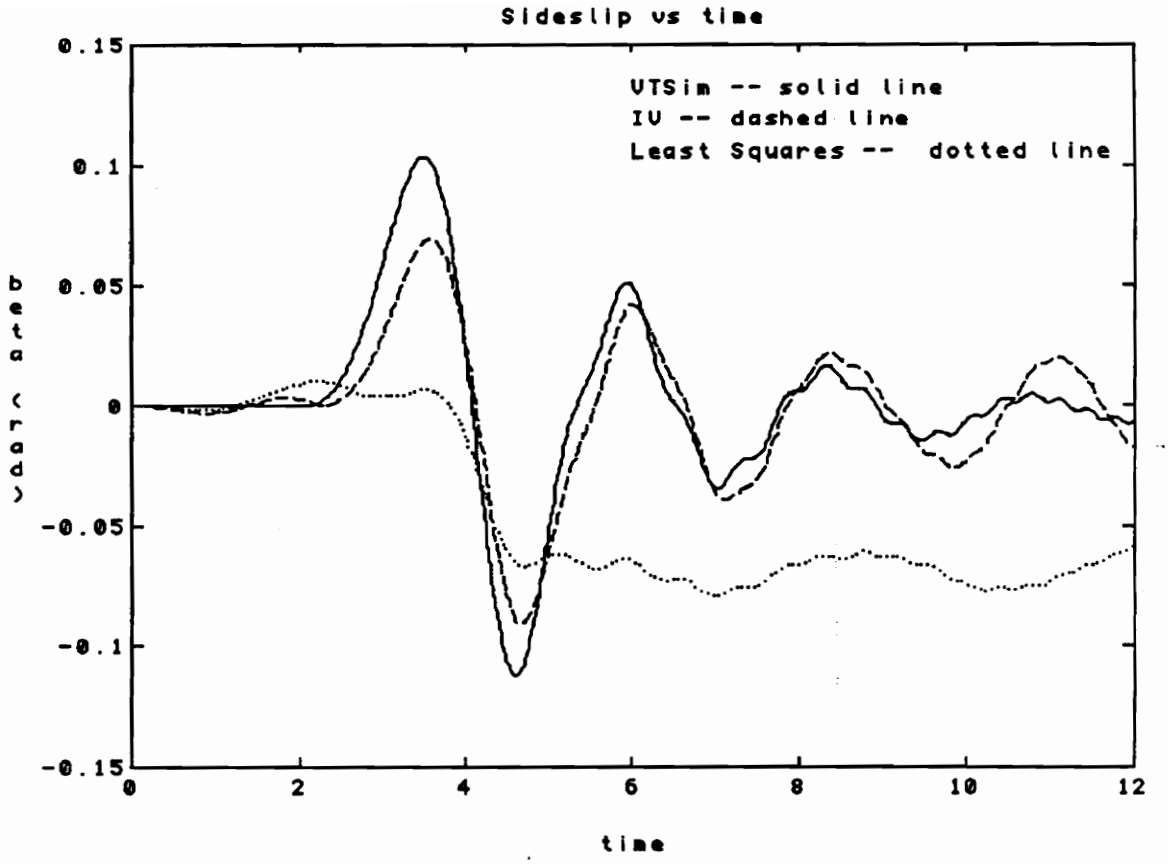

Figure A25: Sideslip; Case 4

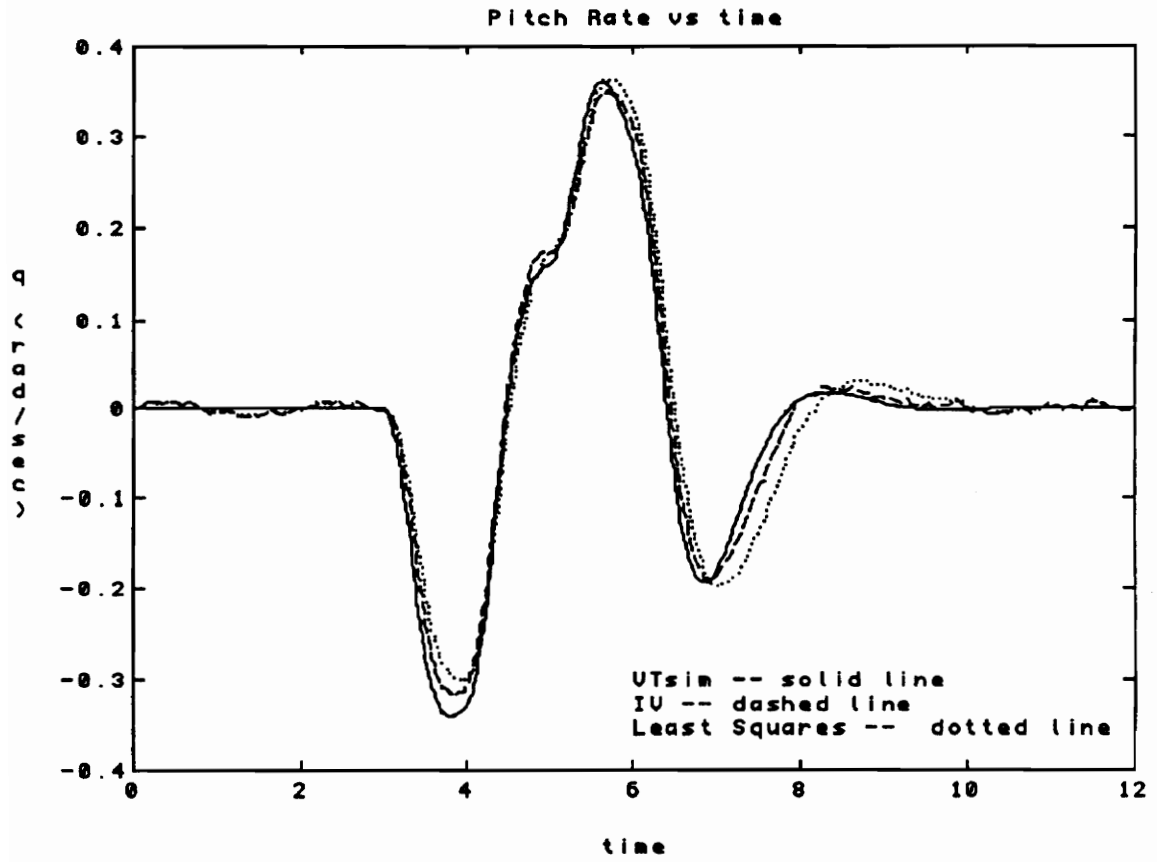

Figure A26: Pitch rate; Case 5

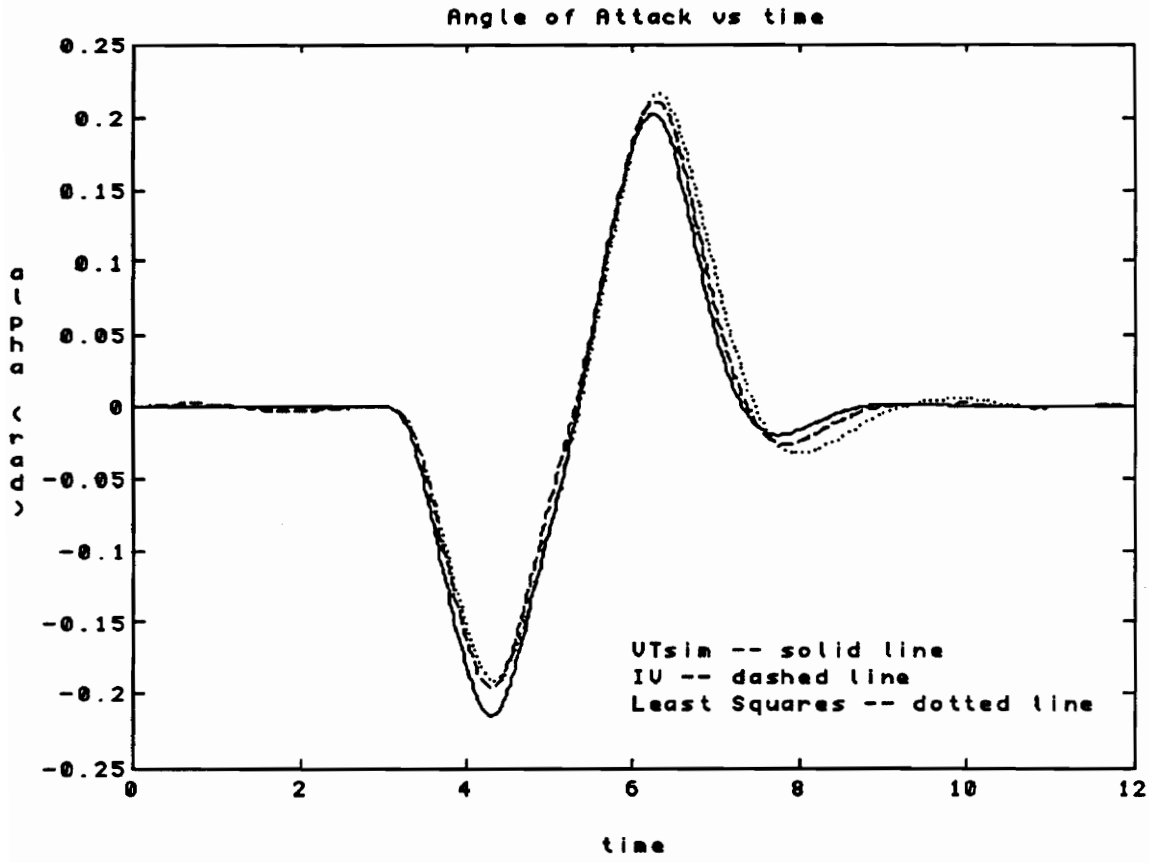

Figure A27: Angle of attack; Case 5

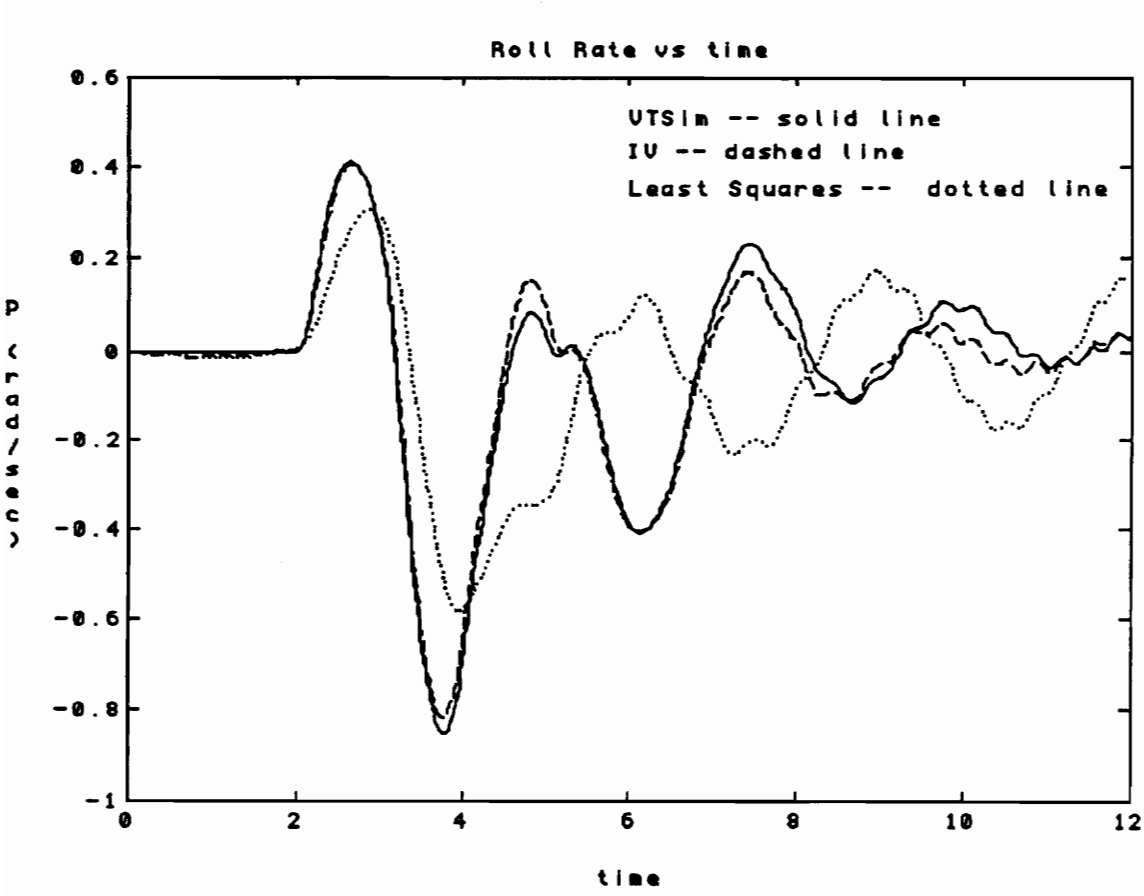

Figure A28: Roll rate; Case 5

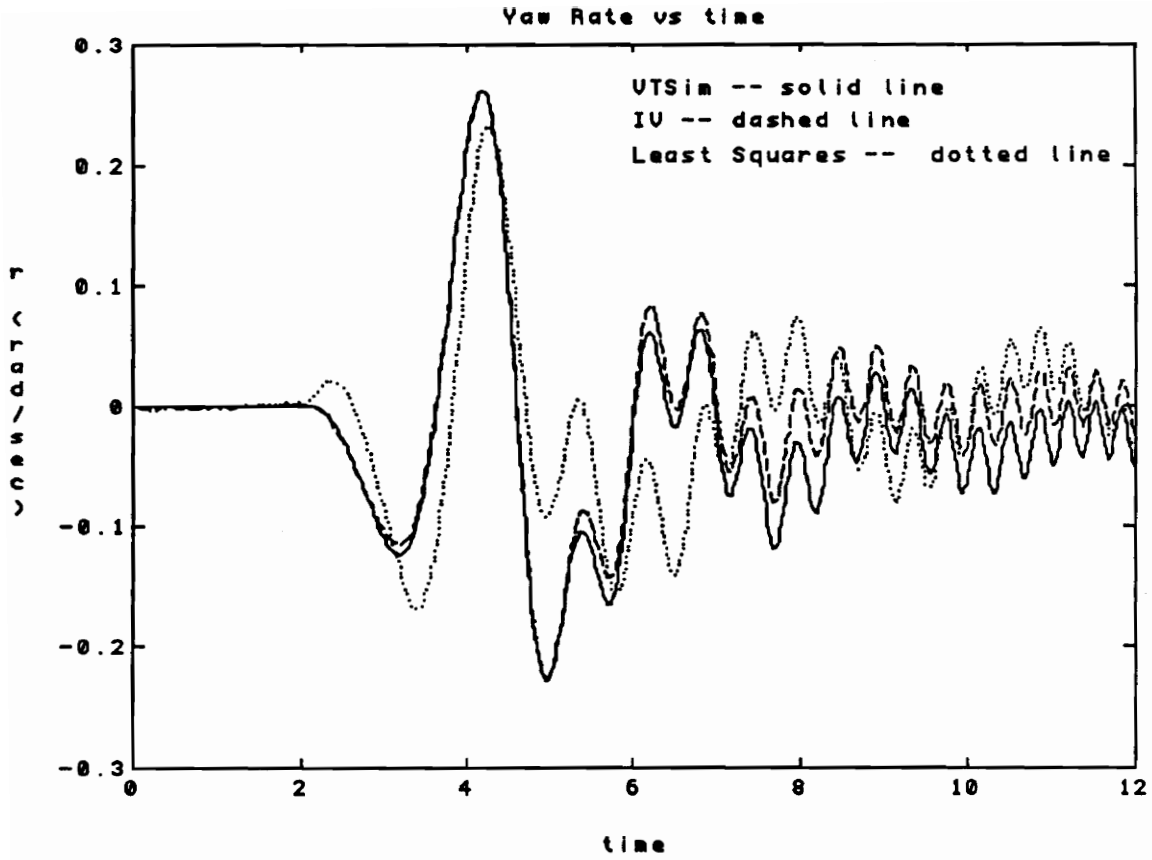

Figure A29: Yaw rate; Case 5

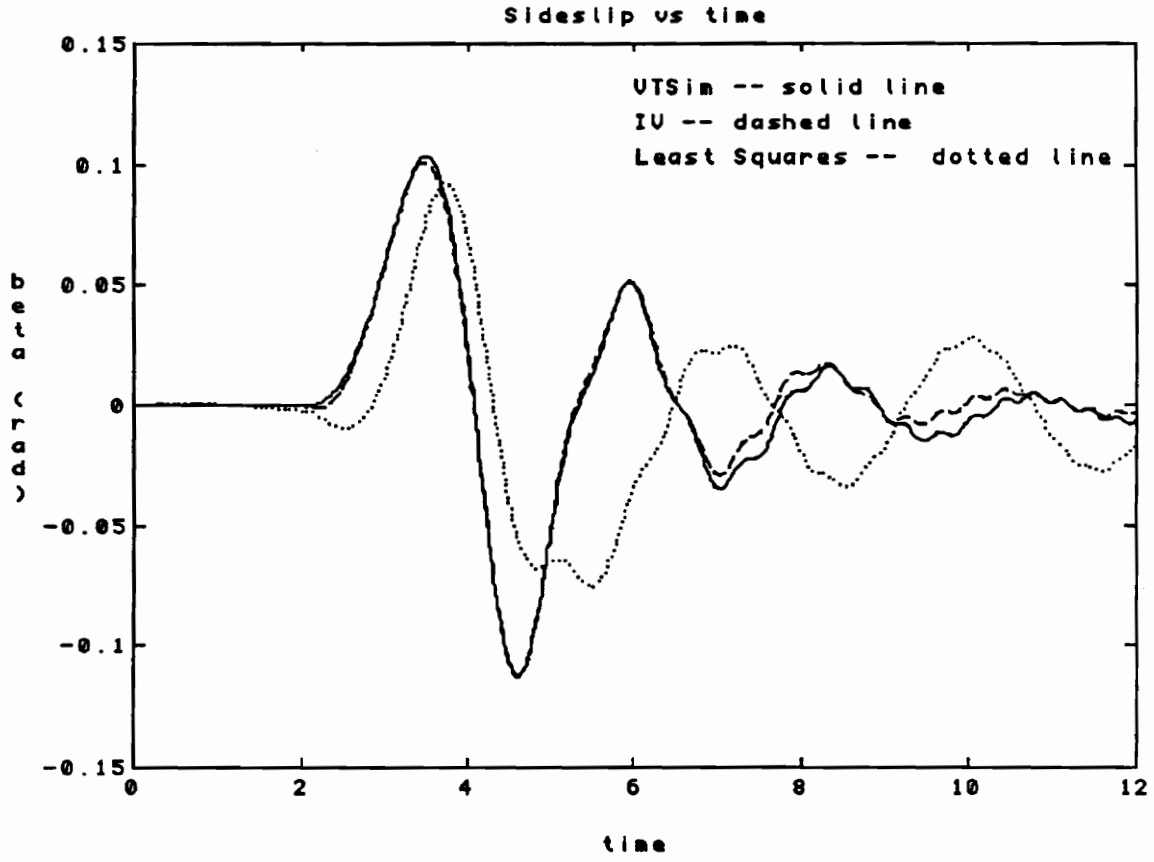

Figure A30: Sideslip; Case 5

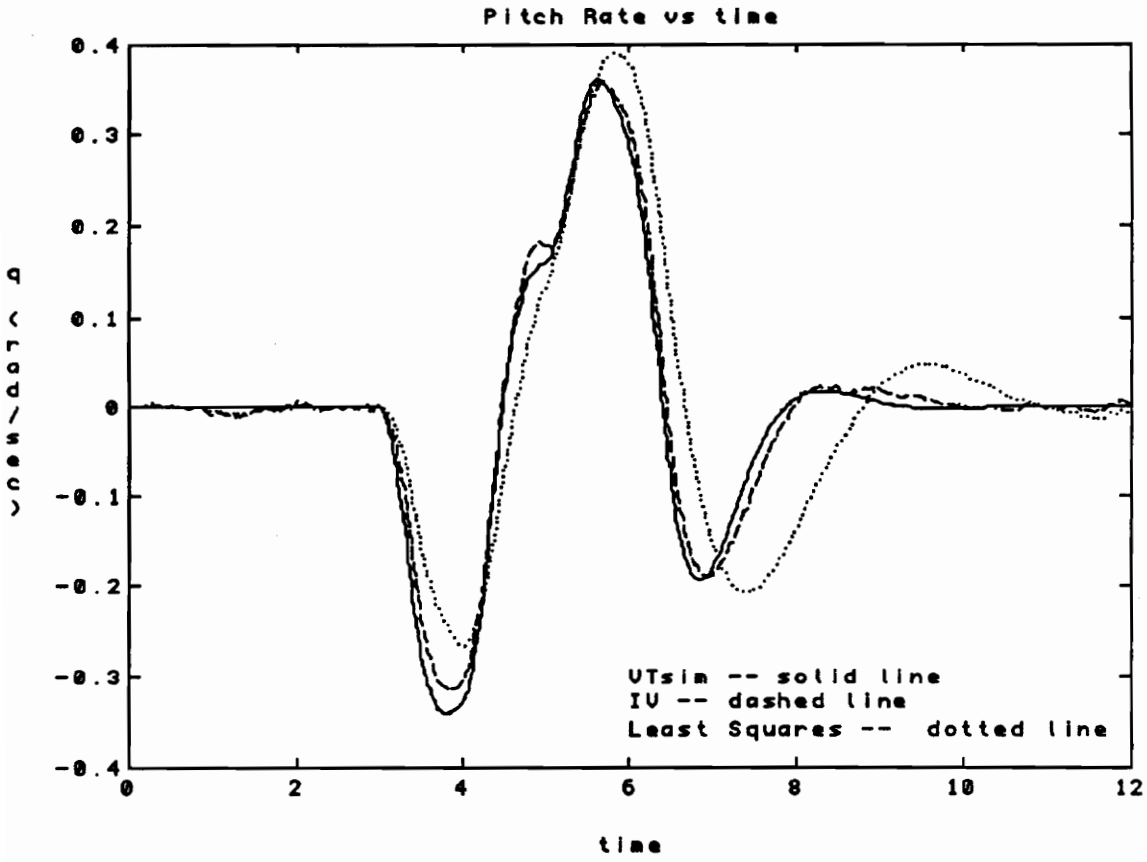

Figure A31: Pitch Rate; Case 6

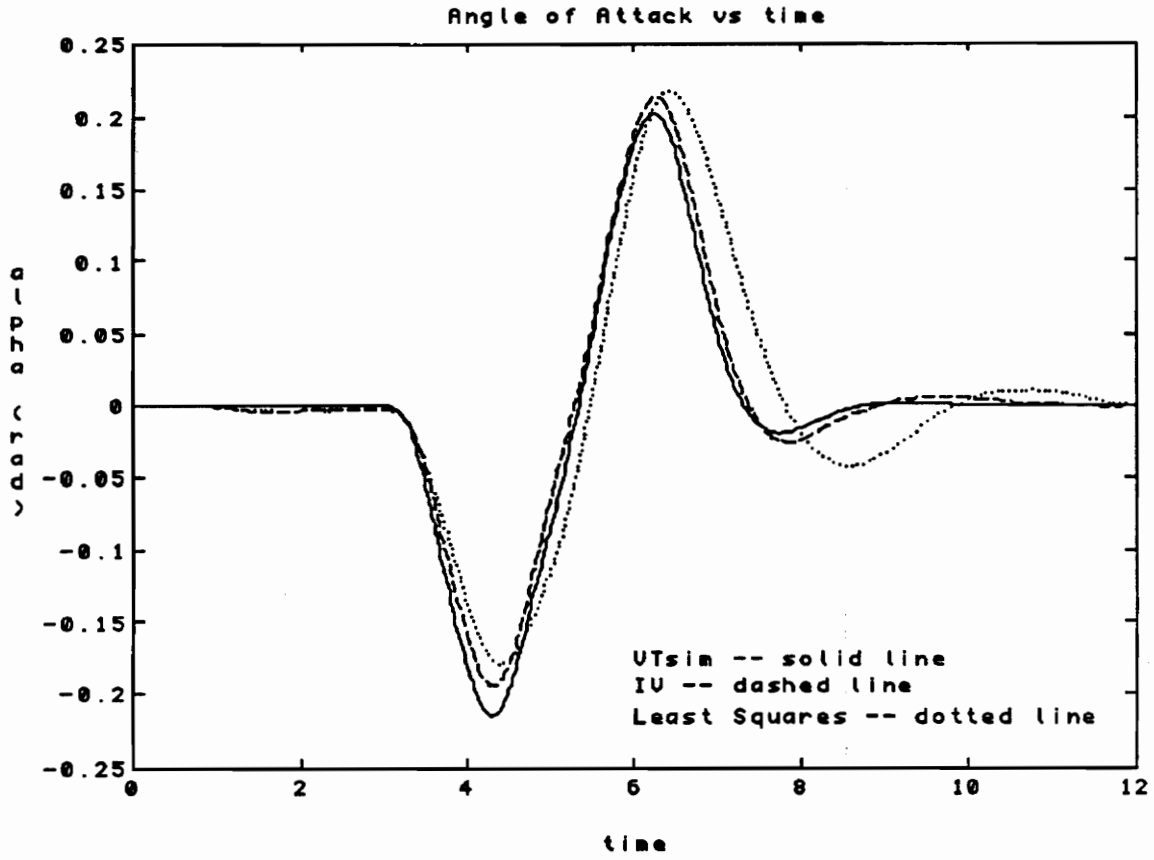

Figure A32: Angle of attack; Case 6

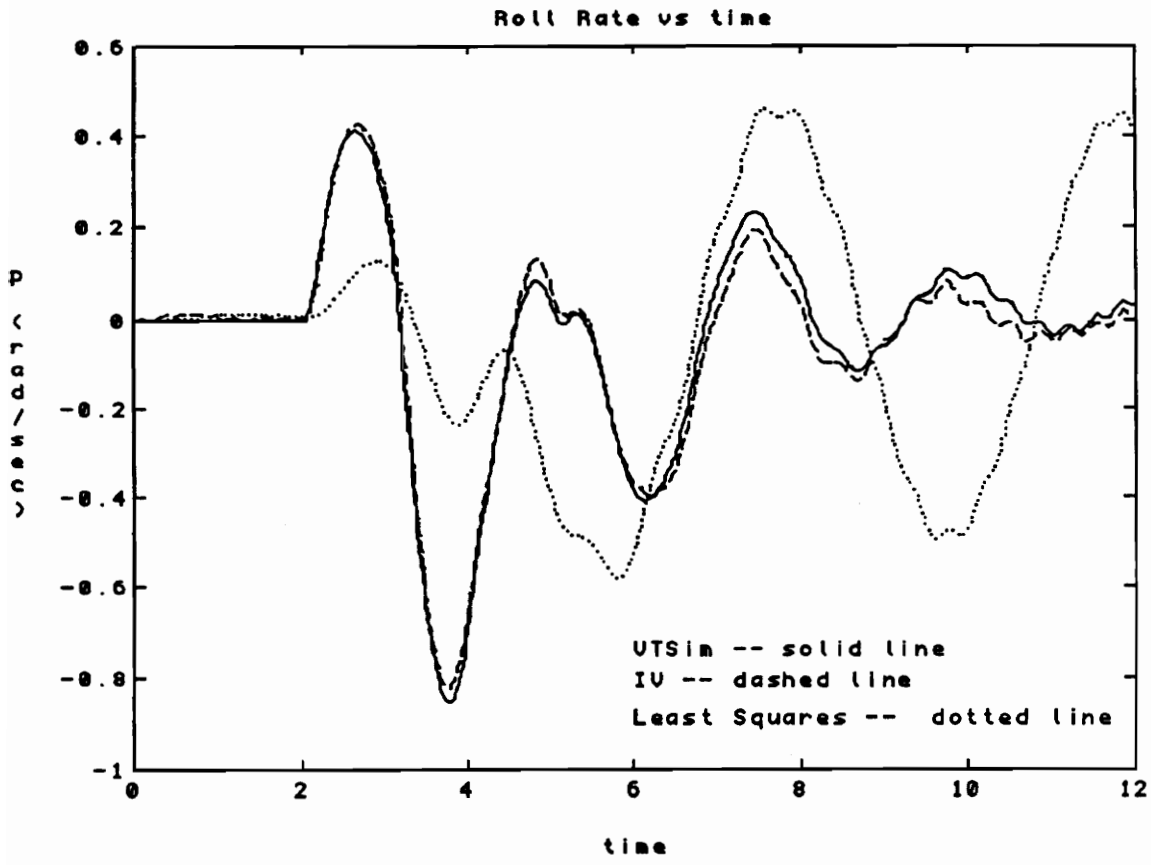

Figure A33: Roll rate; Case 6

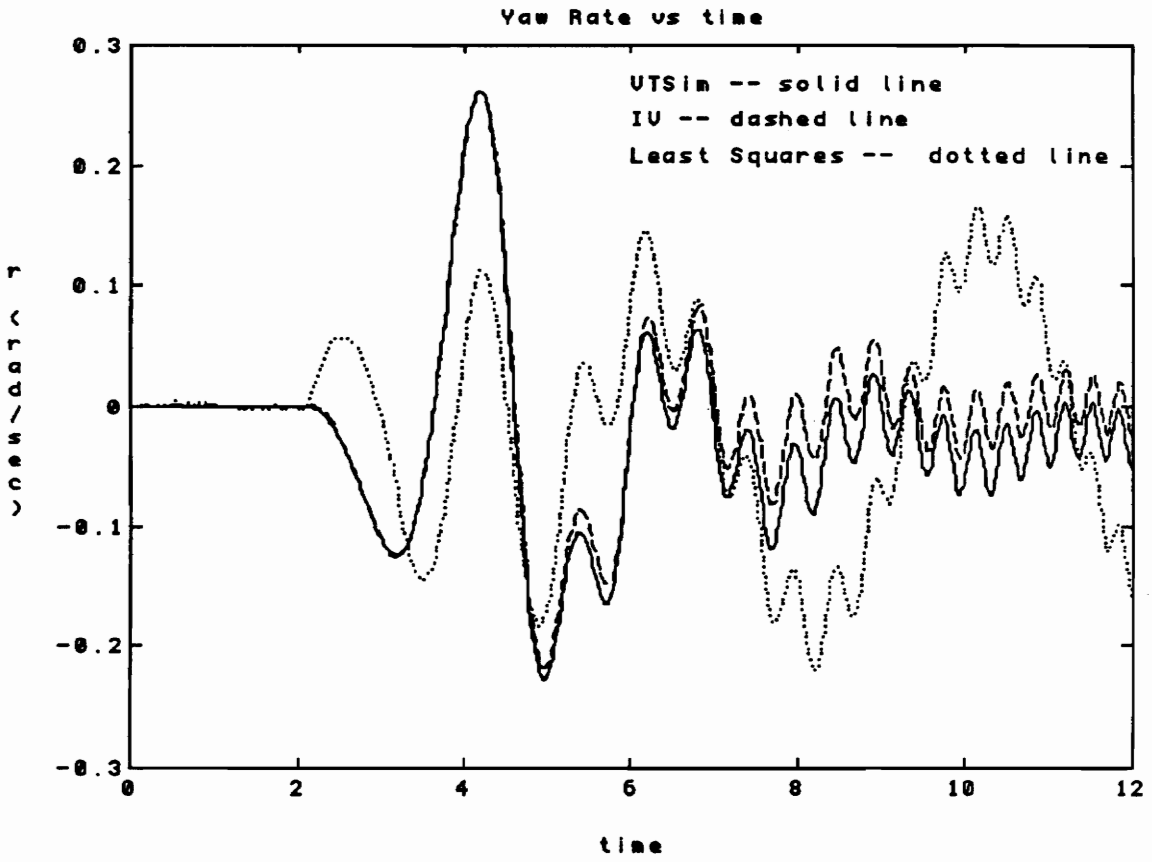

Figure A34: Yaw rate; Case 6

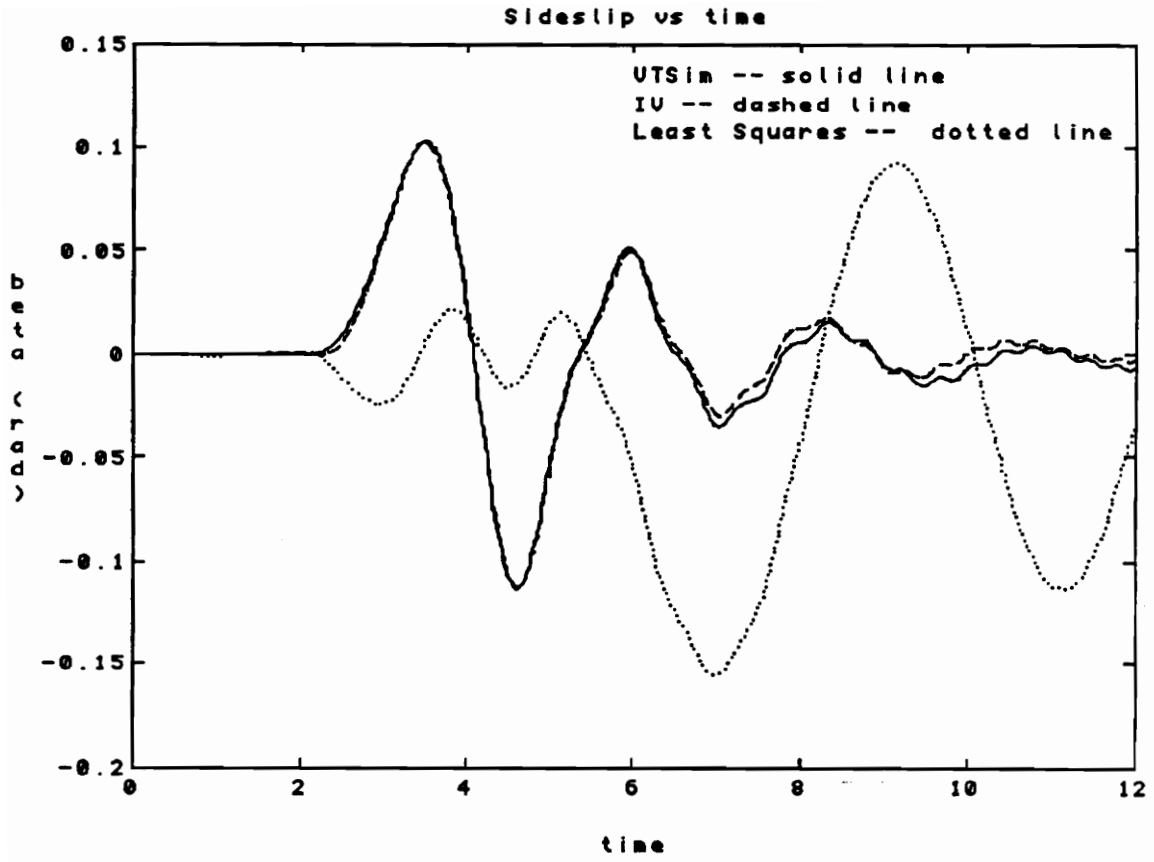

Figure A35: Sideslip; Case 6

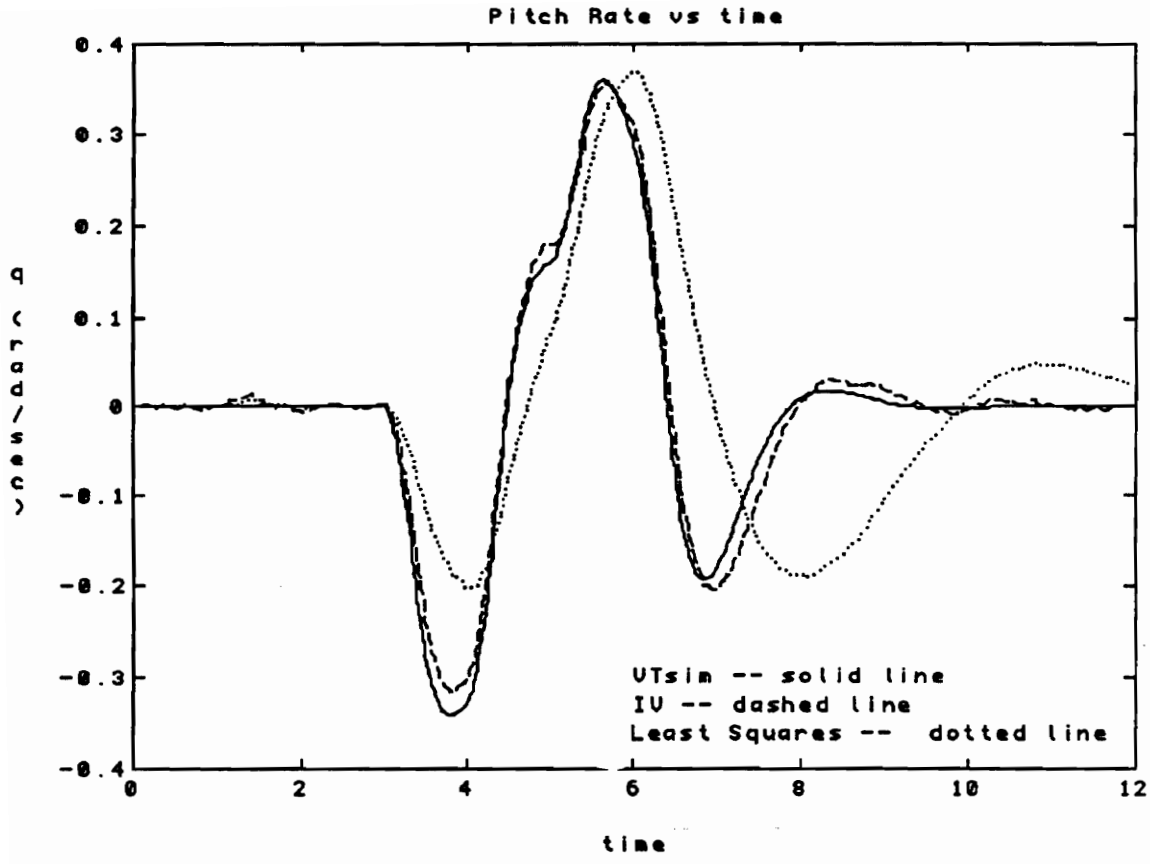

Figure A36: Pitch rate; Case 7

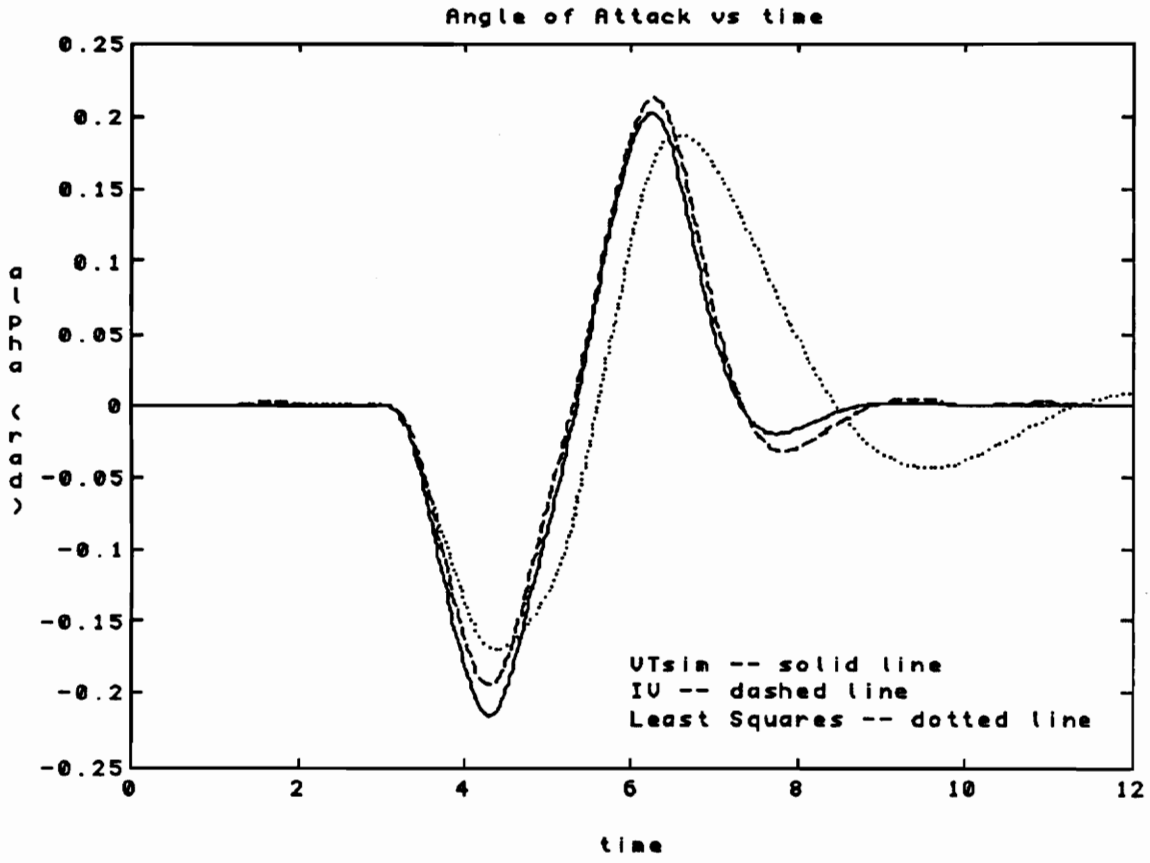

Figure A37: Angle of attack; Case 7

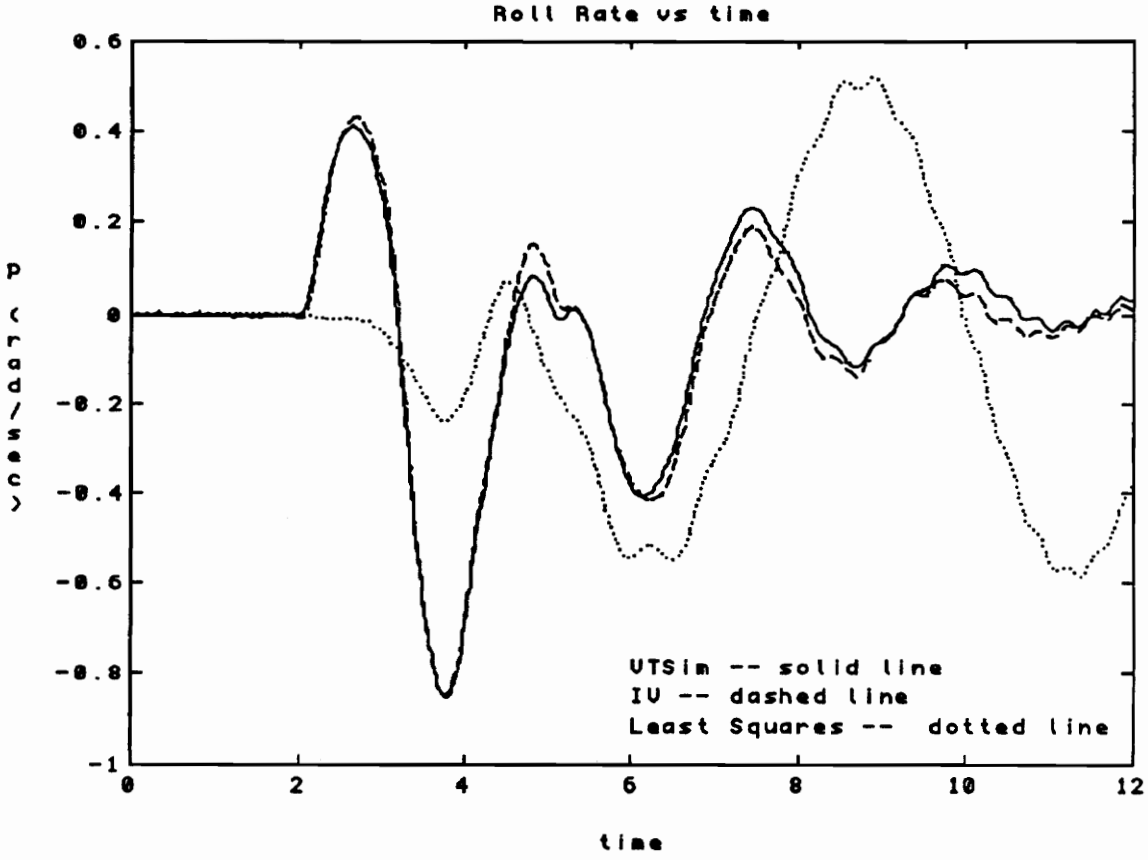

Figure A38: Roll rate; Case 7

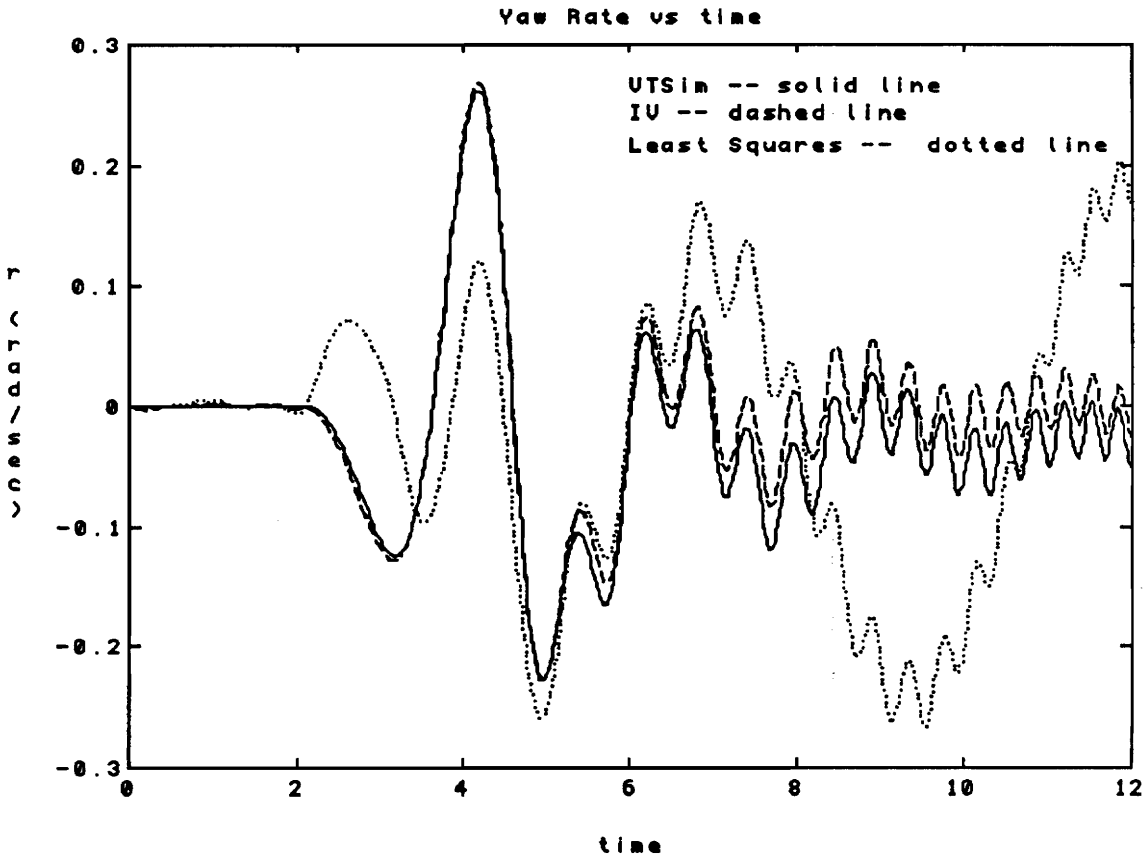

Figure A39: Yaw rate; Case 7

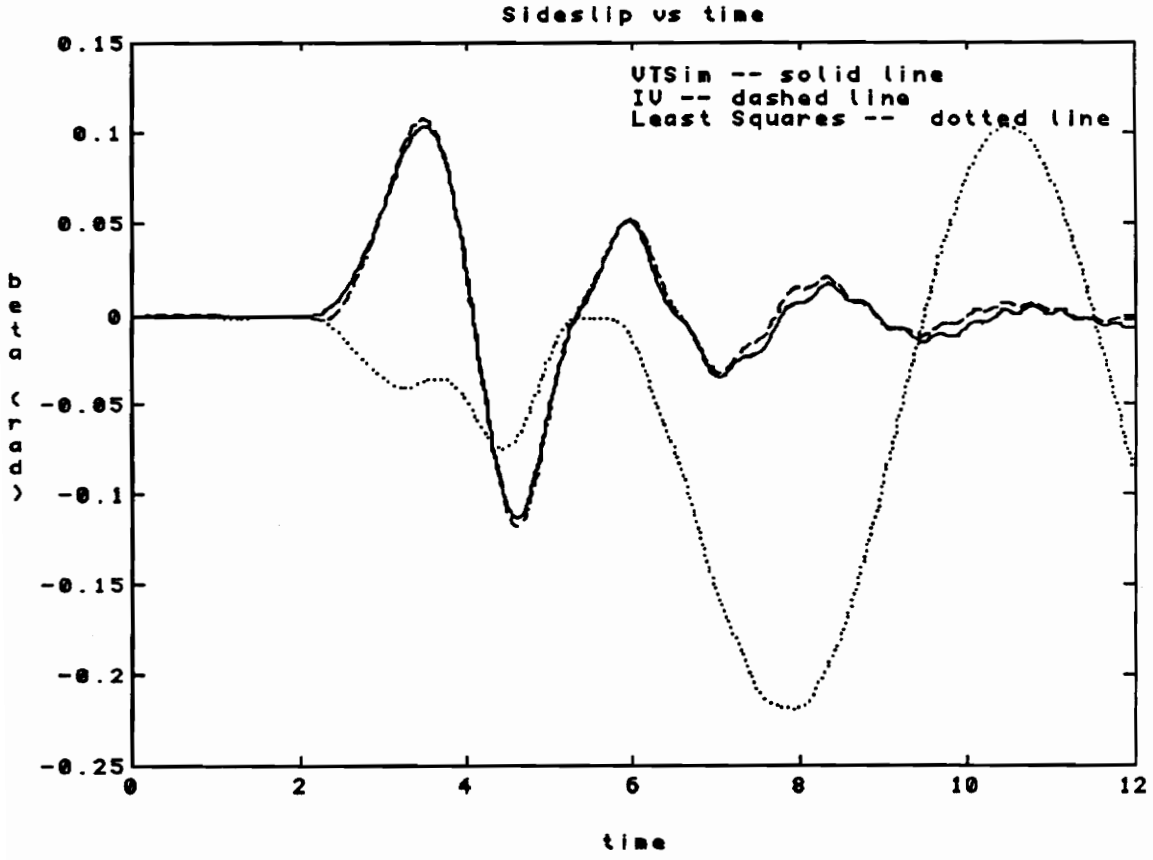

Figure A40: Sideslip; Case 7

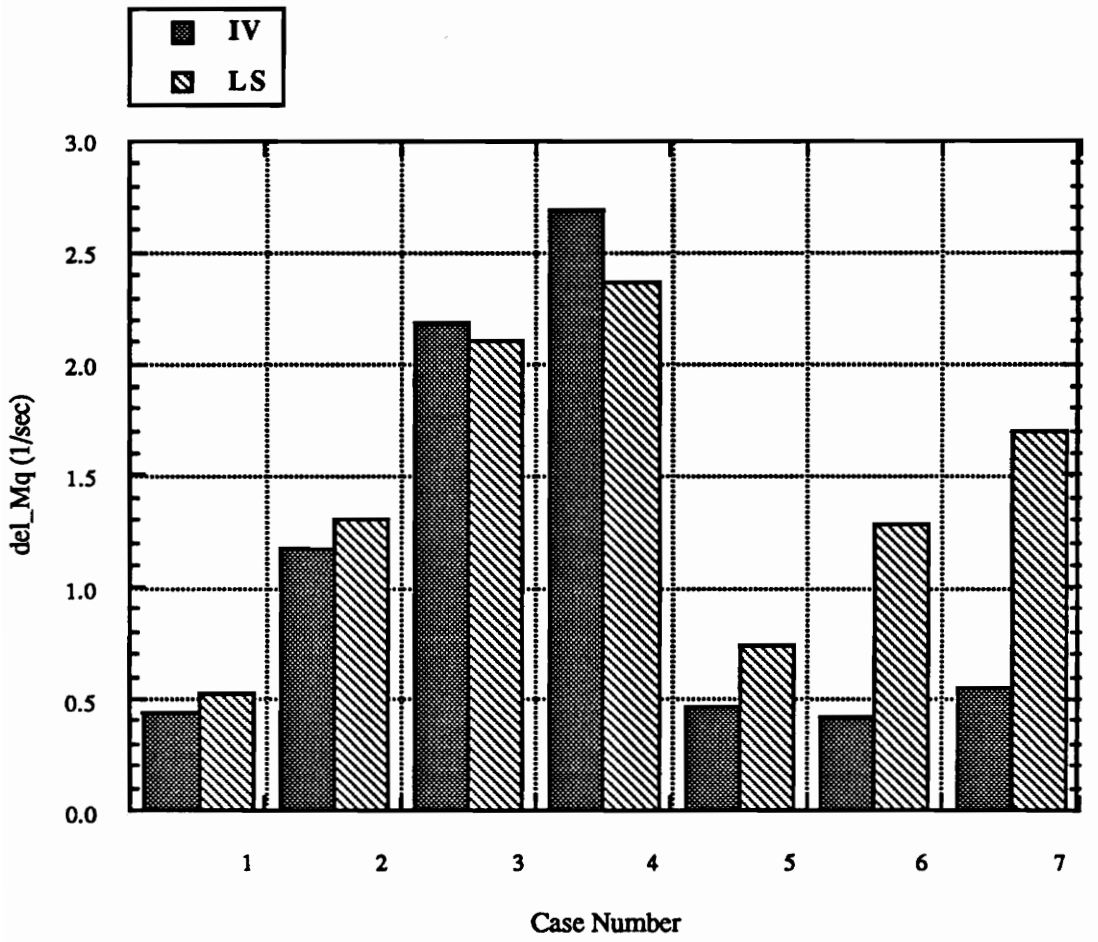

Figure A41: Absolute value of change in Mq from zero noise identified error value

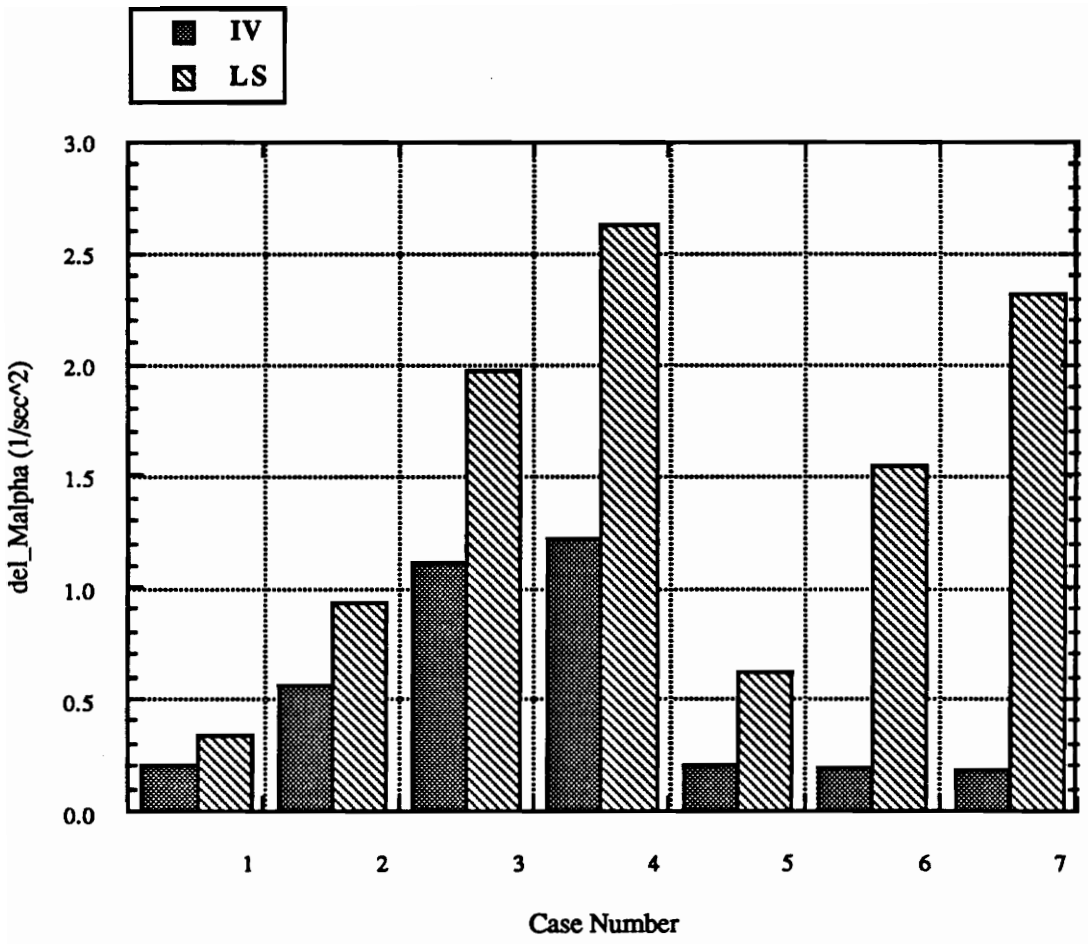

Figure A42: Absolute value of change in Malpha from zero noise identified error value

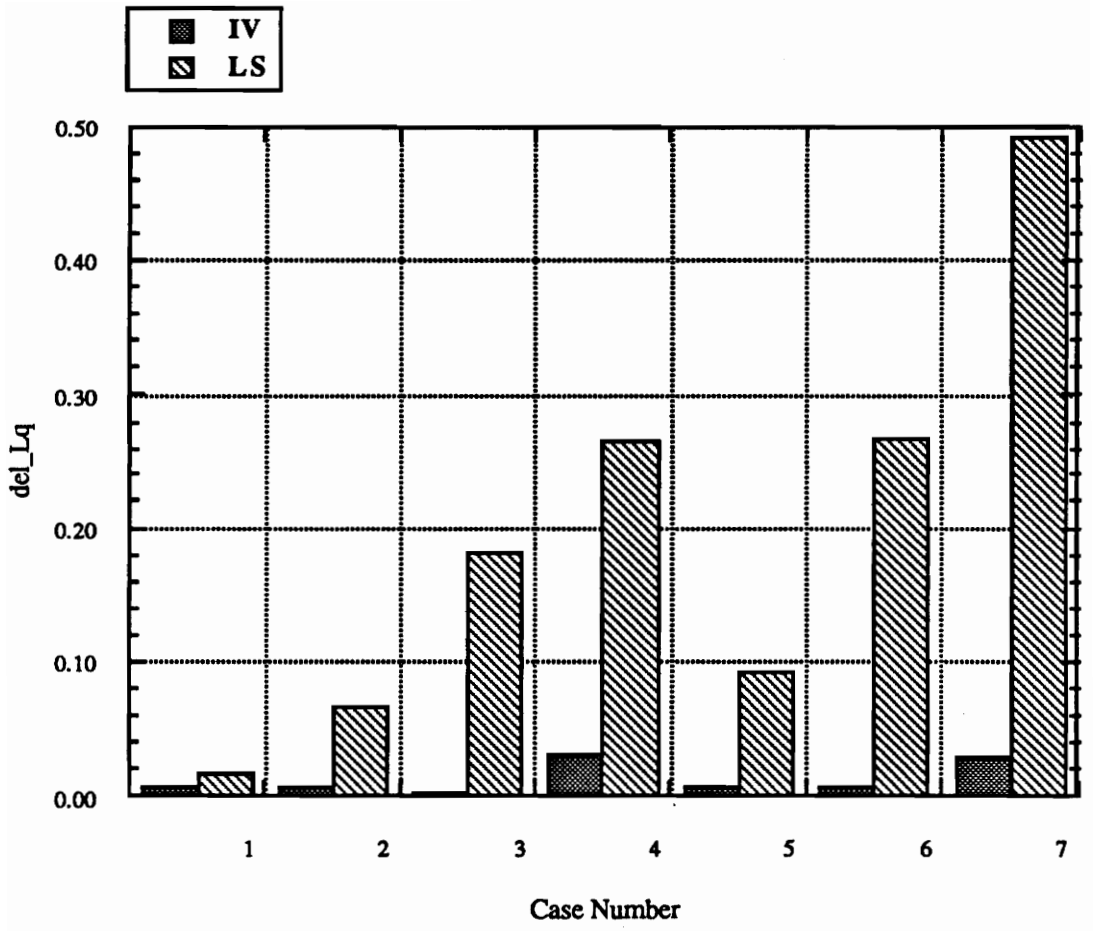

Figure A43: Absolute value of change in Lq from zero noise identified error value

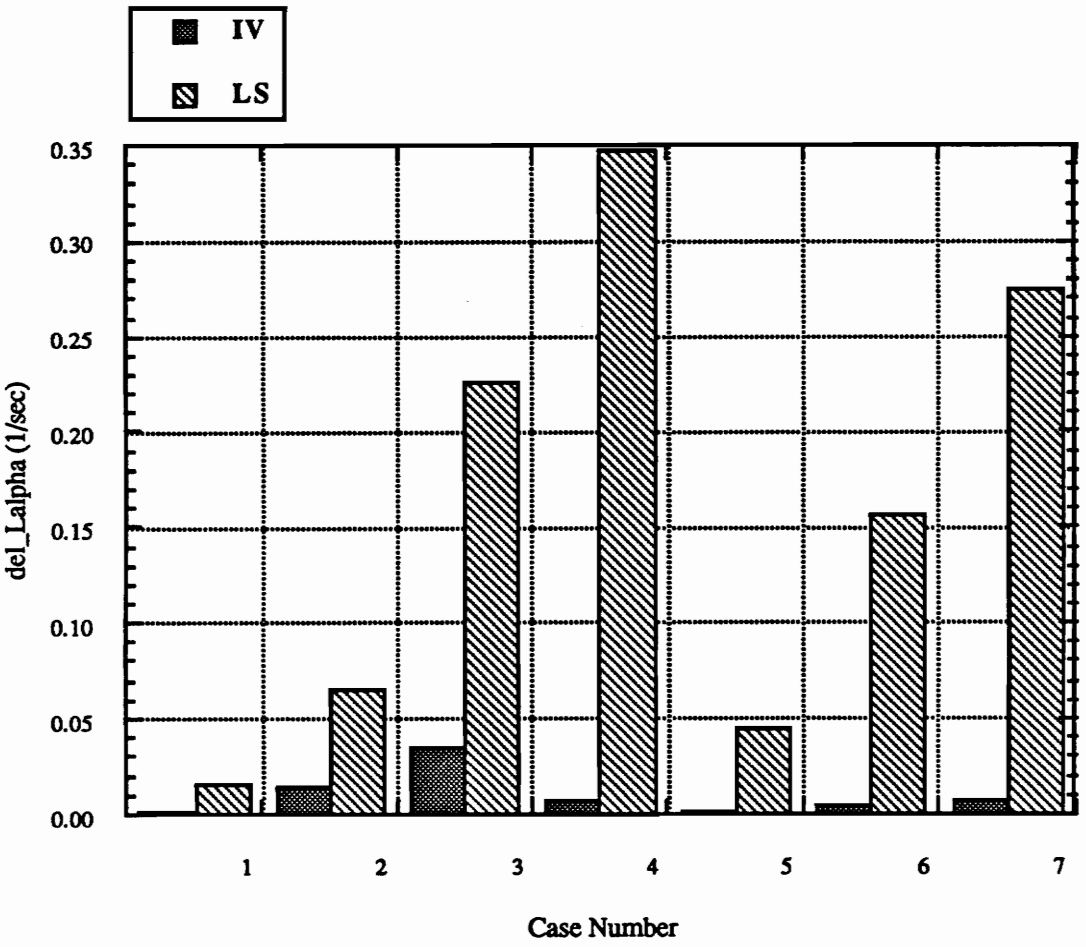

Figure A44: Absolute value of change in Lalpha from zero noise identified error value

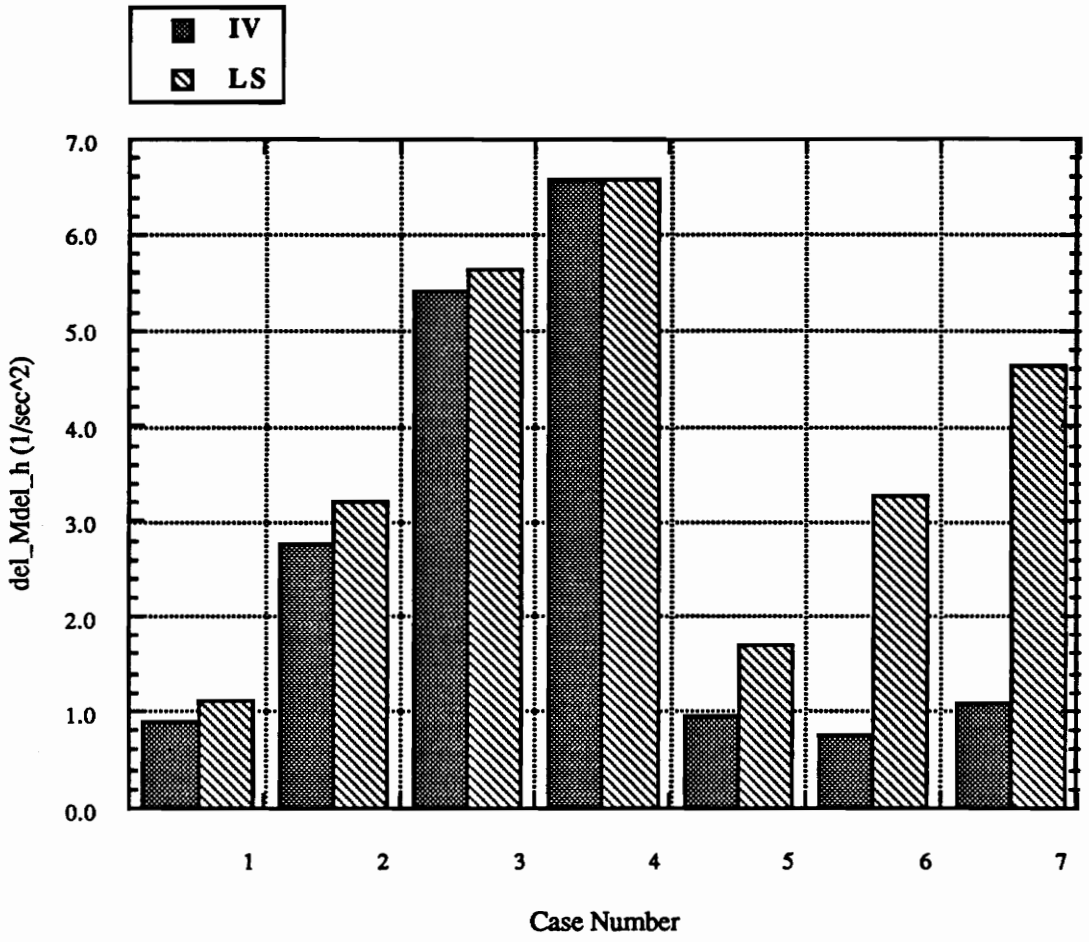

Figure A45: Absolute value of change in M_delta_h from zero noise identified error value

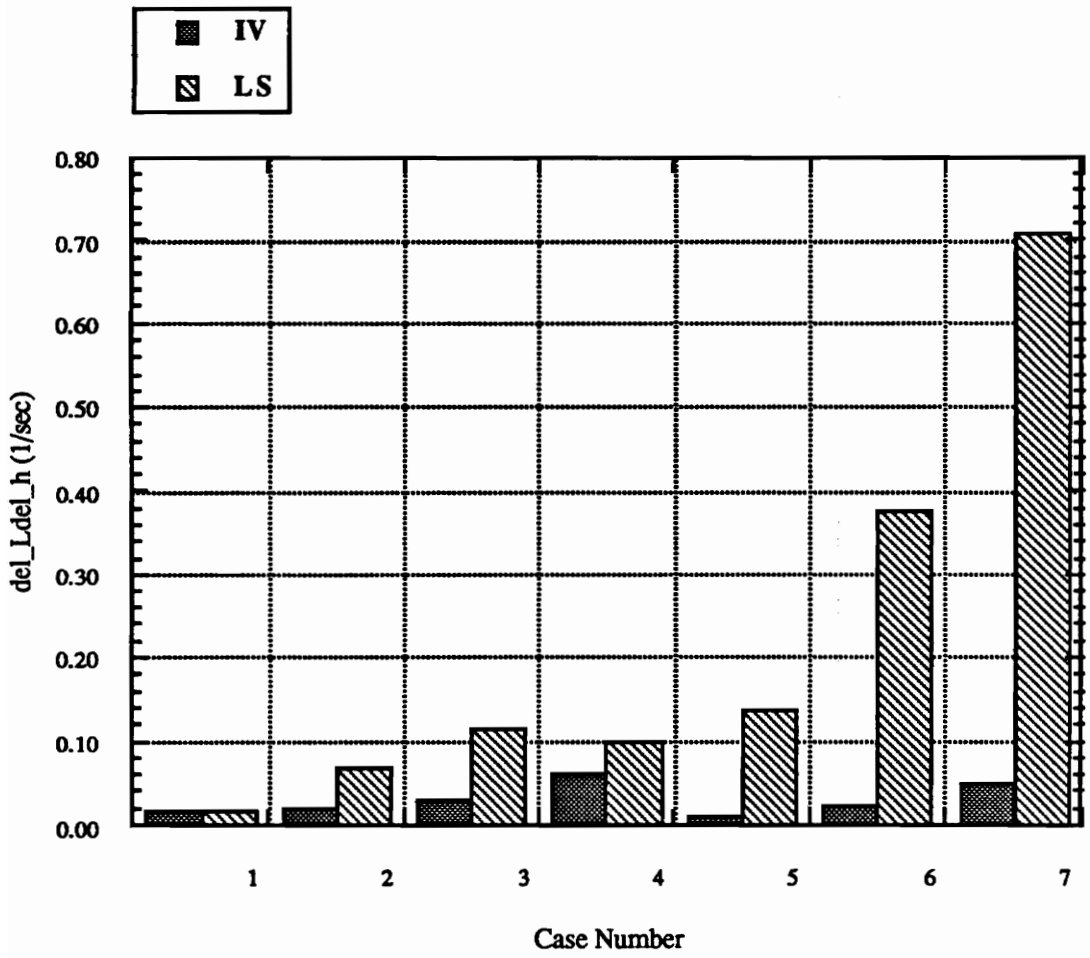

Figure A46: Absolute value of change in L_delta_h from zero noise identified error value

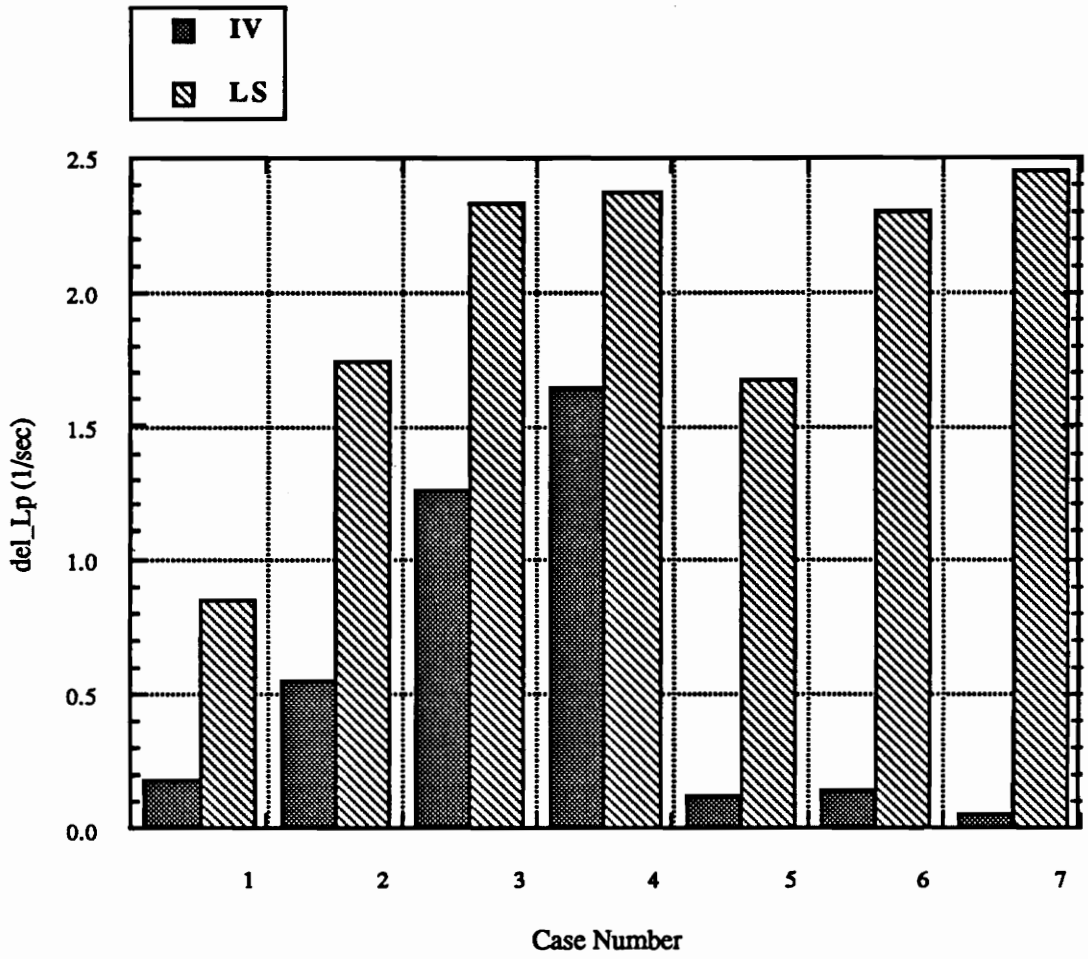

Figure A47: Absolute value of change in Lp from zero noise identified error value

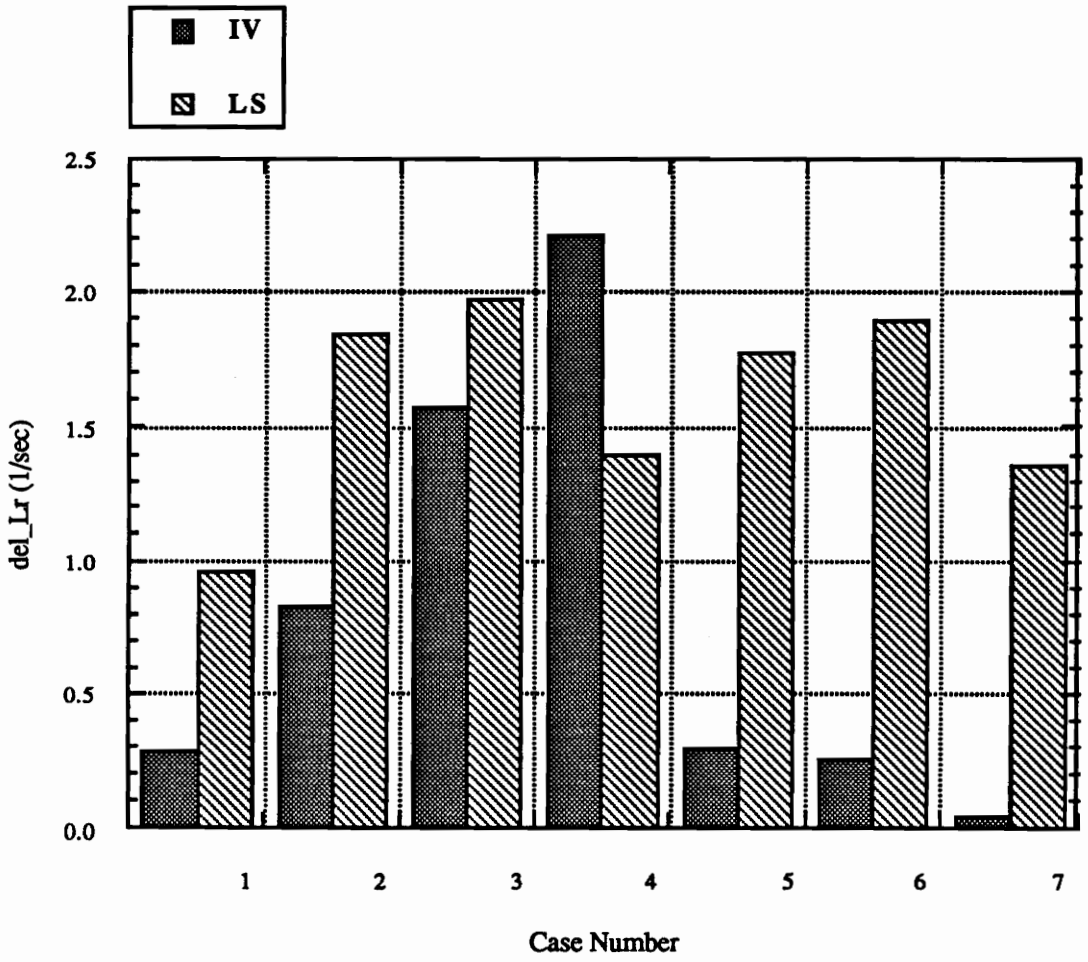

Figure A48: Absolute value of change in Lr from zero noise identified error value

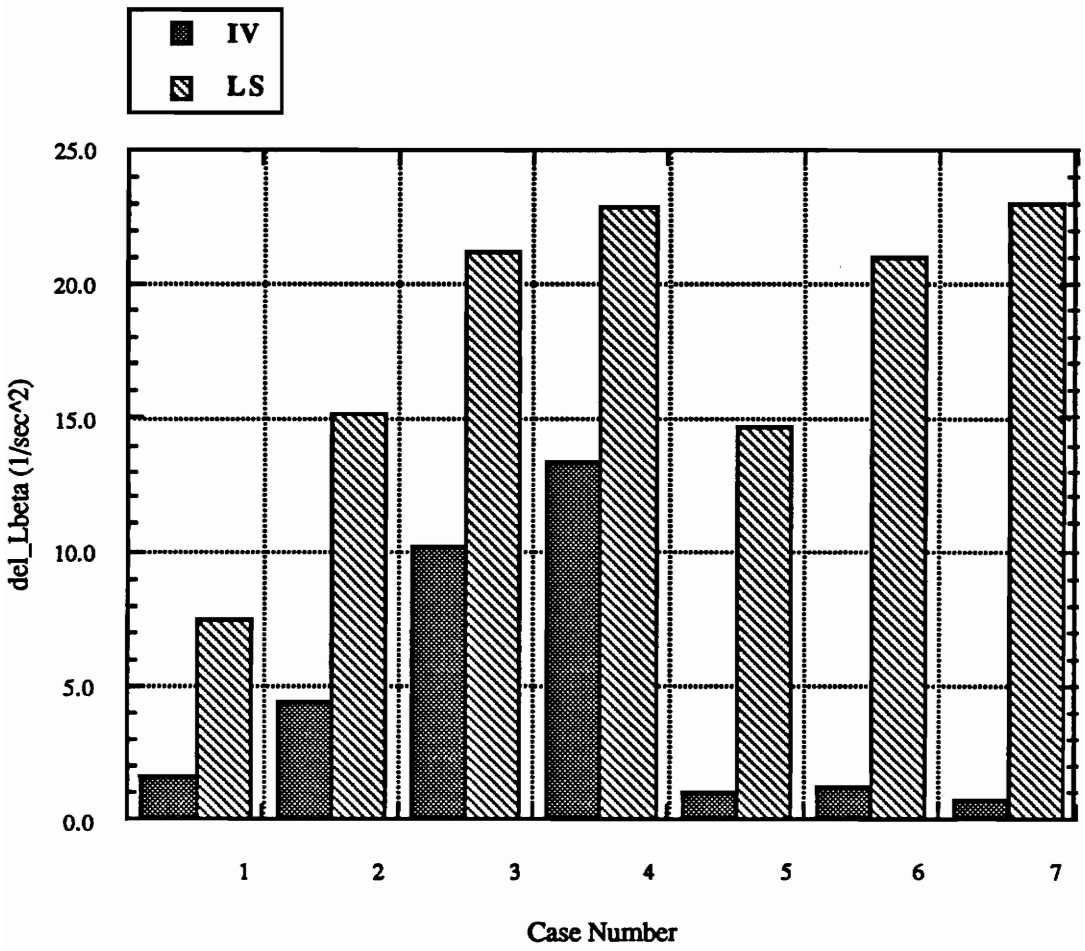

Figure A49: Absolute value of change in Lbeta from zero noise identified error value

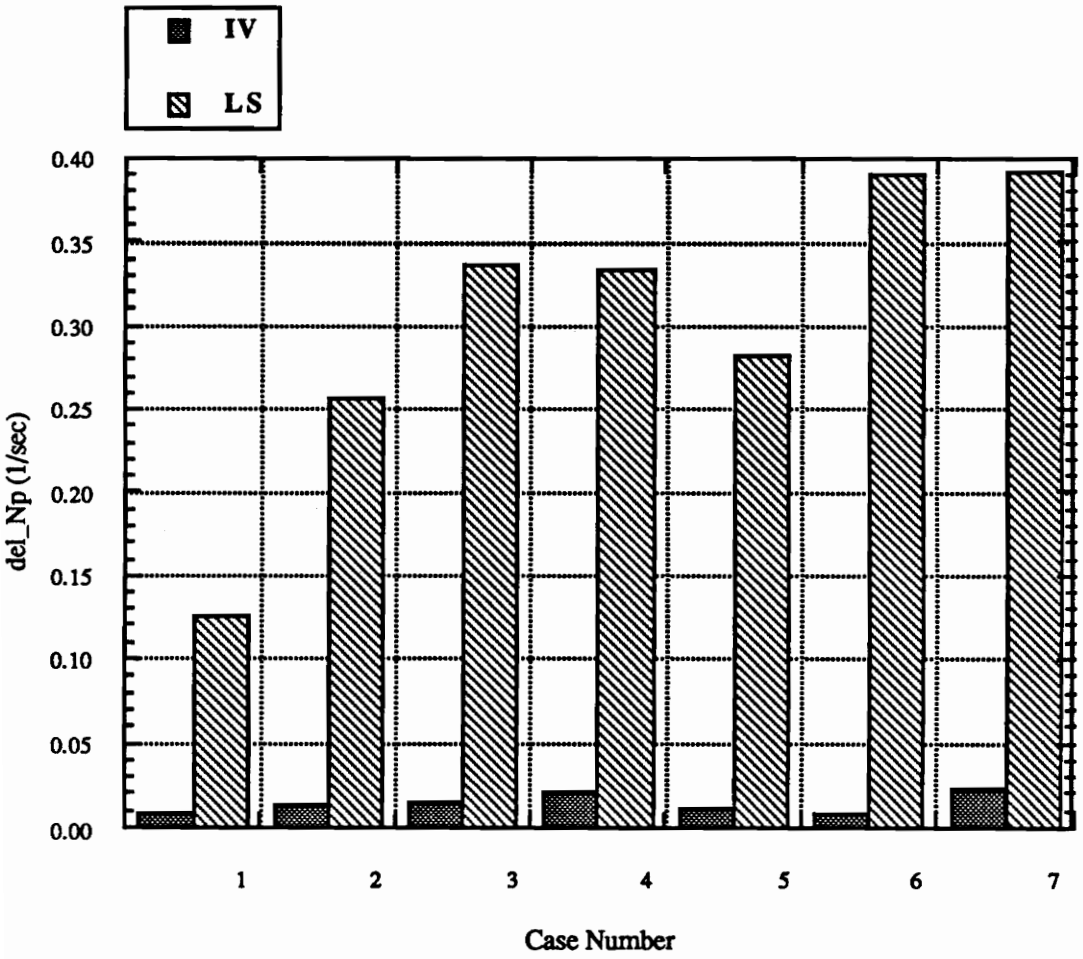

Figure A50: Absolute value of change in Np from zero noise identified error value

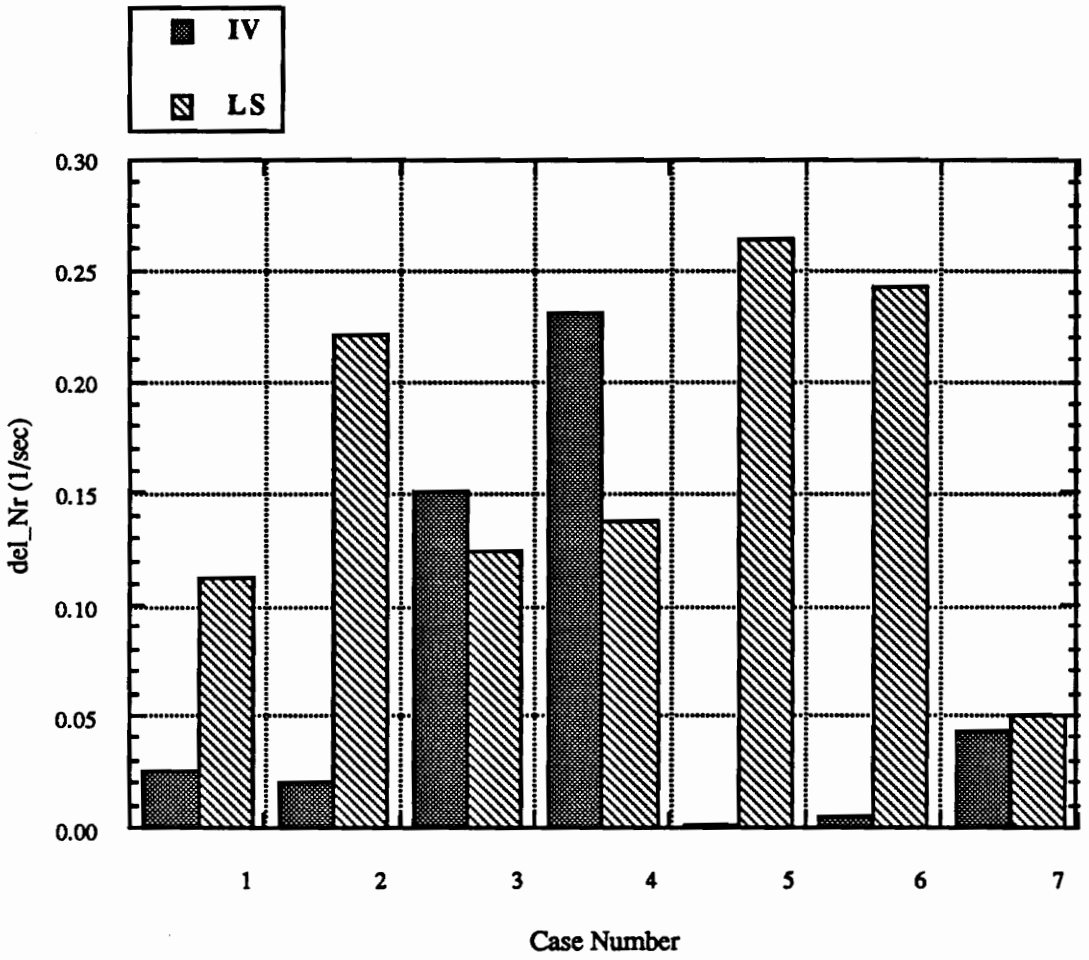

Figure A51: Absolute value of change in Nr from zero noise identified error value

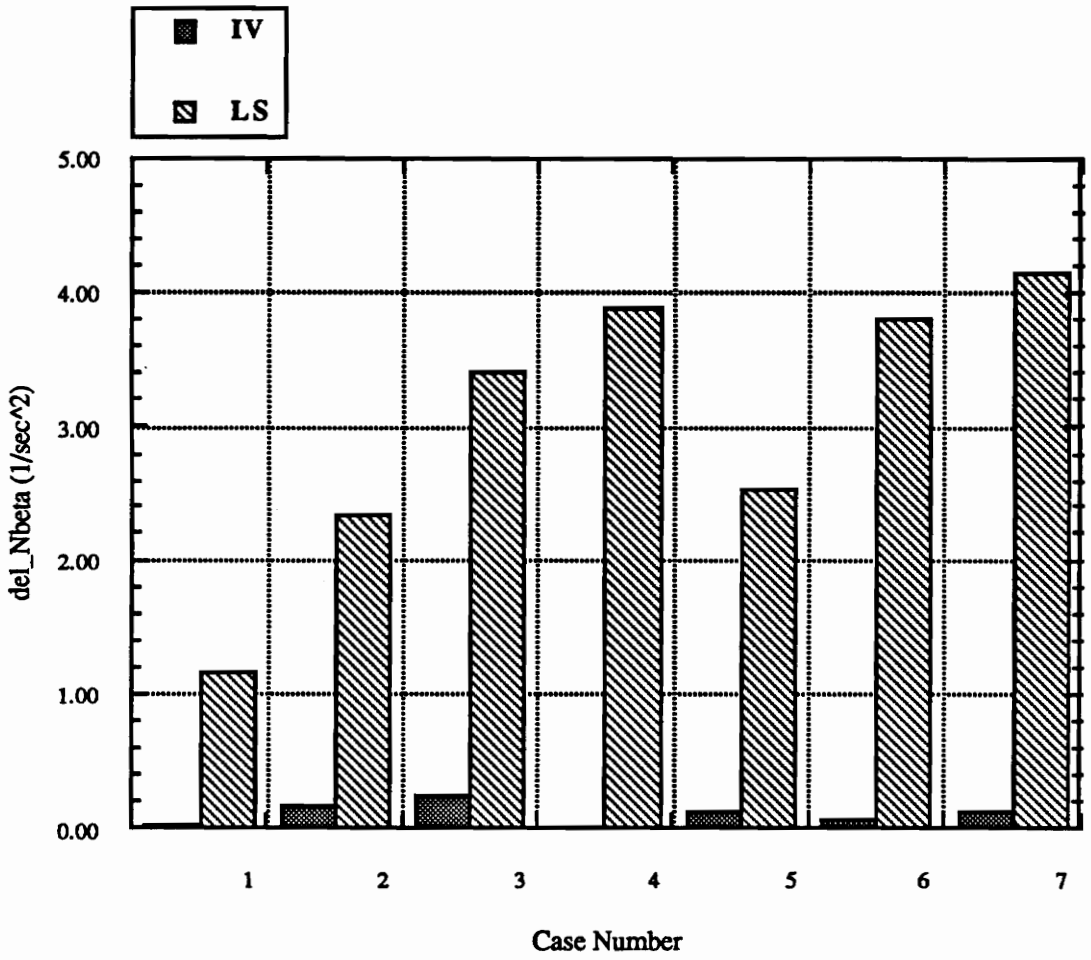

Figure A52: Absolute value of change in Nbeta from zero noise identified error value

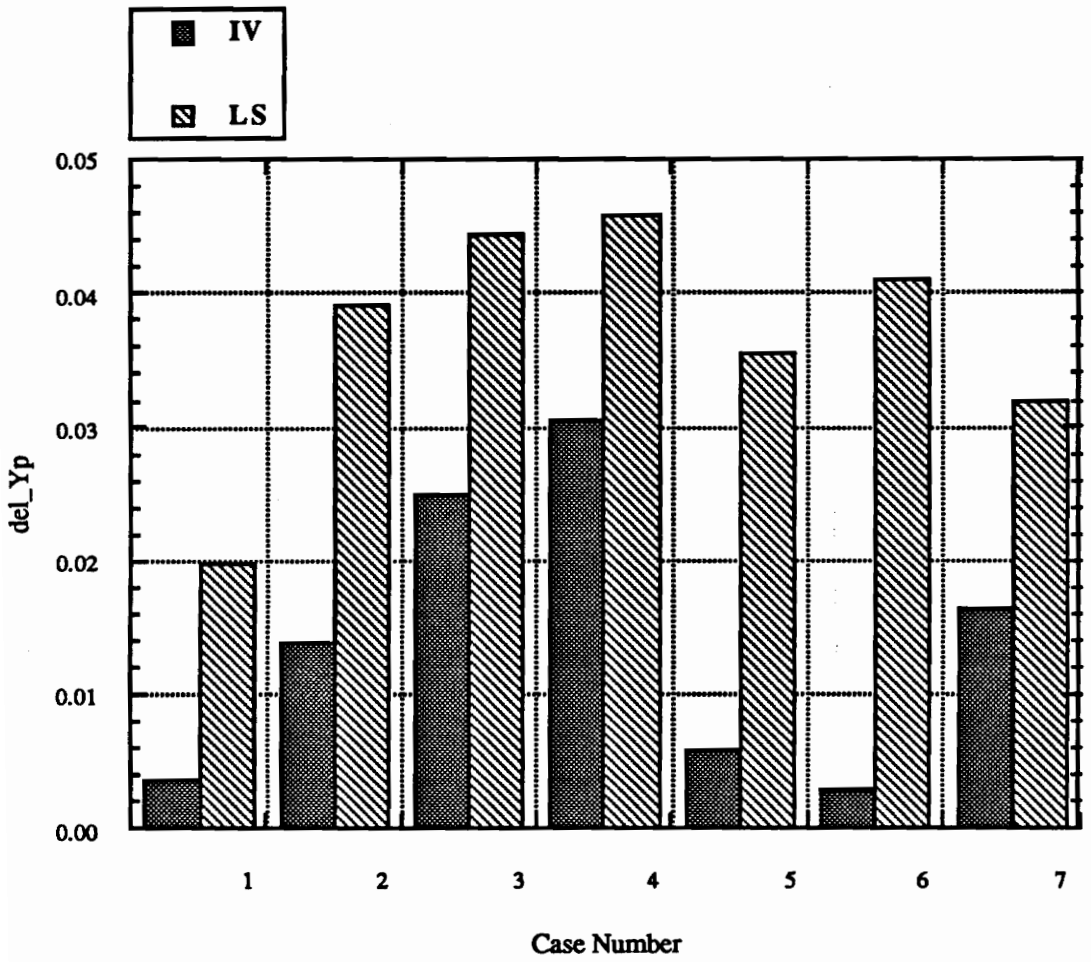

Figure A53: Absolute value of change in Yp from zero noise identified error value

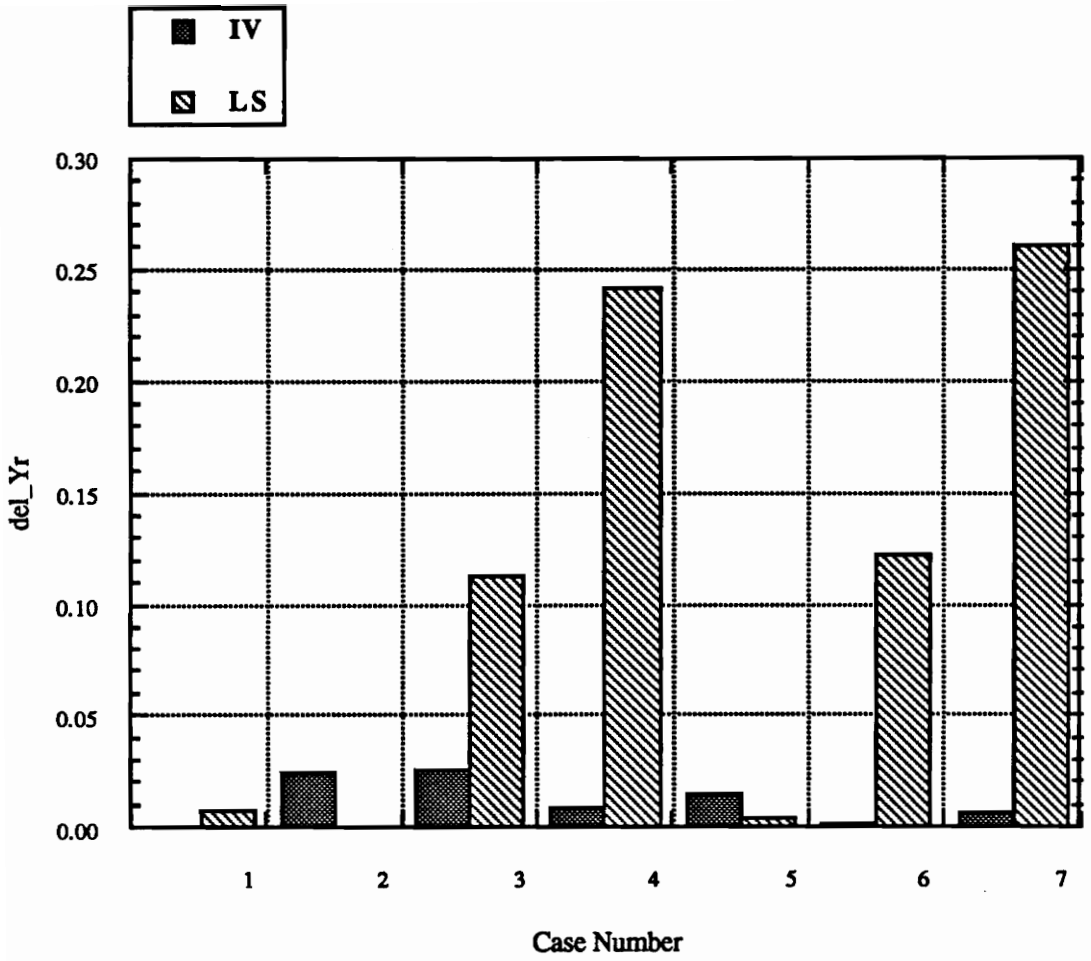

Figure A54: Absolute value of change in Yr from zero noise identified error value

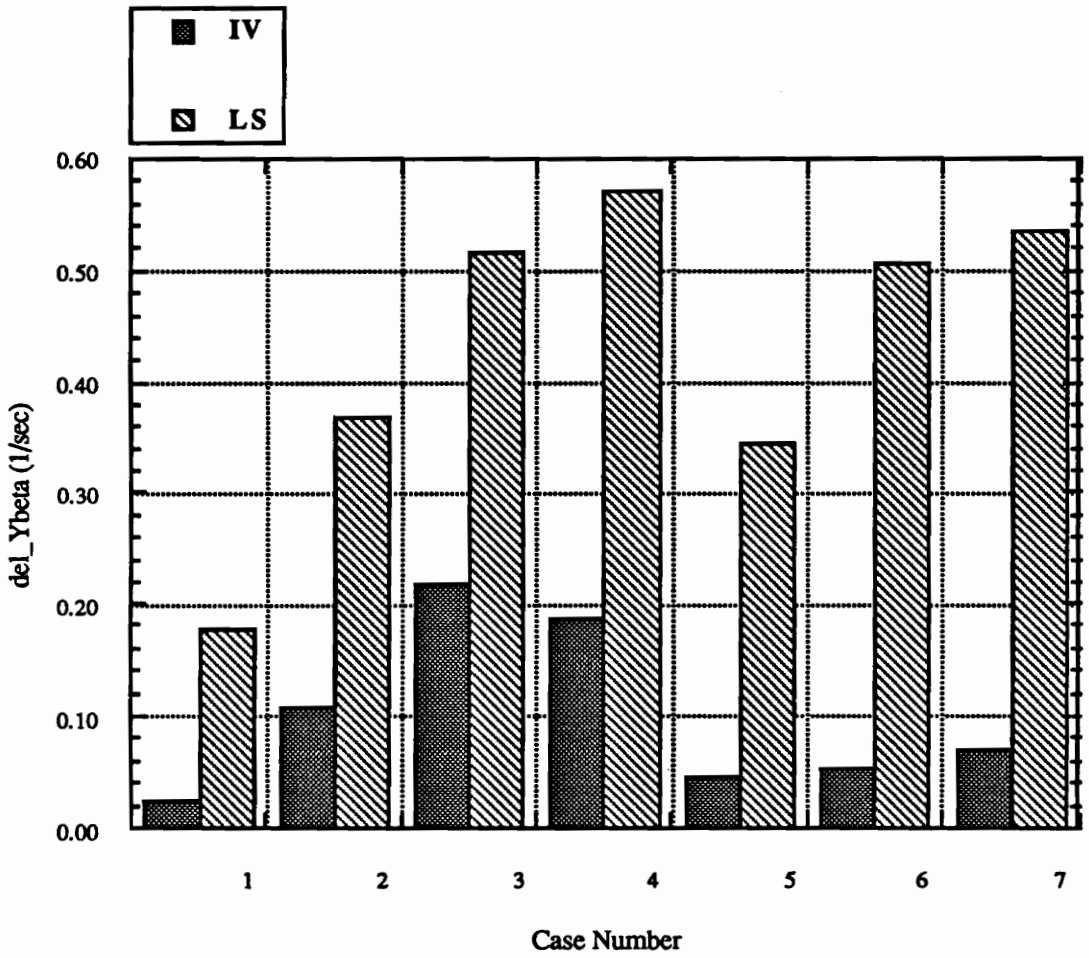

Figure A55: Absolute value of change in Ybeta from zero noise identified error value

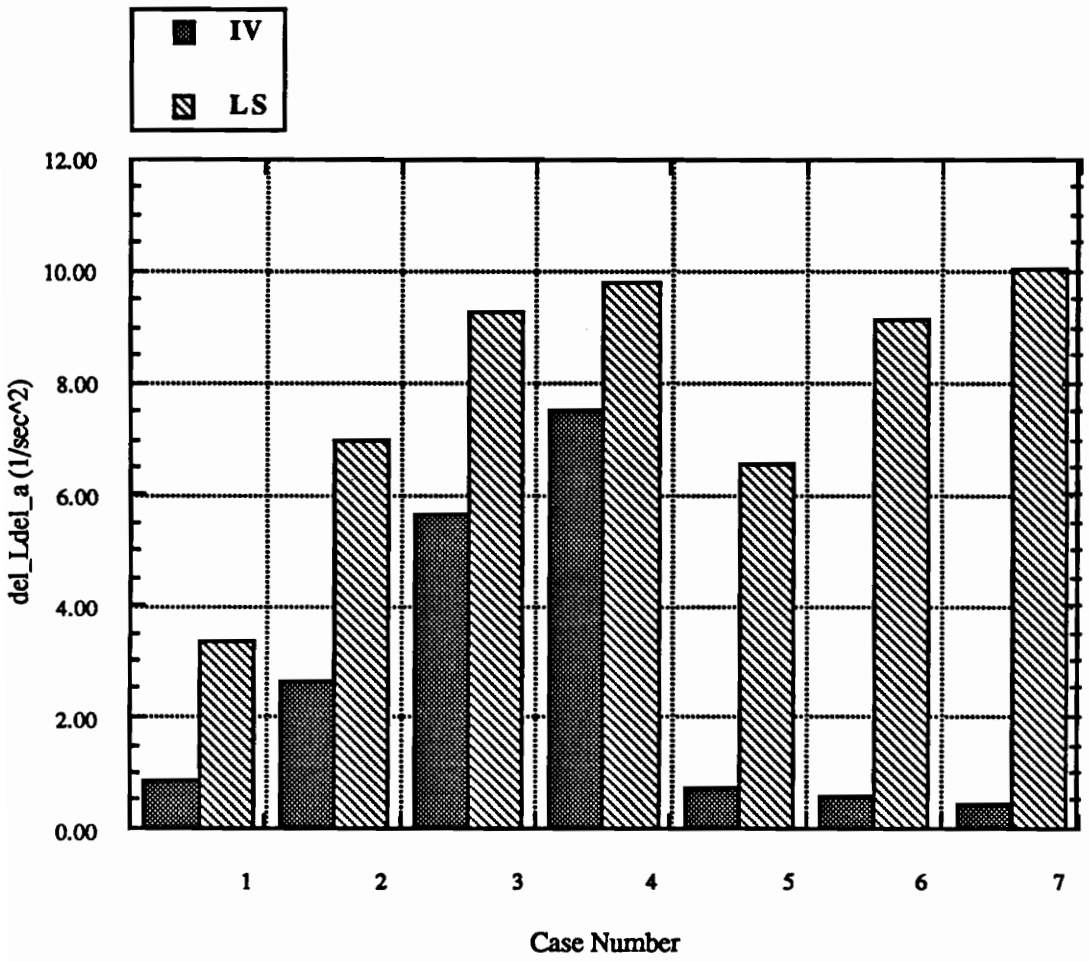

Figure A56: Absolute value of change in L_delta_a from zero noise identified error value

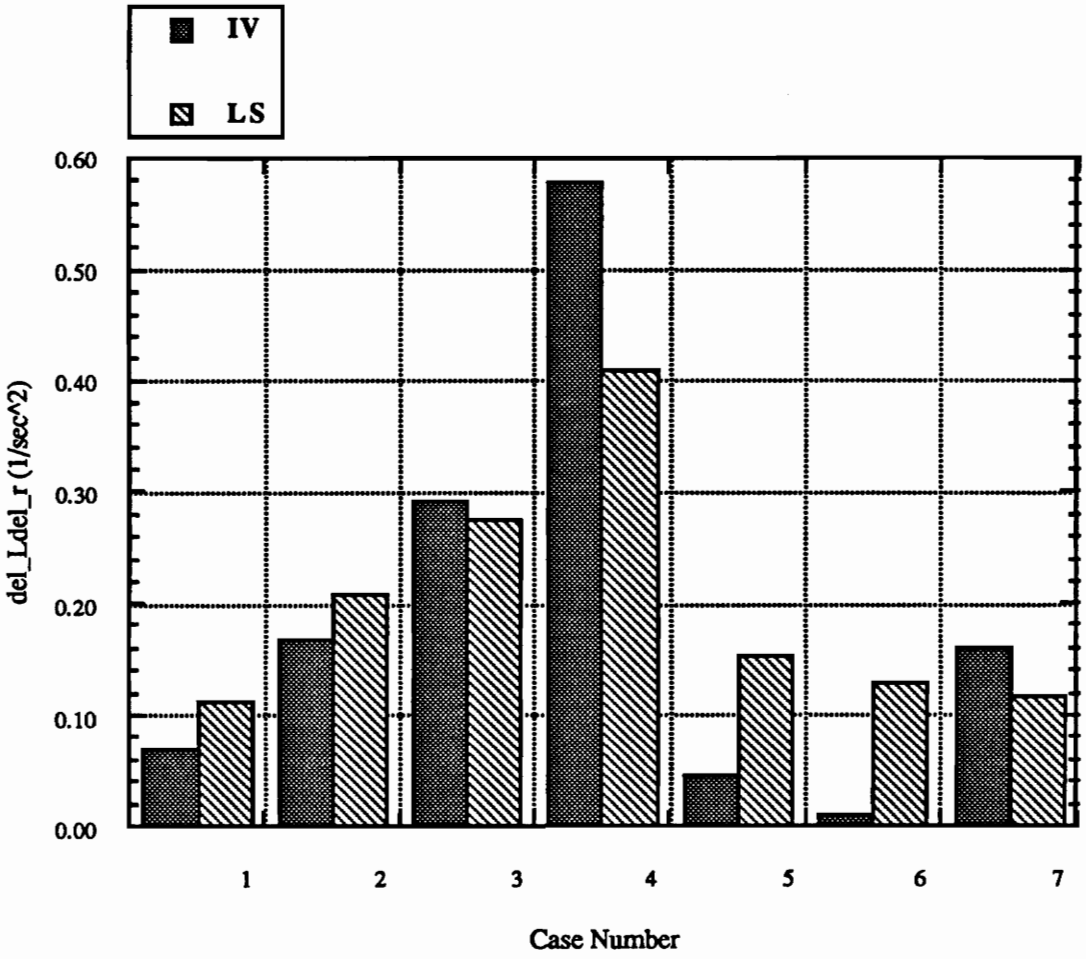

Figure A57: Absolute value of change in L_delta_r from zero noise identified error value

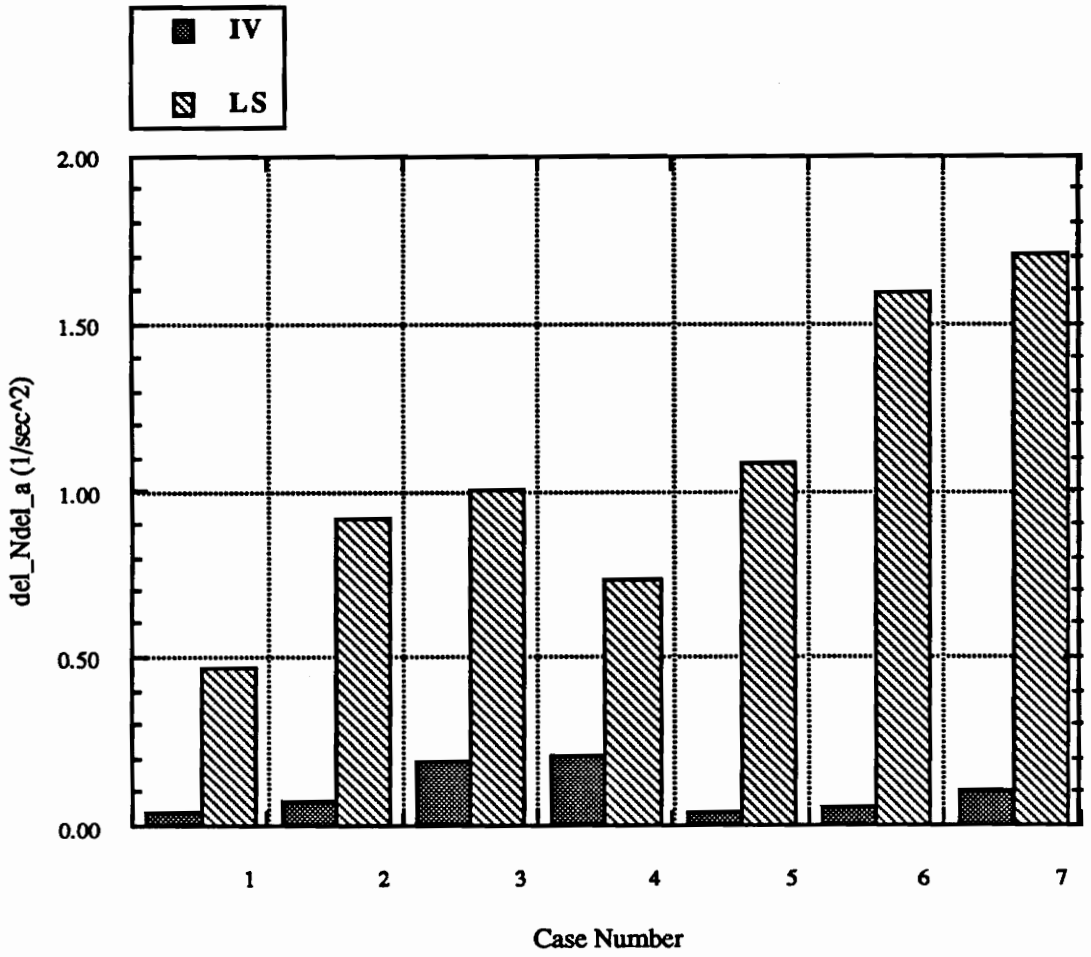

Figure A58: Absolute value of change in N_delta_a from zero noise identified error value

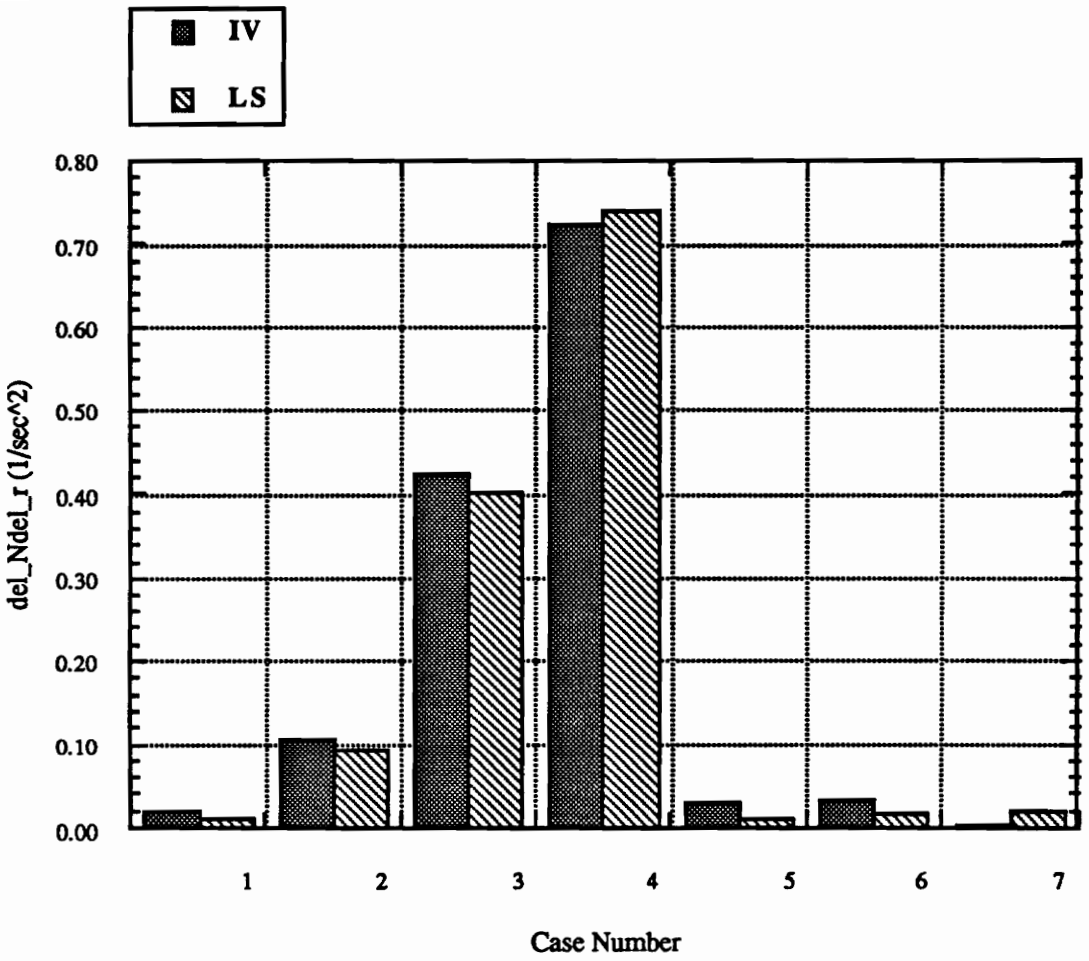

Figure A59: Absolute value of change in N_delta_r from zero noise identified error value

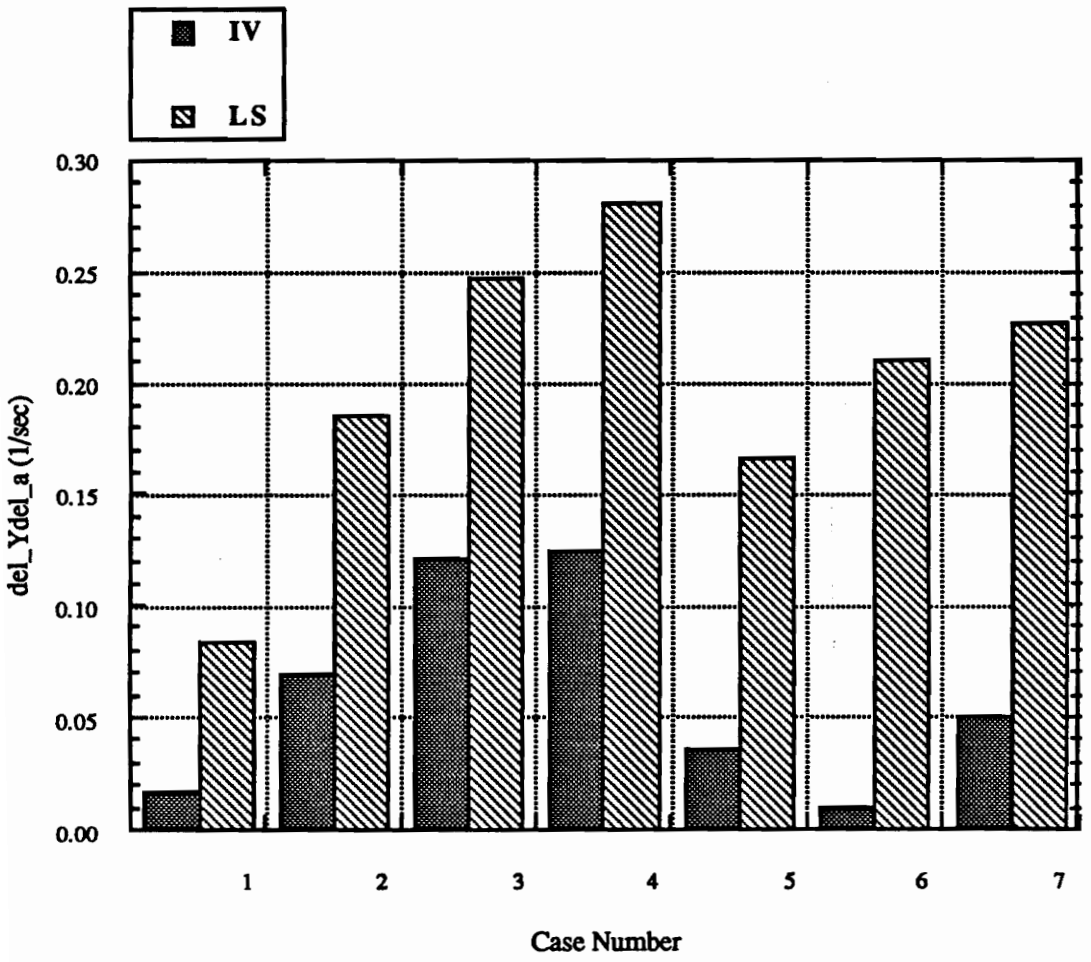

Figure A60: Absolute value of change in Y_delta_a from zero noise identified error value

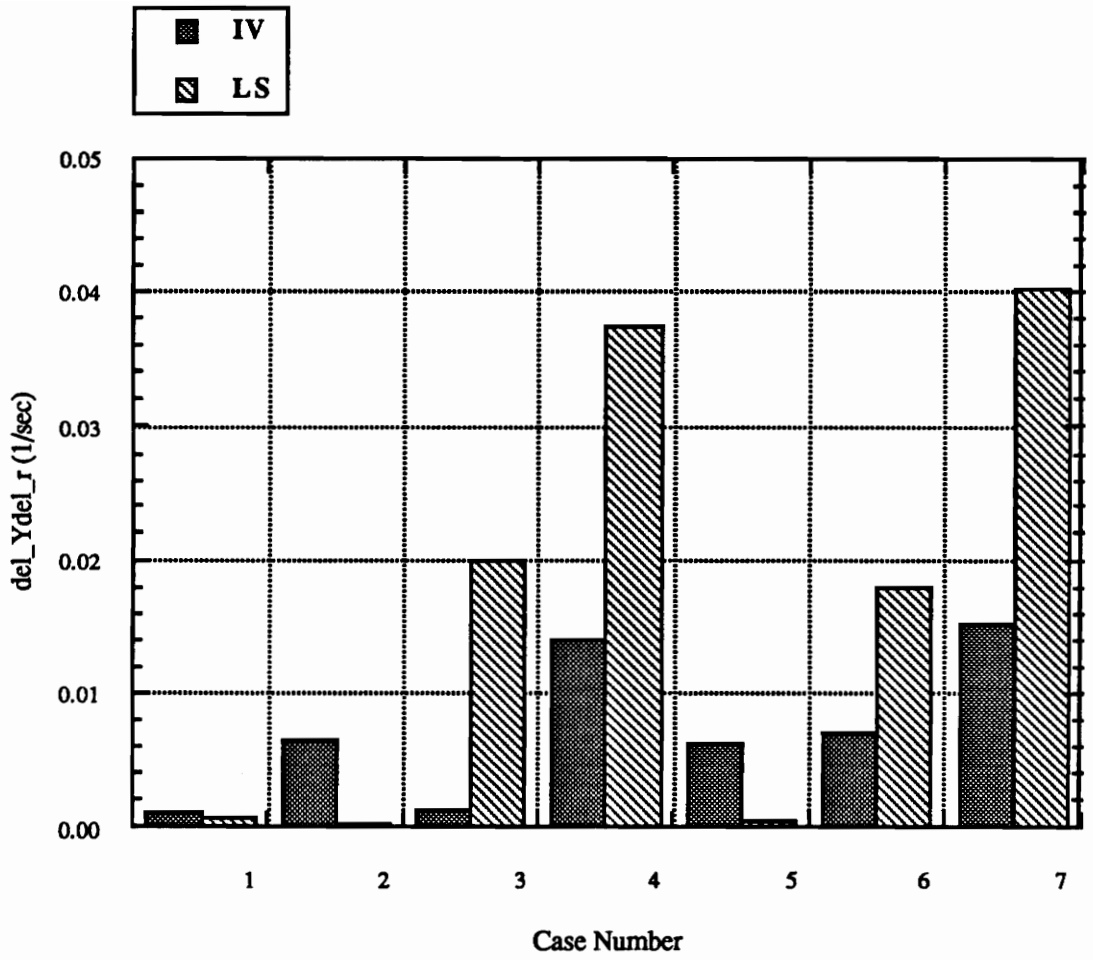

Figure A61: Absolute value of change in Y_delta_r from zero noise identified error value

7.0 Vita

The author was born on December 23, 1967 in Mobile, Alabama. He graduated from Murphy High School in May 1986 and entered The University of Alabama in August 1986. He received a Bachelor of Science degree in Aerospace Engineering in May 1991. He then entered Virginia Polytechnic Institute and State University in August 1991 to pursue graduate studies in Aerospace Engineering and received his Master of Science degree in December, 1992.

Christopher D. Weekley